Epitope Sequence and Modification Fingerprints of Anti-Aβ Antibodies

Talucci Ivan[1, 2]; Leske Timon[1]; Klafki Hans-Wolfgang[3]; Hassan Mohammed Mehedi[3]; Steiert Annik[3]; Morgado Barbara[3]; Bothe Sebastian[1]; van Werven Lars[4]; Liepold Thomas[4]; Walter Jochen[5]; Schindelin Hermann[1]; Wiltfang Jens[3]; Wirths Oliver[3]; Jahn Olaf[3,4]; Maric Hans-Michael[1]

Author affiliations:
[1] Rudolf Virchow Center for Integrative and Translational Bioimaging, Julius-Maximilians-Universität (JMU) Würzburg, Germany
[2] Department of Neurology, University Hospital Wuerzburg (UKW), Würzburg, Germany
[3] Department of Psychiatry and Psychotherapy, University Medical Center Göttingen (UMG), Germany
[4] Neuroproteomics Group, Department of Molecular Neurobiology, Max Planck Institute for Multidisciplinary Sciences, Göttingen, Germany
[5]Center of Neurology, Molecular Cell Biology, University Hospital Bonn, Germany
Correspondence to H.M.M. at hans.maric@uni-wuerzburg.de

Abstract

A hallmark of Alzheimer's disease (AD), the most common form of dementia, is the progressive accumulation of amyloid-beta (Aβ) peptides across distinct brain regions. Anti-Aβ antibodies (Aβ-Abs) that bind specific Aβ variants are essential research tools. Furthermore, the monoclonal Aβ-Abs Aducanumab, Lecanemab, and Donanemab have recently gained approval as the first disease-modifying therapeutics for early AD. In this study, we systematically determined on peptide microarrays the exact binding epitopes of 20 Aβ-Abs, including biosimilars of Aducanumab, Lecanemab and Donanemab. Precise Aβ-sequence and modification requirements were resolved through deep mutational scans and synthetically modified peptide libraries. To address the potential limitations of peptide microarrays employing short Aβ fragments, the observed monovalent Aβ-Ab reactivities were further studied using biochemical approaches, complementary in vitro analysis of Aβ-Ab binding to oligomeric and aggregated Aβ, as well as immunohistochemical staining of patient-derived AD brain samples. The data identifies Aβ-Abs that preferentially recognize critical truncation and modification variants as well as gain and loss of binding mutants in familial AD. Our work provides insights into the mode of binding of currently available Aβ-Ab biosimilars and further classifies the immunological tools for detecting and discriminating distinct Aβ truncations, mutational variants and post-transcriptionally modified derivatives. We expect that this comprehensive resource on Aβ-Ab sequence and modification selectivity will not only advance fundamental research on AD but potentially also support the development of improved diagnostic tools and therapeutic strategies.

Introduction

Alzheimer's disease (AD) is a neurodegenerative disorder characterized by the accumulation of amyloid-beta (Aβ) [1, 2] and tau tangles in the brain, leading to cognitive decline and dementia [3]. Aβ peptides are generated under physiological conditions from Amyloid Precursor Protein (APP) by sequential proteolytic cleavages by beta- and gamma-secretase [4]. The initial β-secretase cleavage of APP results in the release of soluble sAPPβ and the generation of a 99 amino acids (AA) long carboxy (C)-terminal APP fragment (C99) with an amino (N)-terminal Asp-residue. Aβ peptides are generated by subsequent gamma-secretase cleavage of C99 [5, 6].

In human cerebrospinal fluid, a conserved pattern of soluble Aβ1-37, Aβ1-38, Aβ1-39, Aβ1-40 and Aβ1-42 has been observed [7]. Aβ peptides isolated from amyloid plaques have been shown to include several variants differing in length, their N- and C-termini, and post-translational modifications (PTMs) [8], such as cyclization of N-terminal Glu(3) or Glu(11) into pyroglutamate (pE) [9], and racemization or isomerization of Asp(1) and Asp(7) [10-13]. Furthermore, phosphorylated forms of Aβ (pSer(8) and pSer(26)) have been reported in amyloid plaques based on studies employing phospho-selective anti-Aβ antibodies (Aβ-Abs), although these findings have not yet been conclusively confirmed by mass spectrometry [14-16]. In extracellular senile plaques in the brain's functional tissue, the parenchyma, Aβ1-42 is more prevalent than Aβ1-40, and various N- and C-terminally truncated [17-20] as well as N-terminally elongated variants [21] have been described [5, 22]. In particular, those starting with a cyclized pE (3) [12] or Phe at position 4 [21, 23], are highly abundant in AD brains [24]. Genetic mutations [25] further multiply Aβ amino acid sequence variability. The study of the structural polymorphisms of the Aβ peptide resulting from PTMs or mutations and the potential impact on the formation of pathophysiological oligomeric forms and fibrillar aggregates is challenging [26-30]. The majority of PTMs occur in the flexible N-terminal region of the fibrils, encompassing residues 1–16, and were proposed to trigger or accelerate the fibrillation of Aβ [31-33]. The same region is also responsible for metal ion coordination which may influence fibril formation [34]. Similarly, several pathogenic APP mutations within Aβ are associated with altered folds, higher aggregation propensities, and toxicities [35-37].

Importantly, this complexity requires molecular tools with appropriate molecular specificity and sensitivity and poses enormous challenges in designing sensitive diagnostic readouts and effective targeted therapies. Passive immunotherapy using monoclonal Aβ-Abs has been investigated extensively as an approach for AD treatment resulting in Aβ-Abs with several

69 different Aβ selectivity profiles [38] [39]. For example, Aducanumab, a recombinant human
70 antibody, was developed after screening human memory B-cells for reactivity towards
71 aggregated Aβ [40, 41]. Bapineuzumab, the humanized form of the murine antibody 3D6 [42]
72 has been reported to bind to both monomeric and aggregated Aβ.
73 Aβ-Abs are the primary means for the detection and targeting of specific Aβ variants within
74 the outlined Aβ-sequence and -modification space. The precise molecular binding epitopes of
75 Aβ-Abs are fundamental to Aβ research. However, the immunogens used to raise and select
76 Aβ-Abs may not represent precise and reliable predictors of the actual sequence and
77 modification requirements. Furthermore, epitope requirements reported by different mapping
78 methodologies may differ and may thus render a comparison difficult. Here we addressed the
79 range and limitations of the sequence and modification specificity by side-by-side comparison
80 in complementary assays for a panel of Aβ-Abs central to AD research and therapy.

81 Results and Discussion

82 The Aβ-Abs investigated in this study are listed in **Table 1**. The panel encompasses biosimilars
83 of the currently FDA-approved drugs (i) Aducanumab (Biogen), initially approved for the
84 treatment of mild cognitive impairment [43] but discontinued in 2024 (ii) Lecanemab (Biogen)
85 [44], which in contrast to Aducanumab, has been approved via regular approval track and (iii)
86 Donanemab (Eli Lilly) as the most recent expansion of the AD-drug arsenal [45, 46]. The set
87 of Aβ-Abs further encompasses selected antibodies directed against specific Aβ variants such
88 as Aβ1-x with a free N-terminal-Asp(1) (3D6, 82E1, 11H3, 80C2), N-truncated Aβ starting
89 with pE(3) (AβpE3-X) (pE3-Aβ, 2-48 and $Donanemab_{bs}$) and phosphorylated Aβ forms
90 (1E4E11, 5H11C10). Furthermore, the panel covers Aβ-Abs against the N-terminal region of
91 Aβ and a central epitope, as well as antibodies selective for N-terminally elongated and
92 truncated Aβ variants.

Antibody[a]	*Source*[b]	*Clonality*[c]	*Origin specie* [d]	*Immunogen*[e]	*Modification Binding*[f]	*Array*[g]	*Refs.*
3D6	Creative Biolabs (#PABL-011)	Mono	Mouse	1-5	-	1-5	[42, 47-49]
pAb77	Dept. of Psychiatry, Göttingen	Poly	Rabbit	2-14	-	3-16	[50]
4G8	Biolegend (#800701)	Mono	Mouse	17-24	-	17-21	[21, 51]
11H3	Nanotools (#bA4N-11H3)	Mono	Mouse	1-x	-	1-4	-
82E1	IBL (#10323)	Mono	Mouse	1-16	-	1-4	[49, 52]
14-2-4	IBL	Mono	Mouse	(−3)-5	-	(-2)-3	[21]
7H3D6	Center of Neurology, Bonn	Mono	Rat	1-14	-	1-10	[53]
1E4E11	Abcam (#ab219817)	Mono	Mouse	p1-14	pSer8	3-8	[53]
5H11C10	Center of Neurology, Bonn	Mono	Mouse	p20-34	pSer26	19-32	[14]
pAb58-1	Dept. of Psychiatry, Göttingen	Poly	Rabbit	4-9	-	4-9	[52]
Aβ-pE3	Synaptic Systems (#218003)	Poly	Rabbit	pGlu3-7	pE3	3-7	[54]
80C2	Synaptic Systems (#218231)	Mono	Mouse	1-5	-	1-5	[49]
2-48	Synaptic Systems (#218011)	Momo	Mouse	pGlu3-7	pE3	3-7	[55]
101-1-1	Dept. of Psychiatry, Göttingen	Mono	Mouse	(−3)-5	-	(-2)-3	[21, 56]
IC16	Dept. of Neuropathology, Düsseldorf	Mono	Mouse	1-16	-	1-8	[57-59]
6E10	Covance (#SIG-39320)	Mono	Mouse	1-16	-	3-8	[51, 56]
1E8	Nanotools (#bA4N-1E8)	Mono	Mouse	1-x	-	3-8	[48]
Aducanumab$_{bs}$	Proteogenix (#PX-TA1335)	Mono	Human	-	-	1-7	[41]
Donanemab$_{bs}$	Proteogenix (#PX-TA1549)	Mono	Humanized	pGlu3-42	pE3	3-10	[60, 61]
Lecanemab$_{bs}$	Proteogenix (#PX-TA1746)	Mono	Humanized	1-42	-	3-7	[62]

Table 1 – Footnotes: (a) names of the anti-amyloid beta antibodies. (b) Source of the antibodies used in this study, either commercial or academic. (c) Clonality of the antibodies: "mono" indicates monoclonal, while "poly" stands for polyclonal antibodies. (d) Species of origin for the IgGs: mouse, rat, human, or rabbit. (e) Immunogens, as reported in the literature, that were used to generate the corresponding antibodies. (f) If available, the anticipated PTM specificity is indicated: “p” represents phosphoserine (at positions Ser8 or Ser26), and “pE3” refers to an N-terminal pyroglutamate (at position 3). (g) epitope identified in this study on microarrays.

101 # Pre-screening of Aβ-Ab Epitopes

102 Information regarding binding epitopes and /or immunogens for most of the tested Aβ-Abs has
103 been published and is summarized in **Table 1**. However, the binding epitope information was
104 derived with varying methodologies. To provide an initial side-by-side comparison we pre-
105 screened all of the listed Aβ-Abs in array format using copies of peptide libraries and standard
106 antibody concentrations of 0.5-1 µg/mL (**Figure 1a)**. The library comprised the amyloid
107 precursor protein (APP770) residues 649-722, corresponding to the canonical Aβ1-42 amino
108 acid sequence with additional 23 amino terminal and 9 carboxy terminal residues. To enable
109 single amino acid resolution, 60 peptides with a length of 15AA and overlapping by 14AA
110 were synthesized and displayed as cellulose-conjugates incapable of oligomerization (**Figure**
111 **1b**). We first focused on Aβ-Abs with known preference for Aβ starting with a free Asp(1) and
112 initially found that 3D6 and 82E1 also detected Aβ(2-x) and several N-terminally elongated
113 Aβ-related peptides in addition to Aβ(1-x), at least under the generic pre-screening conditions
114 with presumably suboptimal Ab concentrations (**Figure 1b**). Thus, it is clear that antibodies
115 must be titrated for each specific application to obtain selectivity and to reduce non-specific
116 binding. Forfor optimal signal to noise ratios and ideal selectivity profiles on the microarrays,
117 the Aβ-Ab concentrations were adjusted for 3D6, 82E1, 11H3, 80C2 and 7H3D6 (**Figure 1 –**
118 **figure- supplement 1**) and (**Appendix 1-7**). This setup allowed to determine the general
119 location of the binding epitopes within the Aβ sequence for all tested Aβ-Abs as shown by the
120 heatmap in (**Figure 1b).** Similarly, Donanemab [60, 61], 1E4E11 [53], and 5H11C10 [14],
121 which have been previously reported as selective for AβpyGlu3, pSer8-Aβ, AβpE3, pSer8Aβ,
122 and pSer26-Aβ, respectively, produced detectable signals in this pre-screening with
123 unmodified Aβ-related peptides. Again, these findings demonstrate the need for further
124 investigation to confirm selectivity under more appropriate assay conditions, i.e. optimized
125 antibody concentrations and presentation of modified Aβ-fragments as binding partners. The
126 side-by-side determined epitopes are summarized together with their immunogen in **Table 1.**
127 Epitope mapping recapitulated previously reported data, but also further confines (pAb77, 4G8,
128 14-2-4, 101-1-1, 6E10, 1E8, 7H3D6, 1E4E11, 5H11C10) or even expands (Aducanumab$_{bs}$) the
129 required residues for binding. However, although this initial microarray only contained
130 unmodified Aβ sequences, we also observed binding for Aβ-Abs known as PTM-selective.
131 (3)pE(3)Specifically, Donanemab$_{bs}$, 2-48 and Aβ-pE3 were raised against AβpE3-x (**Table 1**)
132 and were expected to show preference for Aβ peptides starting with a pE(3). In the pre-
133 screening with unmodified Aβ sequences, however, Donanemab$_{bs}$ detected Aβ(3-x) starting

134 with non-cyclized Glu(3), Aβ(-3-x) as well as several other N-terminally elongated Aβ-related
135 peptides and Aβ1-x. Since the primary binding mode for AβpE3-x had not yet been tested at
136 this stage these initial screening observations remain preliminary. Similarly, 1E4E11 and
137 5H11C10, which were reported to have high selectivity for phosphorylated Aβ peptides at Ser8
138 and Ser26 [14, 53], both displayed strong signals with several non-phosphorylated Aβ variants
139 in the pre-screening. Although the findings with the modification-selective Aβ-Abs are
140 indicative of cross-reactivity due to the presence of epitopes resembling their target and/or the
141 effect of suboptimal binding conditions, the unbiased microarray screening provided valuable
142 initial information regarding the sequence regions and modifications of interest to be
143 investigated in more detail in the course of our study.

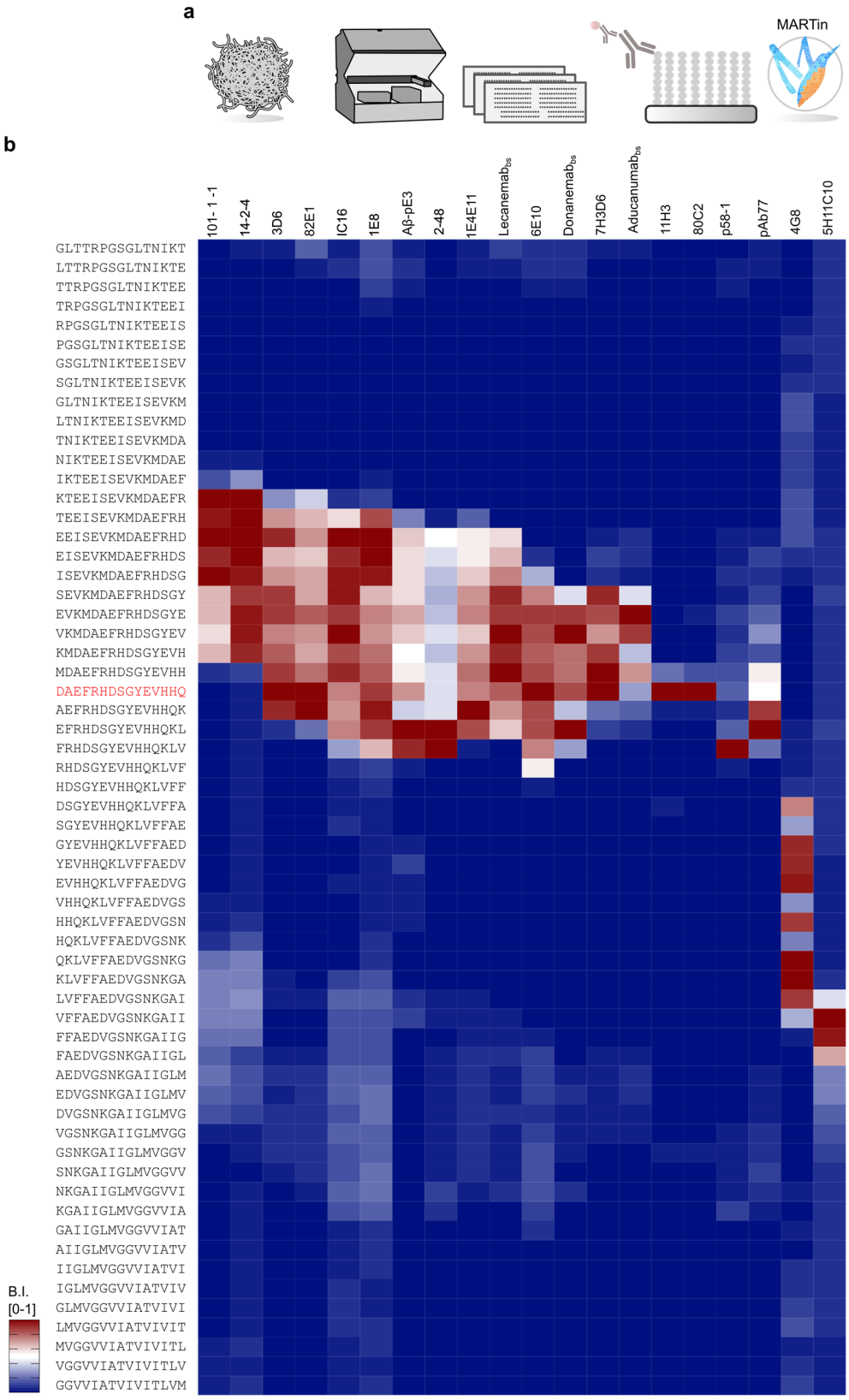

Figure 1 Microarray workflow and Aβ-Ab epitope pre-screening. (a) Schematic of the microarray workflow. The library comprised the amyloid precursor protein (APP) residues 649-722 (APP770 numbering), corresponding to Aβ residues -23 to 51, as a library of 15-mer peptides overlapping by 14AAs, copied in dozens, and probed for Aβ-Abs binding followed by analysis in MARTin. (b). The epitope screening binding data are summarized as a heatmap.

150 The antibody-binding peptides were presented in a semi-quantitative manner. Blue and red
151 shades indicate the relative binding strength of the related arrayed peptides to the left and
152 cognate Aβ-Ab on top. The blue – red scale is visualizing the normalized binding intensity for
153 each antibody individually. The applied antibody concentrations ranged between 0.5-1 µg/mL.
154 Note: Among the 20 tested antibodies, 1E4E11, 5H11C10, 2-48, Aβ-pE3, and $Donanemab_{bs}$
155 have known PTM-selectivity, which could not be fully addressed with the initial microarray
156 consisting of unmodified Aβ fragments only.

157 Titration and Selectivity Assessment of Aβ Abs Directed Against 158 the Aβ N-terminus

159 The sensitivity and selectivity profiles of Aβ-Abs 80C2, 11H3, 3D6, 82E1, which were
160 expected to show preferential binding to Aβ with a free N-terminal Asp(1), and mAb 7H3D6
161 were explored in more detail. The canonical Aβ peptide is typically 40-42 amino acids long. In
162 addition, various N-terminal variants have been reported [49]. Several truncated forms have
163 been detected in brain tissue [21, 24]. Notably, N-terminally truncated Aβ peptides, particularly
164 those starting with Phe at position 4, are abundant in AD brains. The metalloproteinase
165 ADAMTS4, which is expressed in oligodendrocytes, has been linked to APP processing and
166 the generation of Aβ4-X peptides [23] . Additionally, N-terminally elongated Aβ peptides, such
167 as Aβ(-3-X), which can be generated by the same enzyme in cell culture [21], may be of interest
168 in the context of AD biomarker research: Aβ(-3-40) can serve as a reference in a composite
169 blood based biomarker of AD for cerebral Aβ accumulation [63, 64]. Highly sensitive and
170 selective Aβ-Abs for N-terminal Aβ variants are a prerequisite for studying their specific roles
171 in detail. In our microarray experiments, the titration of Aβ-Abs expected to prefer Aβ1-x
172 variants with a free N-terminal Asp (mAbs 80C2, 11H3, 3D6, 82E1) plus the rat monoclonal
173 7H3D6 (Figure 1 Supplement **1**) (**Appendix 1**) broadly classifies the tested mAbs into two
174 groups. One group (80C2 and 11H3) that, on microarray under the tested experimental
175 conditions, displayed exclusive binding towards Aβ1-x over the entire titration range albeit
176 with limited sensitivity. A second group showed high sensitivity but concentration-dependent
177 and limited Aβ1-x selectivity over related Aβ variants under the tested conditions (3D6, 82E1
178 and 7H3D6). Among the 20 tested antibodies, 1E4E11, 5H11C10, 2-48, Aβ-pE3, and
179 $Donanemab_{bs}$ exhibited the previously reported preferences for PTMs, which will be addressed
180 in detail in the following paragraphs.

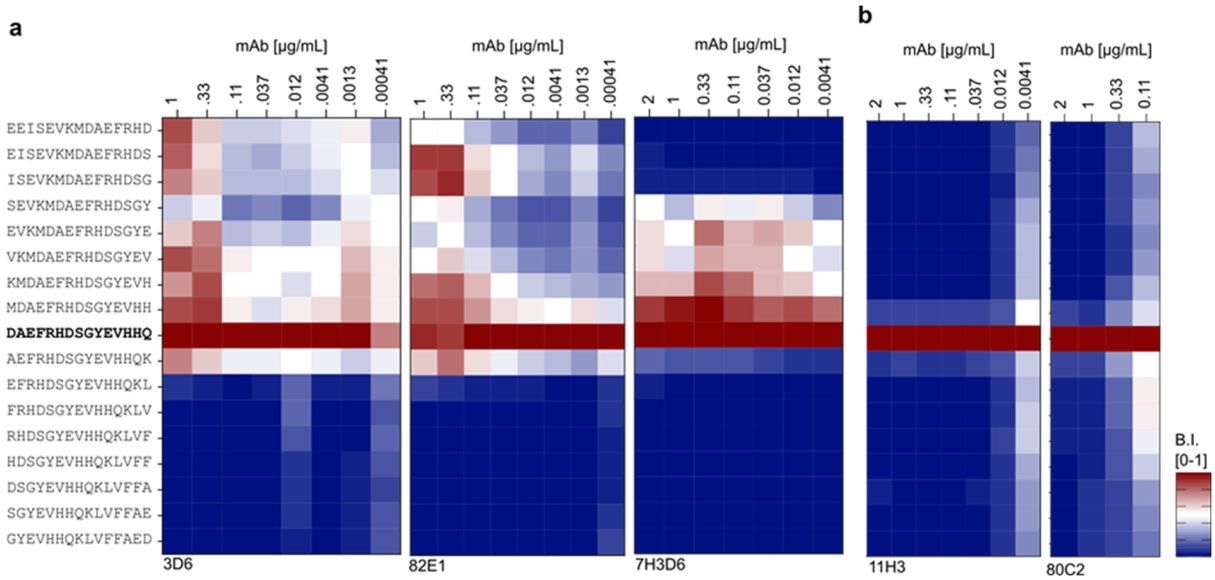

Figure 1 - figure supplement 1. Titration series of N-terminal specific Anti-Aβs (a) Titration of monoclonal Aβ-Ab 3D6, 82E1 and 7H3D6 at concentrations ranging from 2 to 0.00041 µg/mL to study the selectivity for free-Asp(1) over Asp(1) within an N-terminal elongated peptide. The signals were normalized internally and presented as a heat map with blue-to-red shades ranging from 0 to 1 (b) monoclonal Aβ-Ab 11H3D6 and 80C2 exhibited high selectivity towards free-Asp(1) across the chosen concentration range of 2 µg/mL down to 0.0041 µg/mL.

Deep Mutational Scans Provide Information on Aβ-Abs Binding Requirements

Next, we further explored the reactivities observed during the epitope pre-screening (**Figure 1**) and probed in total 14 selected monoclonal antibodies with matched deep mutational libraries. Apart from the biosimilar Abs and the Abs directed against the Aβ N-terminus described above, we also selected three generic Aβ Abs as references (IC16, 1E8, 6E10) and two Abs selective for N-terminally elongated Aβ variants (14-2-4, 101-1-1), the core epitope of which we have described earlier [21]. Display and binding evaluation of all possible point-mutants systematically resolved the sequence requirements for these 14 Aβ-Abs towards the binding region corresponding to the Aβ(-10-18) amino acid sequence (**Figure 2A - figure supplement 1**) in three different 18-meric positional scans. Peptides covering Aβ(-10-8) **(Figure 2b)**, Aβ(-3-15) **(Figure 2c)** and Aβ1-18 **(Figure 2d)** regions were generated. As these three peptide regions showed binding to most of the N-terminal antibodies (**Figure 1**), we postulated that these 18-mers should cover the main antigen-antibody (Ag/Ab) contact regions. The three Aβ-related wild-type sequences were sequentially scanned from N-terminus to C-terminus by replacing each position by every proteinogenic amino acid (342 different peptide

205 sequences in total). A customized criterion was utilized to identify the core motif for each
206 monoclonal antibody tested. While the identified core motifs are essential for binding, they
207 may not fully represent the specificity of the antibodies but rather indicate where the majority
208 of the Ag/Ab contact takes place. Specifically, the raw mean intensities for all peptide variants
209 were measured and normalized against the corresponding wildtype sequence. Amino acid
210 exchanges that reduced binding by >50% were designated as dominant negative. This process
211 was reiterated for each exchange at that position. Positions were considered as major
212 contributor to the core motif when more than 50% of the exchanges were marked as dominant
213 negative. The resulting core motifs are summarized in **Figure 2 – figure supplement 1D**. The
214 findings highlight both similarities and differences in the binding mode of different Aβ-Abs,
215 affirming binding to epitopes located in the N-terminal region of the Aβ sequence. Overall, this
216 comprehensive binding data provides guidance for sorting monoclonal Aβ-Abs based on
217 epitope properties. For two of the tested antibodies, namely 3D6 and Aducanumab, crystal
218 structures are publicly available [41] [42], and indicate binding in the regions Aβ1-5 (3D6) and
219 3-7 (Aducanumab), respectively. Here, the microarray results recapitulated the epitope of 3D6
220 (murine precursor of Bapineuzumab) and expanded the binding interface for Aducanumab$_{bs}$
221 binding to monomeric short Aβ fragments by two residues, namely Asp(1) and Ala(2) (**Figure
222 2D, Figure 2 - figure supplement 1A, B**). Donanemab is known to recognize Aβ starting with
223 cyclized pE3 [60, 61], however, on our initial microarray screen, Donanemab$_{bs}$ showed clear
224 signals with AβpE3-x and several other Aβ related peptides starting N-terminally of Glu(3),
225 including Aβ1-x (**Figure 1**). To further explore this unexpected observation, Donanemab$_{bs}$ was
226 tested on the Aβ (1-18) deep mutational scan. Consistent with its expected preference for the
227 Aβ3-x region, the primary Ag/Ab contacts for the binding to Aβ1-18 involved the amino acids
228 *EFRHDSGY*. Asp(1) and Ala(2) were not highly conserved. Importantly, the murine precursor
229 antibody mE8 from which Donanemab was derived was previously shown to have a very strong
230 preference for truncated AβpE3(starting with pyroglutamate) [61]. This particular point is
231 further addressed in detail in the paragraph "Modification selectivity of monoclonal Aβ-Abs
232 mAbs" (see below). The monoclonal Ab 1E4E11, which was previously reported to be highly
233 selective for phosphorylated pSer(8)-Aβ [53], bound to unphosphorylated Aβ2-16 and several
234 other unphosphorylated Aβ-related peptides on the initial screen (**Figure 1**). Interestingly, the
235 profiling of Ser(8) did not show elevated binding to the phospho-mimetic exchanges (Asp or
236 Glu) (Figure 2D). The effect of phosphorylation at Ser(8) is also addressed in detail in the
237 paragraph "Modification selectivity of monoclonal Aβ-Abs" mAbs(see below). As shown in

238 (**Figure 2 - supplement 2D**), several Aβ-Ab exhibited altered binding strength with exchanges
239 R5G or Y10F which may be valuable information when studying the co-aggregation dynamics
240 between exogenous (human) and endogenous (mouse) Aβ in transgenic models.

241 The data set presents the sequence requirements of 14 Aβ-Abs for binding to 18-mer Aβ-related
242 peptides in a microarray setup, thereby complementing previous structural insights and further
243 improving our understanding of their molecular mode of action.

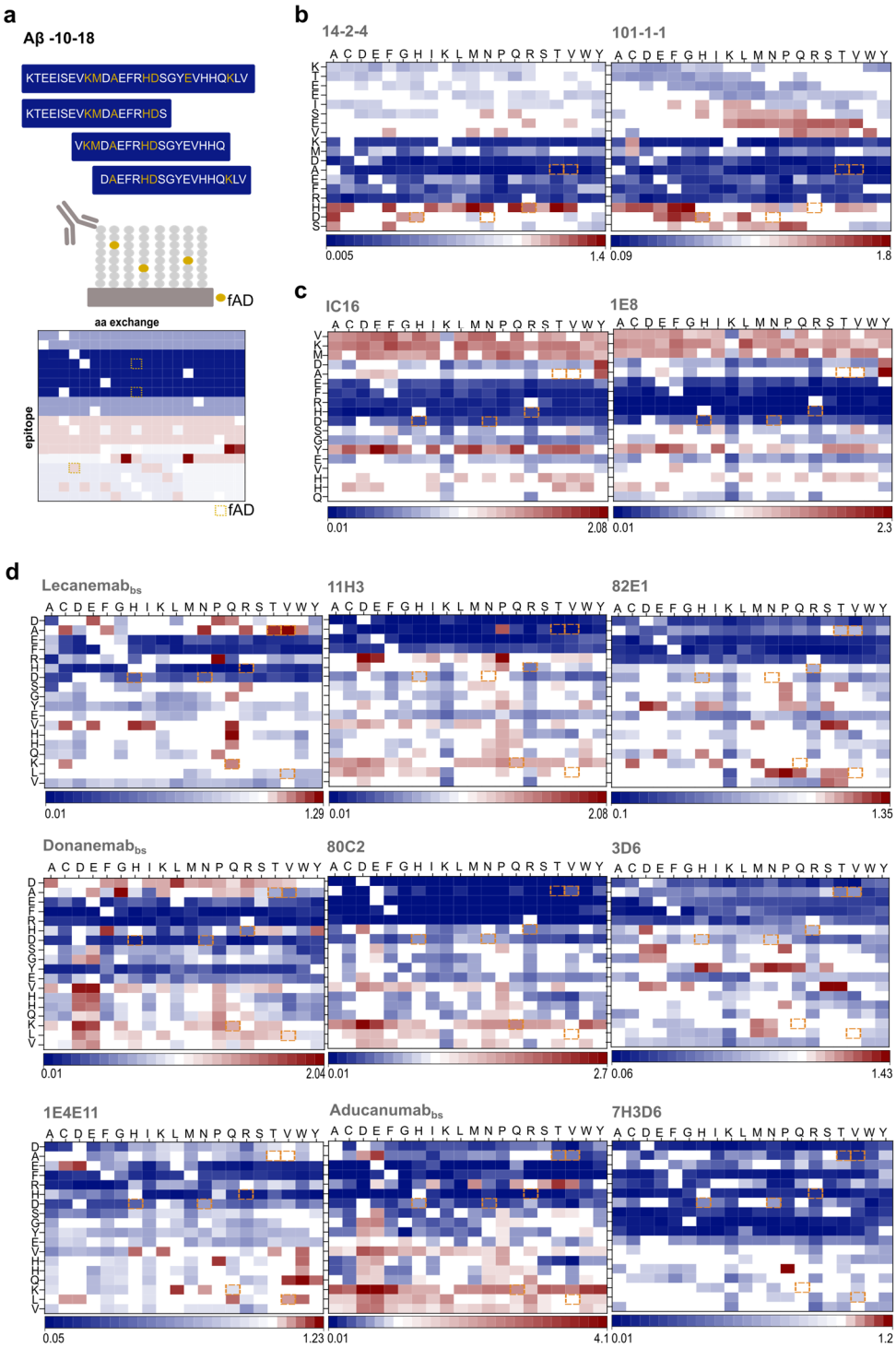

244

245 **Figure 2- Deep Mutational Scans Define Aβ-Ab Core Sequences** (a) Schematic summary
246 of the three deep positional scans in the N-terminal region. Seven reported APP mutations are
247 indicated as yellow boxes. From each 18-mer epitope, positional substitutions were generated
248 (342 variants for each epitope) and tested semi-quantitatively in microarray format. The wild-
249 type sequence was sequentially scanned from N to C terminal by turning each position into
250 every proteinogenic amino acid. Consequently, the contribution of each residue is depicted in
251 blue-white-red shades, with white corresponding to no variation from wt [1] and blue-to-red
252 representing loss or gain of binding strength. (b) Fingerprint analysis for the first peptide group
253 covering the sequence *KTEEISEVKMDAEFRHDS*. The Aβ-Abs tested here are *101-1-1* and
254 *14-2-4* (c) Fingerprint analysis for the second peptide group covering the sequence
255 *VKMDAEFRHDSGYEVHHQ*. The Aβ-Abs tested here are IC16 and 1E8 (d) Fingerprint
256 analysis for the third peptide group covering the sequence *DAEFRHDSGYEVHHQKLV*. The
257 Aβ-Abs tested here are Aducanumab, Donanemab and Lecanemab biosimilars. In addition,
258 commercially available Aβ-Abs such as 3D6, 82E1, 11H3, 80C2, 7H3D6 and 1E4E11 were
259 included. Note: The antibodies, 1E4E11 and Donanemab$_{bs}$ have known reported PTM-
260 preference which will be addressed in the next paragraphs.

261 Hereditary APP Mutations Affect Antibody Binding

262 Next, we studied the impact of some reported hereditary mutations in the *APP* gene resulting
263 in amino acid exchanges within the Aβ sequence [25]. Specific familiar *APP* gene mutations
264 [25, 65] are reported to either lead to aggressive forms of AD or to exert a protective effect.
265 Several mutations in the Aβ peptide have been reported to cause familial AD (fAD), with all
266 but two having a dominant pattern of inheritance [65, 66]. These alterations can lead to
267 enhanced aggregation and increased cytotoxicity, contributing to the onset and progression of
268 early-onset AD. The following APP mutations within the Aβ amino acid sequence were
269 included in the microarray screen: D7H [67], D7N [68], H6R [69], A2V[70], A2T [71, 72],
270 K16Q [73, 74], L17V [75].

271 Our analysis indicates that genetic mutations causing amino acid exchanges in or close to the
272 Aβ sequence can affect antibody binding. Regarding the biosimilar antibodies Lecanemab$_{bs}$,
273 Donanemab$_{bs}$ and Aducanumab$_{bs}$, this may potentially have relevance for rare fAD and their
274 therapeutic implications. The APP mutants D7H/7N, H6R and A2T/V, K16Q and L17VL17V
275 are highlighted in the deep mutational scan data (**Figure 2** and **Figure 2 - Supplement 1**), as
276 they were identified within the core motifs of the Aβ-Abs. The mutations A2V, D7H, D7N,
277 and H6R can lead to an increased aggregation propensity of Aβ and contribute to early onset
278 fAD [76]. Specifically, D7H (Taiwan), D7N (Tottori), and H6R (English) mutations may alter
279 the structural features and thermodynamics of Aβ42, leading to increased β-sheet [77] content
280 For confirmation and for highlighting the importance of considering genetic variability to
281 therapeutic responses, we next paradigmatically explored the effects of the D7H, D7N, H6R,

A2V and A2T APP mutations [69] on Aducanumab$_{bs}$ binding to short monomeric Aβ-related peptides on microarray.

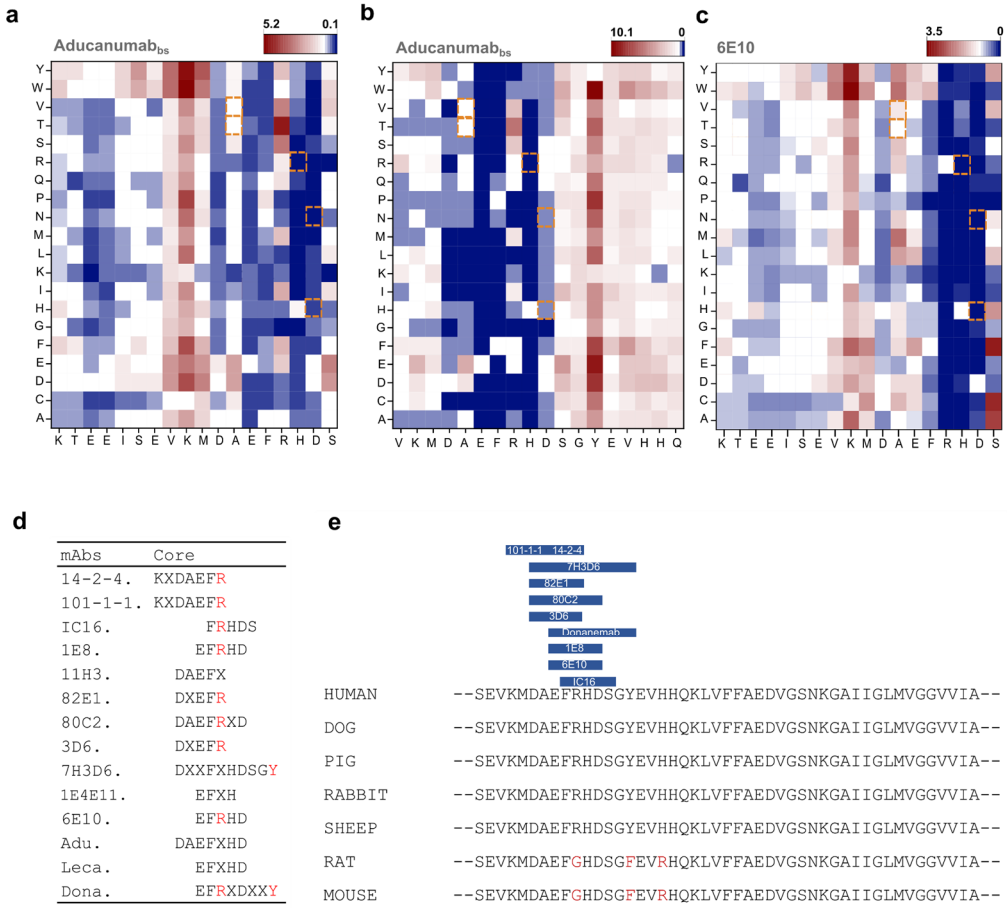

Figure 2 - figure supplement 1. N-terminally elongated Deep Mutational Scans of Aducanumab$_{bs}$ and 6E10 with core motifs summary (a) Fingerprint analysis for the first peptide group covering the sequence *KTEEISEVKMDAEFRHDS*. The Aβ-Ab tested here is Aducanumab$_{bs}$ (b) Fingerprint analysis for the second peptide group covering the sequence *VKMDAEFRHDSGYEVHHQ*. The Aβ-Ab tested here is Aducanumab$_{bs}$ (c) Fingerprint analysis of 6E10 on the sequence *KTEEISEVKMDAEFRHDS*. (d) Summary of the antibody core motifs, "X" within the sequence stands for non-conserved residue. When an amino acid variation led to a decrease below 50% wt it was marked as dominant negative. If more than 10 amino acid substitutions were dominant negative, the entire position was designated as part of the core motif (represented in single-letter coding). (e) Aβ-Ab species preferences. In red, amino acid positions which are different in rat and mouse are highlighted. These specific positions were probed. Antibodies showing altered binding strength after replacing R5 or Y10 in the human Aβ sequence by G5 or F10 (rat/mouse Aβ sequence) are highlighted in blue. Human: Homo Sapiens; Dog: Canis Lupus Familiaris; Pig: Sus Scrofa; Rabbit: Oryctolagus Cuniculus; Sheep: Ovis Aries; Rat: Rattus Norvegicus; Mouse: Mus Musculus.

The Mutation H6R Abolishes Aducanumab Binding

Consistently across the two deep positional scans, Aducanumab$_{bs}$ and 6E10 showed significantly reduced binding intensity to 18-mer peptides on the array in case of the fAD H6R mutation [69]. This aligns closely with previous findings [51], which identified *RXD* as the minimal sequence required for 6E10 binding via phage mapping (present in 53% of immunoprecipitated sequences). Our data indicate that 6E10 exhibits binding to a broader motif, *EFRHD* and shows that H6 is necessary for binding. To confirm our findings and underscore the potential significance of genetic variability in possible therapeutic strategies, we subsequently measured the binding affinity of Aducanumab$_{bs}$ to Aβ1-15 H6R [69]. First, we spotted the corresponding purified peptides *DAEFRHDSGYEVHHQ* and *DAEFRRDSGYEVHHQ* (**Figure 2 - supplement 2a**) (**Appendix 8**) at 2-fold dilutions. The semi-quantitative on chip titration confirmed a reduced binding strength of Aducanumab$_{bs}$ for the H6R Aβ1-15 variant. For complete quantification including kinetic evaluation, we next conducted Biolayer Interferometry (BLI) experiments (**Figure 2 – supplement 2b**). The BLI response of Aducanumab$_{bs}$ for the H6R was completely abolished when compared with the wildtype sequence. These data confirm the array profiling and, in broader context, highlight a possible gap in efficacy for monoclonal Aβ-Abs in individuals with certain rare hereditary mutations associated with AD, which may have implications for personalized treatment approaches. However, whether or not the H6R amino acid replacement could impact also the binding of Aducanumab$_{bs}$ to aggregated Aβ is still unclear.

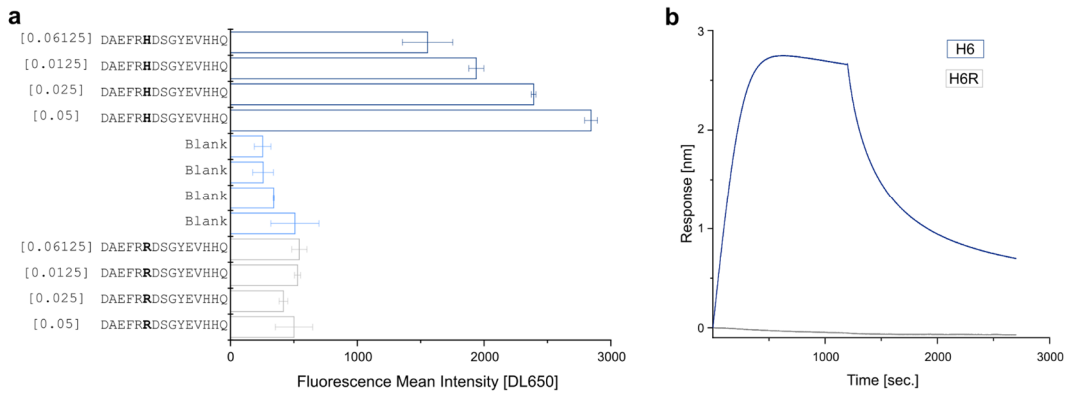

Figure 2 - Supplement 2 Aβ1-15 carrying the English mutation (H6R) shows reduced affinity for Aducanumab$_{bs}$ (a) Dot Blot from the purified 6xHis peptides *DAEFR**H**DSGYEVHHQ* and *DAEFR**R**DSGYEVHHQ* was printed using Slide Spotter robot. IgG signals were detected using Goat anti-human DL650, in square brackets the µg/mL of Aducanumab$_{bs}$ (b) The Biolayer interferometry responses of Aducanumab$_{bs}$ (10nM) over the NTA-loaded *DAEFR**H**DSGYEVHHQ* and *DAEFR**R**DSGYEVHHQ* peptides are shown.

327 ## Modification Selectivity of Monoclonal Aβ-Abs MAbs

328 PTMs of Aβ can significantly impact aggregation propensity [31], clearance mechanisms, and
329 toxicity in AD. Specific PTMs might be associated with different stages of AD progression and
330 severity, offering potential biomarkers for diagnosis and prognosis. Targeting PTMs represents
331 a potential therapeutic strategy to prevent Aβ aggregation and neurotoxicity, thereby slowing
332 disease progression. *In vitro*, Aβ cyclization of N-terminal Glu into pE, and
333 racemization/isomerization of Asp were shown to increase the aggregation propensity and
334 neurotoxicity [12, 78]. Therefore, a selected group of PTM-carrying Aβ peptides (PTM-Aβ)
335 were incorporated to the Aβ chip to explore the potential binding preference of selected Aβ-
336 Abs, under optimized concentrations (**Figure 3**). The antibodies were tested with both PTM-
337 Aβ and the corresponding unmodified variants to provide a head-to-head comparison. This
338 screening was performed in the presence of phosphorylated Aβ at positions Ser(8) or Ser(26),
339 N-terminal pE at position 3, racemization/isomerization of Asp at position 1, and unmodified
340 N-terminal variants. The dataset is divided into sections (**Figure 3 a-f**) for enhanced
341 visualization, where each antibody was screened simultaneously against all peptides to locate
342 their epitope preferences. Post-hoc mass spectrometry (MS) analysis validated the correct
343 display of the PTM variants included in the microarray (**Appendix 1-6**). A set of antibodies
344 without reported PTM preference was applied here as controls (**refer to Table 1**), namely
345 11H3, 101-1-1, IC16, 82E1 and 3D6. Antibody 6E10 has been previously shown to be unable
346 to detect Aβ-pSer(8) and was included as a control antibody [79]. On the microarray and under
347 the tested experimental conditions, Aducanumab$_{bs}$ and 1E4E11 (**Appendix 10**) showed
348 preference for Aβ peptide fragments phosphorylated at Ser(8) (pSer(8)). Donanemab$_{bs}$, 2-48,
349 and pE-Aβ exhibited high selectivity for Aβ peptides starting with an N-terminal pE (**Figure**
350 **3D**) over Aβ3-x starting with a non-cyclized Glu and other Aβ variants. In contrast, mAb IC16
351 showed weaker binding to AβpE3-x than to Aβ3-x. MAbs 7H3D6 and 11H3 did not recognize
352 Iso-Asp(1), while 11H3 interestingly showed no affinity for D-Asp(1)-modified Aβ peptides.
353 As expected, all of the tested antibodies, which are directed against the N-terminal Aβ region,
354 did not show appreciable binding, and only 5H11C10 bound to the phosphorylated Ser(26)
355 within Aβ19-32 to mid-region peptides (**Figure 3E**),

356

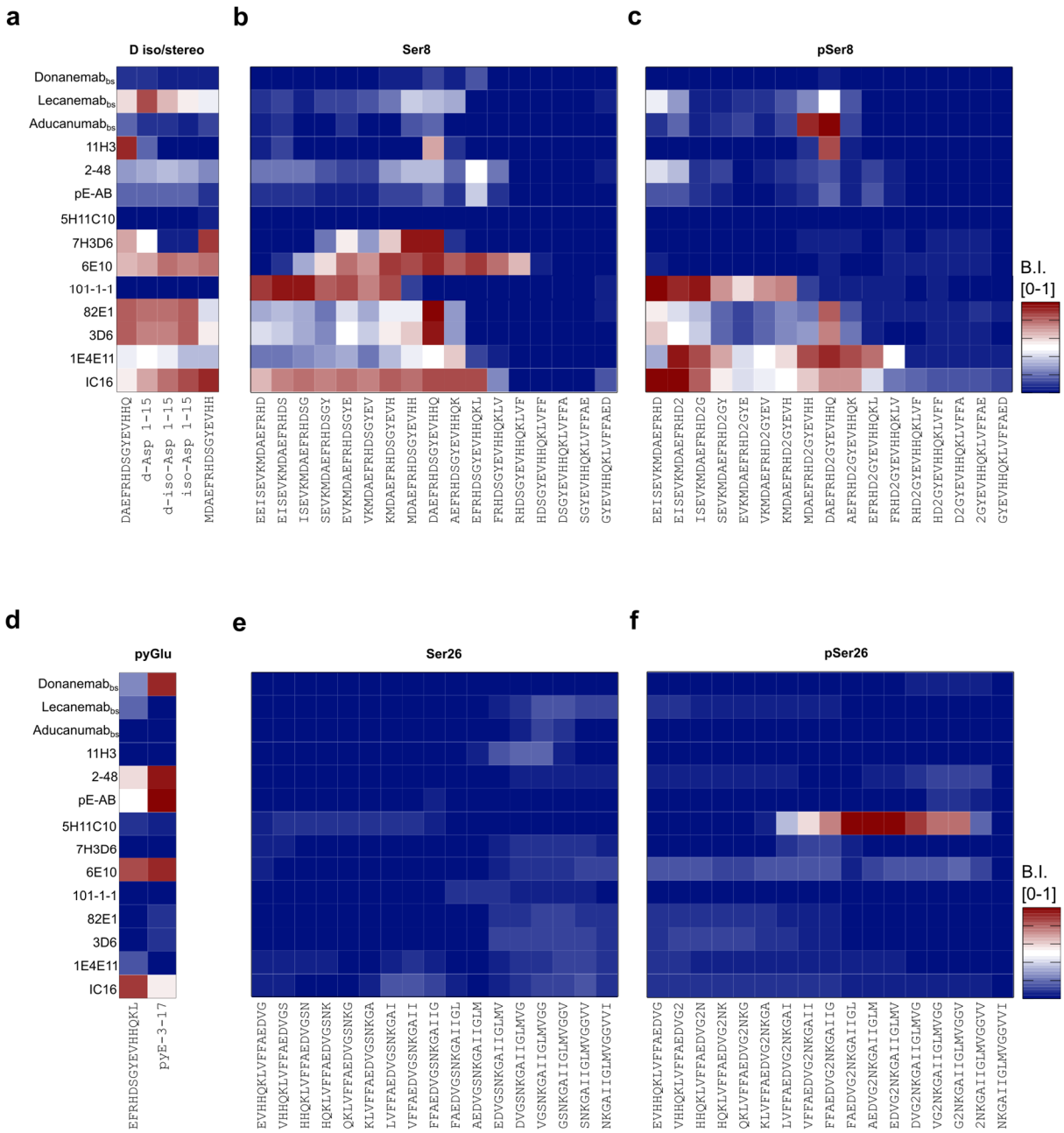

Figure 3 – Multiplex Analysis of Aβ-Abs with preference for post-transcriptionally Modified Abeta variants

The signals were normalized internally and presented as a heat map ranging from 0 to 1. Blue and red shades indicate the binding strength over the related arrayed post-transcriptionally modified peptide shown on top and cognate anti-Aβ antibody to the left. The antibodies were tested under optimal dilutions: 6E10, IC16, pEAB, 1E411, 101-1-1, 5H11C10, 2-48 at 0.25µg/mL; Lecanemab$_{bs}$, Donanemab$_{bs}$ at 0,0012µg/mL; Aducanumab$_{bs}$ at 0.02µg/mL; 3D6, 11H3, 82E1 at 0.037 µg/mL; 7H3D6 at 0.012µg/mL. The dataset is split over different sections (a-f) to allow proper visualization. Each antibody was screened in parallel against all modifications. (a) The control peptide Aβ(-1-14) was used alongside Asp(1) isomers and stereoisomers. (b) The region overlapping with unmodified Serine 8. (c) the region overlapping with modified phospho Serine 8 (represented as '2') , (d) the control unmodified 3-17 was used

370 alongside pE3. (e) The region overlapping with unmodified Serine 26 (f) region overlapping
371 with modified phospho Serine 26 (represented as '2').

372 A pSer8-Preference of Aducanumab$_{bs}$?

373 Aducanumab has been reported to preferentially target aggregated Aβ [40] and bind
374 monomeric Aβ with low micromolar affinity [41], tetrameric Aβ1-15 with low nanomolar
375 affinity and aggregated Aβ with sub-nanomolar affinity corresponding to a roughly 10.000-
376 fold enhanced affinity for Aβ aggregates [40, 41]. However, in our hands, on microarray and
377 under the tested experimental conditions, we observed appreciable binding of Aducanumab$_{bs}$
378 to short, monomeric Aβ-related peptides (**Figures 1, 2, 3**), which we followed up by studying
379 some molecular details. Prompted by the observed preference of Aducanumab$_{bs}$ for
380 phosphorylated pSer8-Aβ(−(-1-14) and pSer8-Aβ1-15 over unphosphorylated Aβ-related 15-
381 mers on our microarrays (**Figure 3, Figure 3 - supplement 2A**), we sought to quantify the
382 underlying relative affinity differences using the purified epitope variants in BLI as a proof-of-
383 concept experiment with the caveat that the assay may affect the absolute affinity due to
384 multivalency and high-density effects. As a reference, mAb 1E4E11 was titrated over the
385 immobilized phosphorylated Aβ variant (**Supplementary Figure 3A S2 - top**) (**Appendix 9**).
386 As expected, mAb 1E4E11 showed a strong response in the nanomolar affinity range with fast
387 on rates and very slow off rates, resulting in a K_D of 4.1nM (**Figure 3A S2 – bottom).** In
388 contrast, the overall response was at least within an order of magnitude lower with the
389 unphosphorylated peptide **(Figure 4BS2 – top)** and showed fast off rates, resulting in a
390 quantified K_D of only 1.3μM for mAb1E4E11 binding **(Figure 4BS2 – bottom**). Overall, mAb
391 1E4E11 showed a 300-fold preference for the phosphorylated Aβ variant in this assay.

392 Henceforth, we applied this methodology to Aducanumab$_{bs}$ (**Figure 3 - supplement 2**) and
393 observed a preference for monomeric Aβ1-15 phosphorylated at Ser(8) over unphosphorylated
394 Aβ1-15. Initially, both modified and unmodified Aβ1-15 peptides were loaded onto the BLI
395 sensors and tested with different antibody concentrations. The affinity for the phosphorylated
396 variant was at least 6 times higher than for the unmodified peptide, however, on microarray,
397 the EC50 for the pSer8-Aβ1-15 was 300 times lower than that for the corresponding
398 unphosphorylated peptide (**Appendix 10**). Importantly, this was only detectable on semi-
399 quantitative array analysis, which can be explained by multivalency effects that may lower the
400 observed antibody off-rate. Overall, the affinity quantification in BLI did not result in a large
401 difference between the two variants and we thus concluded that Aducanumab$_{bs}$ has agnostic

402 preference for a negative charge, either provided by a carboxylic (Asp or Glu – see **Figure 2**)
403 or phosphoserine group (**Figure 3 – Supplement 2**), as it was not selective for the latter. This
404 is in strong opposition to the state-of art pSer(8) antibody 1E4E11, which did not recognize
405 phoshomimetic amino acid exchanges such as aspartate or glutamate (**Figure 2**). This
406 observation raised the question of whether Aducanumab$_{bs}$ is involved in electrostatic
407 interaction.

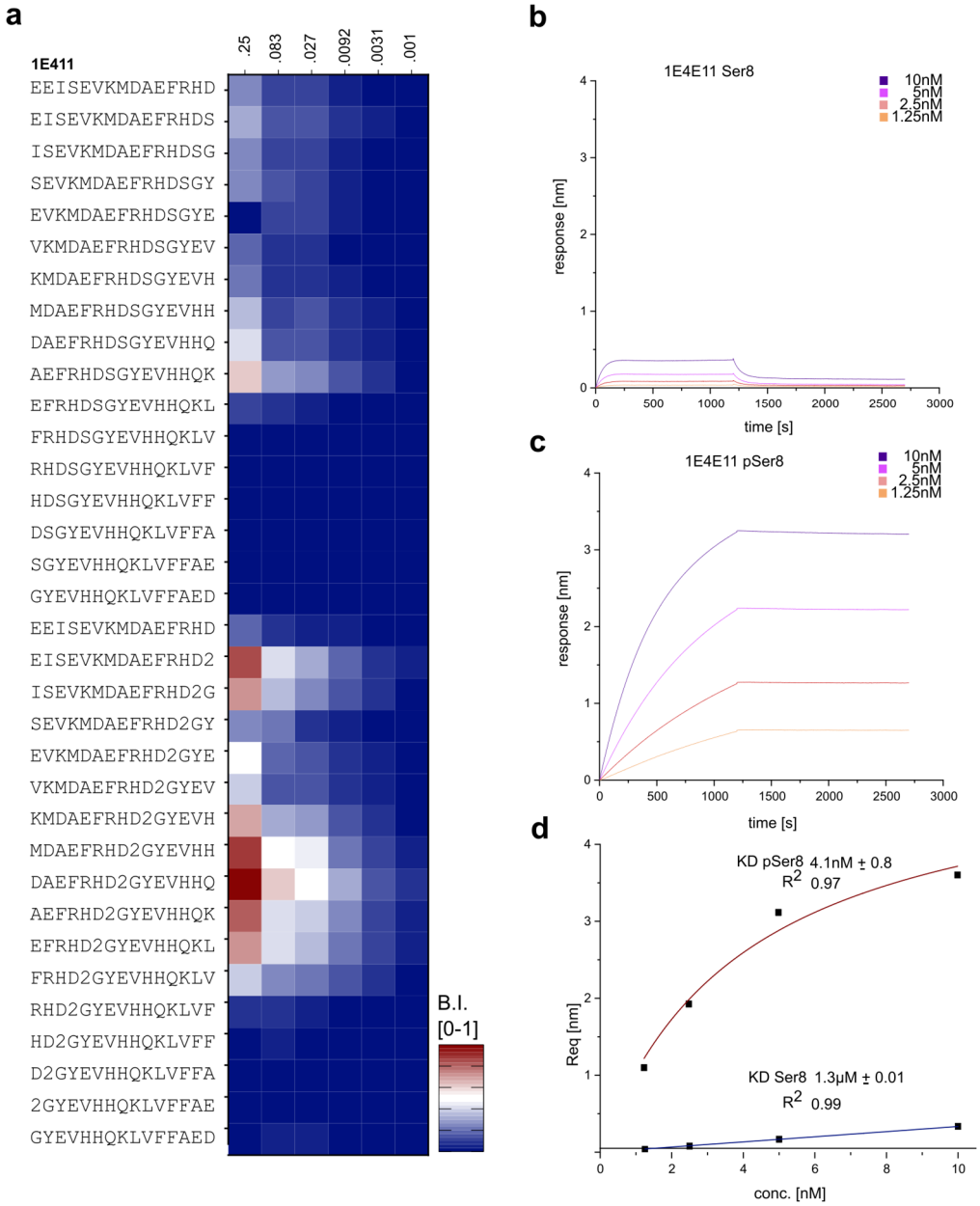

408

409 **Figure 3 – figure supplement 1 – Antibody 1E4E11 shows high preference for**
410 **phosphorylated pSer8 Aβ1-15 in μSPOT and BLI assays.** (a) presents the titration of
411 monoclonal Aβ-Ab 1E4E11 at concentrations ranging from 0.25 to 0.001 μg/mL to achieve
412 high selectivity for Aβ1-15 phosphorylated at Ser(8). The modified pSer is represented as '2'.
413 The signals were globally normalized against *DAEFRHDpSGYEVHHQ* and presented as a heat

map with blue-to-red shades ranging from 0 to 1. (b) The Biolayer interferometry dose-response curve of mAb 1E4E11 binding to the NTA-loaded *DAEFRHDSGYEVHHQ-6xHis-amide* peptide is shown. (c) The Biolayer interferometry dose-response curve of mAb 1E4E11 binding to the NTA-loaded *DAEFRHDpSGYEVHHQ-6xHis-amide* peptide is shown. (d) BLI steady-state analysis revealed K_Ds of 4.1nM and 1.3µM for Aβ1-15 with phosphorylated and unphosphorylated Ser (8), respectively (1:1 model).

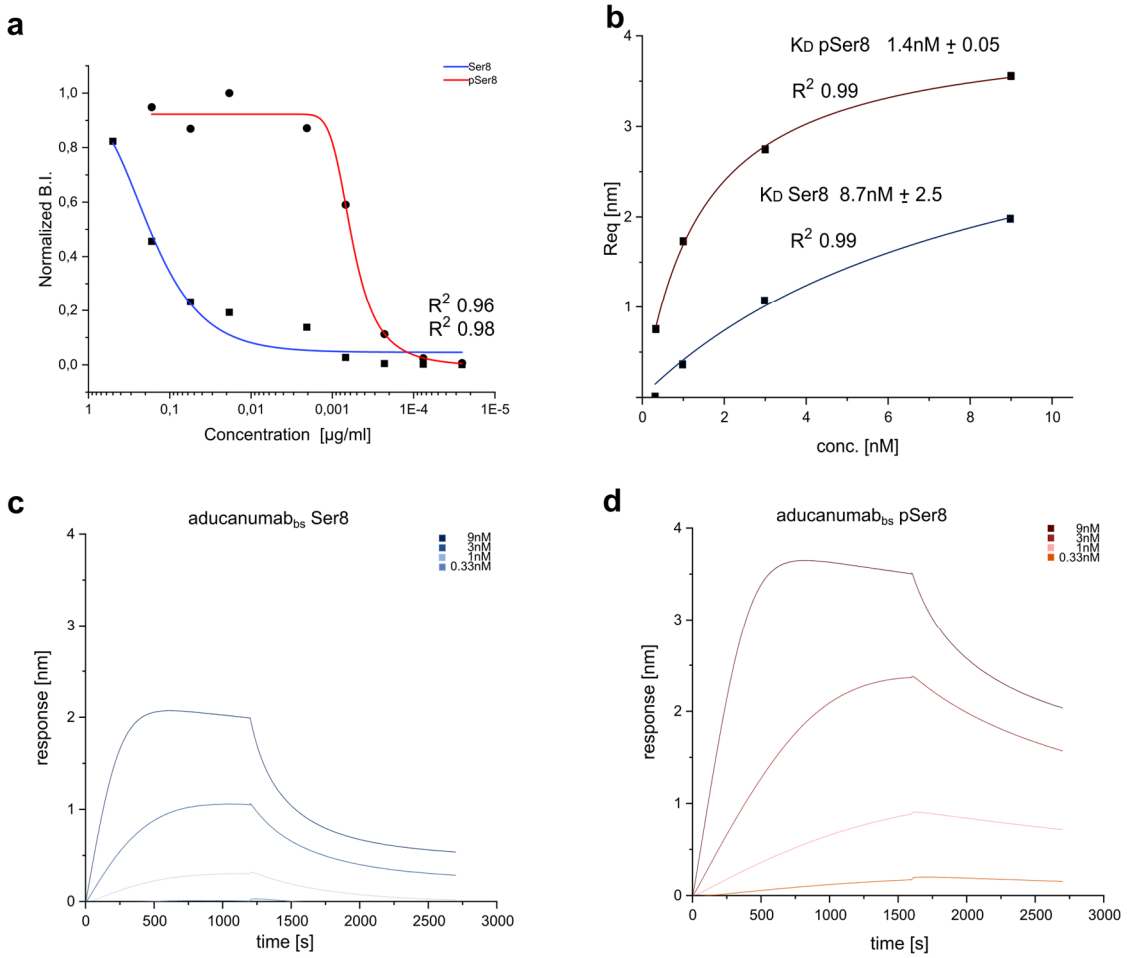

Figure 3 – figure supplement 2 Phosphorylation aids Aducanumab$_{bs}$ binding to synthetic monomeric Aβ1-15. (a) shows the titration of Aducanumab$_{bs}$ at different concentrations to achieve high selectivity for phosphorylated pSer8-Aβ1-15 over unphosphorylated Aβ1-15. The signals were internally normalized and fitted as a sigmoidal curve (Boltzmann). The phospho signal for pSer8-Aβ1-15 is shown in red (r^2 0.98) and the signal for unphosphorylated Aβ1-15 is shown in blue (r^2 0.96). (b) BLI steady-state analysis revealed KDs of 1.4nM and 8.7nM for phosphorylated and unphosphorylated Aβ1-15, respectively (1:1 model) (c) The Biolayer interferometry dose-response curve of Aducanumab binding to the NTA-loaded *DAEFRHDSGYEVHHQ-6xHis-amide* peptide is shown. (d) The Biolayer interferometry dose-response curve of Aducanumab binding to the NTA-loaded *DAEFRHDpSGYEVHHQ-6xHis-amide* peptide is shown.

To further explore the relevance of the observed interaction between Aducanumab$_{bs}$ and the N-terminal phosphorylated Aβ fragment, we conducted molecular dynamics (MD) simulations (**Figure 3 - supplement 3**) using the published crystal structure of Aβ2-7 and Aducanumab

435 Fab complex (PDB: 6CO3). These simulations were performed using Molecular Operating
436 Environment (MOE) software. Specifically, we investigated two different short Aβ peptide
437 sequences, *AEFRHDS* and *AEFRHDpS*, to examine how phosphorylation at Ser(8) affects the
438 binding stability of the antibody-antigen complex.

439 By assuming that fewer fluctuations in the system correlate with a higher affinity, these data
440 provide insights into the preferential binding mode of Aducanumab to phosphorylated short N-
441 terminal Aβ fragments. By assuming that fewer fluctuations in the system lead to higher
442 affinity, the root mean square deviation (RMSD) diagrams indicate greater stability (average
443 conformation over 600ns) for the phosphorylated peptide due to its reduced fluctuations
444 (**Figure 3 - supplement 3**). Additionally, the phospho group enhances the interaction with
445 extra hydrogen bonds compared to the unmodified peptide (**Figure 3 - supplement 3**).
446 Conversely, the non-phosphorylated peptide exhibits more fluctuations (**Figure 3 -**
447 **supplement 3**). Thus, under these conditions, the MD simulation results confirm the findings
448 from the microarray and BLI analyses.

449

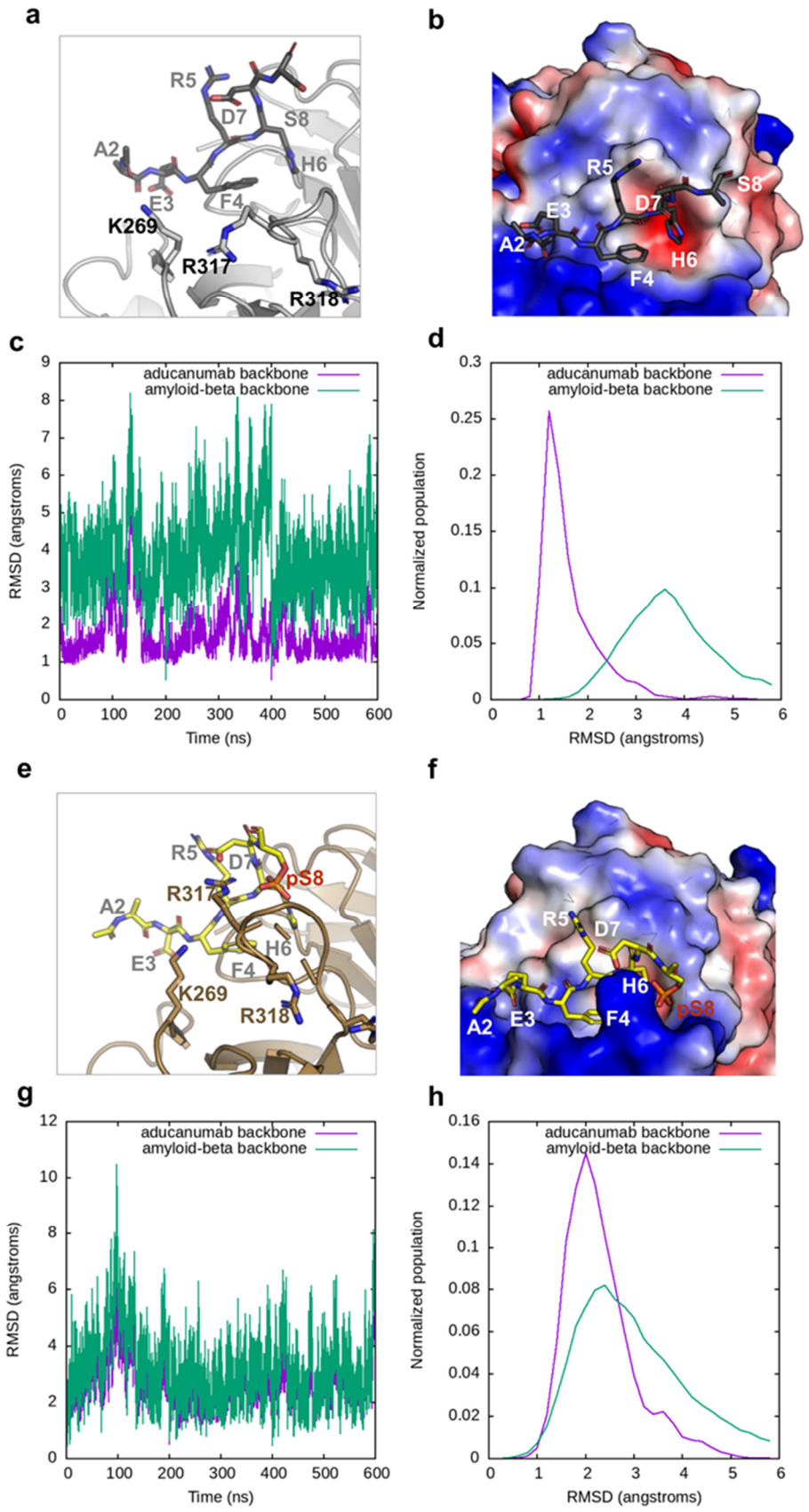
a
R5
D7
S8
A2
H6
E3
F4
K269
R317
R318
b
R5
S8
D7
E3
A2
H6
F4
c
aducanumab backbone
amyloid-beta backbone
RMSD (angstroms)
Time (ns)
d
aducanumab backbone
amyloid-beta backbone
Normalized population
RMSD (angstroms)
e
R5
D7
pS8
R317
A2
H6
E3
F4
K269
R318
f
R5
D7
H6
pS8
A2
E3
F4
g
aducanumab backbone
amyloid-beta backbone
RMSD (angstroms)
Time (ns)
h
aducanumab backbone
amyloid-beta backbone
Normalized population
RMSD (angstroms)

450

Figure 3 – figure supplement 3 - MD simulation of Aducanumab with pSer(8)-Aβ2-8 (a) sticks and cartoon depiction of the MD simulations between Aducanumab and AEFRHDS **(b)** electrostatic density for the non phosphorylated sequence interaction **(c-d)** RMSD analysis of the backbone atoms of the unphosphorylated candidate (average conformation over 600ns) **(e)** sticks and cartoon depiction of the MD simulations between Aducanumab and AEFRHDpS **(f)** electrostatic density for the pSer8 sequence interaction **(g-h)** RMSD analysis of the backbone atoms of the PTM candidate (average conformation over 600ns)

Taken together, the MD simulations rationalize the unexpected preference of $Aducanumab_{bs}$ towards monovalent pSer8Aβ1-15 we observed on microarray. The observation underscores the complexity of $Aducanumab_{bs}$ binding to Aβ. This is further substantiated by comparing the previously resolved structure [41] with the MD simulation for short non-phosphorylated and pSer(8) Aβ-related peptides. Here, pSer8-Aβ2-8, unlike the corresponding non-phosphorylated Aβ, replicates the structurally determined binding mode. In the MD simulation, using the resolved epitope peptide EFRHDpS allows for the binding mode that has R317 and R318 contributing to the paratope. Similarly, the crystal structure (PDB 6CO3) includes a sulfate ion [41] that neutralizes the positive charges of R317 and R318 (**Figure 3 – supplement 4**). In summary, the monomeric binding mode benefits from the neutralization of a positive patch on Aducanumab Fab, which likely explains the phospho-preference.

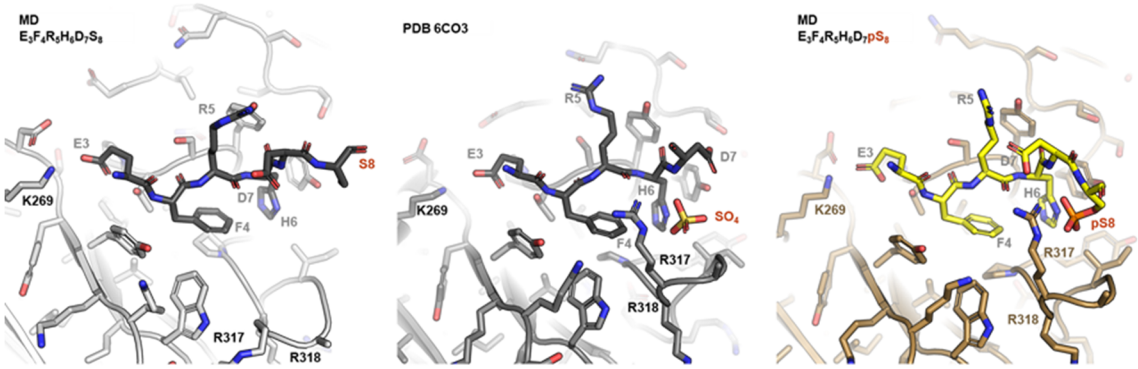

Figure 3 – supplement 4 – pSer8 but not Ser8-Aβ recapitulate the X-Ray resolved binding mode. Comparison of MD simulations with the structural data. The MD simulation was conducted with the resolved epitope peptide *EFRHDS,* but no additional ions predict a largely altered binding mode characterized by over 10 Å movements of R317 and R318. In contrast, the crystal structure (PDB 6CO3) harbors a sulfate ion that neutralizes the positive charge introduced by R317 and R318. Strikingly the MD of the pSer(8) modified peptide recapitulates the resolved X-ray binding mode to monomeric Aβ. Aducanumab targets aggregated Aβ, while still engaging with low micromolar affinity a monomeric Aβ.

IP-MS characterization of Biosimilar Aβ-Abs

Our next goal was to further elaborate the screening results obtained with short Aβ fragments and extend the analyses to intact AβX-40 and X-42 variants. To this end, we tested the

481 monoclonal Aβ-Abs 4G8, Donanemab$_{bs}$, Lecanemab$_{bs}$, Aducanumab$_{bs}$, and 1E4E11 as
482 representative examples in terms of their capacity in selecting specific Aβ variants out of a
483 mixture of ten synthetic Aβ peptides on immunoprecipitation (**Figure 4, Appendix 11-12**).
484 The mixture included Aβ1-40 and 1-42, N-terminal truncated Aβ(2-40, 3-40, pE3-40, 4-40, 5-
485 40, 11-40), N-terminal elongated Aβ(-3-40) and phosphorylated pSer8-Aβ1-40 (amidated C-
486 terminal carboxyl group). The antibodies were covalently coupled to magnetic beads and
487 incubated, separately, with aliquots of the Aβ peptide mixture. After washing the magnetic
488 bead immune complexes, the bound Aβ peptides were eluted, and the immunoprecipitated
489 products were analyzed using MALDI-TOF-MS on TOPAC matrix (**Figure 4**). As previously
490 established [39][80], the TOPAC matrix allows for improved detection of phosphorylated Aβ
491 with minimal phosphate loss. Two control antibodies, 4G8 (core epitope 17-21 according to
492 our microarray data) and 1E4E11, were used to set up the system, representing respectively,
493 "pan-Abeta" and pSer8-Aβ1-40 profiles.

494 The IP-MS signature of 4G8, after incubation with the 10 peptide mix, showed signals from all
495 constituents thus acting as positive control, with major intensities for Aβ5-40, intermediate
496 signals for Aβ4-40, Aβ3-40, Aβ2-40, and Aβ1-40, and only minor signals for Aβ1-42, Aβ(-3-
497 40) and pSer8 Aβ1-40 (**Figure 4**). Additionally, pyroglutamate AβpE3-40 was clearly
498 recognized by mAb 4G8. As expected from its central epitope 17-21, 4G8 was the only Ab that
499 showed an intense signal for N-terminally truncated Aβ11-40. The monoclonal antibody
500 1E4E11 preferentially precipitated pSer8-Aβ1-40-amide and, additionally, Aβ2-40, Aβ1-42
501 and Aβ1-40. The phosphorylated pSer8-Aβ1-40-amide produced the highest signal, suggesting
502 a certain degree of preference (but not specificity) of 1E4E11 for phosphorylated pSer8-Aβ-
503 amide under the tested conditions (**Figure 4**).

504 In line with the PTM-microarray screening (**Figure 3**), Donanemab$_{bs}$ exhibited highly
505 preferential binding to AβppE3-40, with only minor signals for Aβ3-40 and Aβ2-40 (**Figure**
506 **4**). The IP-MS spectra obtained with Lecanemab$_{bs}$ showed predominant peaks for Aβ2-40,
507 Aβ1-42, and Aβ1-40 confirming the location of the epitope in the N-terminal region of Aβ
508 (**Figure 4**). For Aducanumab$_{bs}$, we observed clear signals for Aβ2-40, Aβ1-42, Aβ1-40, but
509 not for phosphorylated pSer8-Aβ1-40-amide (**Figure 4).** This was in contrast to the binding

510 data from array and BLI towards the minimal monovalent epitopes (**Figure 3 – supplement 2**
511 **and 3).**

512 For Aducanumab$_{bs}$, microarray, BLI and IP-MS data suggest three binding modalities. One
513 presumably aggregation specific site (*EFRHDS*) as predicted by previous molecular dynamics
514 studies [81], primarily via neutral V_L, where the Ser(8) would only contact the Tyr-92 [81], in
515 line with previous data [41]. A second, binding site (EFRHDpS) relevant for the binding of
516 short synthetic N-terminal Aβ fragments as resolved by our pSer(8) MD primarily contacting
517 the positively charged V_H chain paratope via Arg-317-318 and in agreement with the sulfate-
518 ion containing structure (**Figure 3 – supplement 4**). Lastly, in a similar way the binding of
519 Aducanumab to monomeric A*EFRHDS* (Aβ2-8) can benefit from the presence of negatively
520 charged sulfate ions [41] (pdb: 6CO3). Of note, a recent molecular dynamics study suggested
521 the presence of an N-terminal neutral domain in Aβ protofibrils (Aβ:Fab contact Ser8:Tyr92)
522 [34], which may contribute for the preferential binding of Aducanumab to aggregated forms of
523 Aβ.

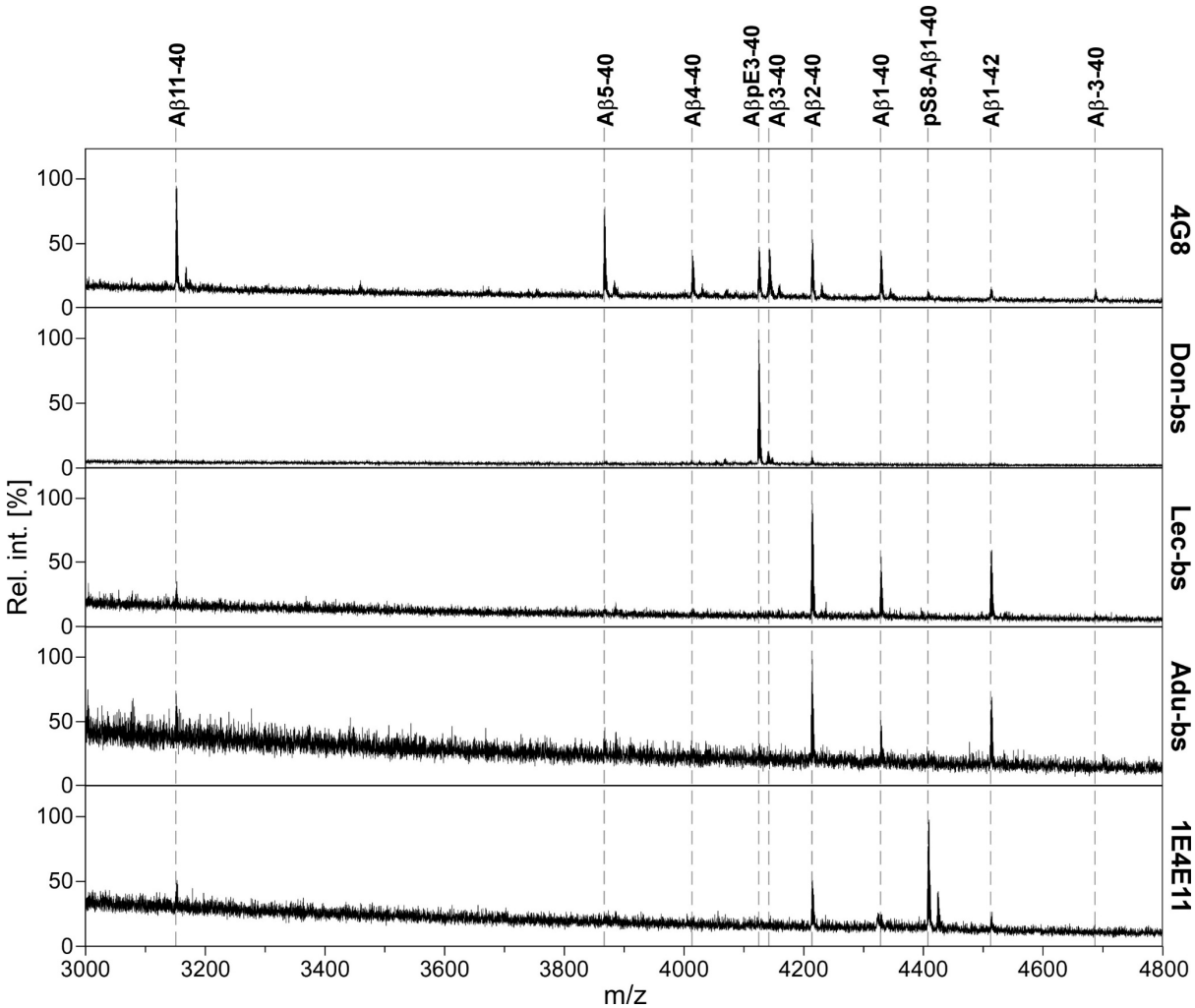

524

525 **Figure 4: IP-MS signature of different biosimilar Aβ-Abs.** A mixture of synthetic Aβ
526 peptides was immunoprecipitated with the following Aβ-Abs (from top to bottom): 4G8 (pan-
527 antibody), Donanemab$_{bs}$ (Don-bs), Lecanemab$_{bs}$ (Lec-bs), Aducanumab$_{bs}$ (Adu-bs), and
528 1E4E11 (phospho-selective control). Mass spectra were generated by MALDI-TOF-MS in
529 reflector mode from TOPAC matrix and are representative for two independent experiments.
530 We noted that the signal pattern slightly varied between experiments, which we mainly
531 attributed to some immunoprecipitation of co-aggregated Aβ species, an effect that has to be
532 considered under the experimental conditions applied.

533 Biosimilar Binding to Monomeric and Aggregated Aβ Variants

534 To further complement the characterization of the biosimilar Aβ-Abs, we applied gel
535 electrophoretic separations of Aβ peptides followed by Western blotting, automated Capillary
536 Isoelectric Focusing immunoassays with charge-based separation of Aβ peptides (CIEF-
537 immunoassay), and immunohistochemistry (IHC) experiments on brain tissue with pre-
538 adsorption of Aβ-Abs.

539 Aducanumab and Lecanemab are known to have a clear preference for aggregated forms of Aβ
540 over monomeric forms [38, 40, 41]. In agreement with these reports, our analysis showed that
541 Aducanumab$_{bs}$ clearly detected highly aggregated fibrillar Aβ1-42 on Bistris-SDS gradient
542 PAGE/Western blot. In contrast, it generated essentially no appreciable signals with
543 monomerized hexafluoroisopropanol (HFIP)-treated or oligomeric Aβ1-42 preparations under
544 the tested conditions (**Fig. 5 A**). On peptide Bicine-Tris SDS-PAGE/Western blot and on CIEF-
545 immunoassays we observed substantial variances with Aducanumab$_{bs}$ between different
546 experiments (data not shown), making reliable interpretations difficult [82]. The observed high
547 variance of the Aducanumab$_{bs}$ results on CIEF-immunoassay and peptide SDS-PAGE/Western
548 blot might be related to the low affinity of Aducanumab for monomeric Aβ [41] and the
549 possibility that Aβ dimers or low order oligomers might form during the experiment [82]. In
550 good agreement with the strong preference of Aducanumab$_{bs}$ for highly aggregated fibrillar Aβ
551 (see above), pre-adsorption with fibrillar Aβ1-42 largely blocked Aducanumab$_{bs}$
552 immunoreactivity of vascular and parenchymal Aβ deposits in AD brain tissue, in contrast to
553 pre-adsorption with an excess of Aβ1-42 monomers (**Fig. 5 B**).

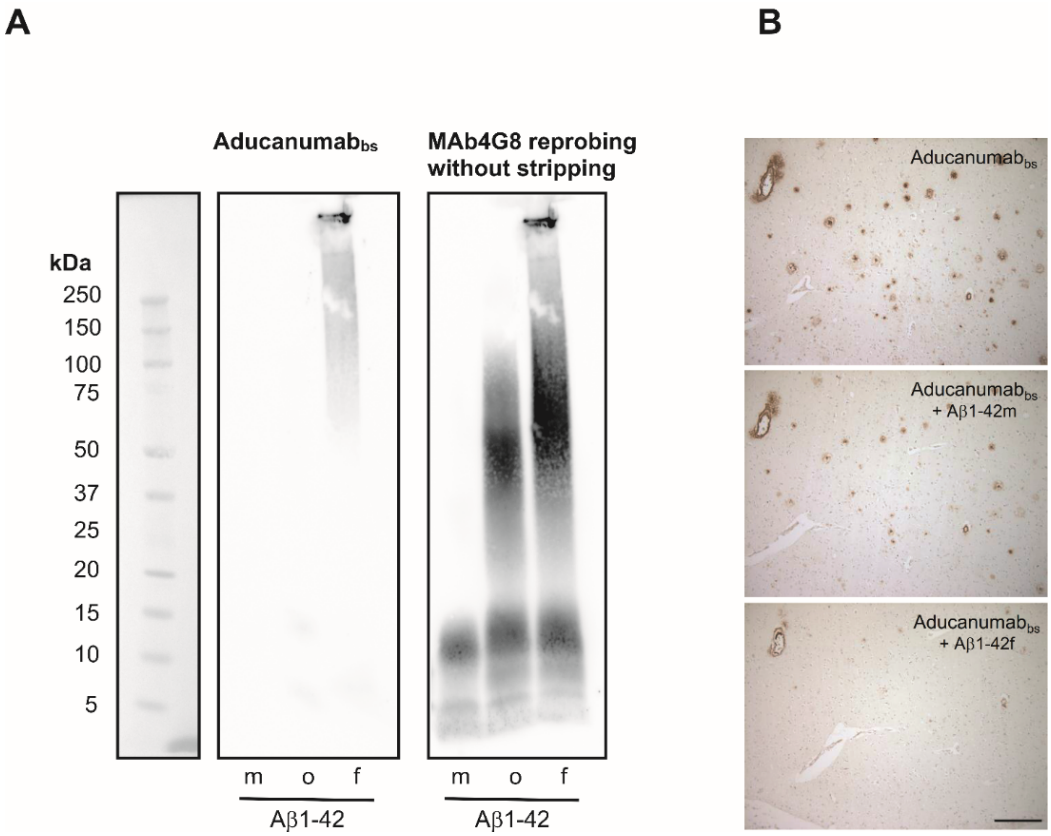

554

555 **Figure 5**: **Aducanumab$_{bs}$ shows strong preference for highly aggregated fibrillar Aβ1-42**.
556 (A) HFIP-treated Aβ1-42 monomer (m), oligomer (o) and fibril preparations (f) (1.44 µg each)
557 were separated by 4-12% Bistris SDS-PAGE, blotted onto nitrocellulose and probed with
558 Aducanumab$_{bs}$ (5 min exposure, F 0.84, image display: High: 65535; Low: 0; Gamma: 0.85).
559 Following image recording the blot membrane was reprobed without prior stripping (no
560 removal of primary and secondary antibodies) with mAb4G8 (1 min exposure, image display:
561 High: 54971; Low: 0; Gamma: 0.99). That way the 4G8 signals were essentially added on top
562 of the initial Aducanumab$_{bs}$ signals and background artifacts. The positions of pre-stained
563 protein marker bands on the blot membrane are shown on the left-hand side. (B) Parallel
564 sections from an AD patient were stained with Aducanumab$_{bs}$ and Aducanumab$_{bs}$ that had been
565 pre-adsorbed with either Aβ1-42 monomers (Aβ1-42m) or Aβ1-42 fibrils (Aβ1-42f). Scale bar:
566 200 µm.

567 Lecanemab$_{bs}$ recognized Aβ1-40, Aβ1-42, Aβ3-40, Aβ-3-40 and phosphorylated pSer8-Aβ1-
568 40 on CIEF-immunoassay and Bicine-Tris SDS-PAGE/ Western blot, indicating that the
569 Lecanemab$_{bs}$ epitope is located in the N-terminal region of the Aβ sequence. On gradient Bistris
570 SDS-PAGE/Western blot and under the tested conditions, Lecanemab$_{bs}$ showed a certain, but
571 not absolute preference for aggregated forms of Aβ1-42 over monomeric and low-n oligomeric
572 forms in the HFIP-treated Aβ1-42 preparation (**Figure 6**). The immunohistochemical detection
573 of Aβ in vascular and parenchymal deposits by Lecanemab$_{bs}$ in brain sections from an AD-
574 patient was efficiently blocked by antibody pre-adsorption with monomerized, oligomeric and
575 fibrillar preparations of Aβ1-42 (**Figure 6 E**).

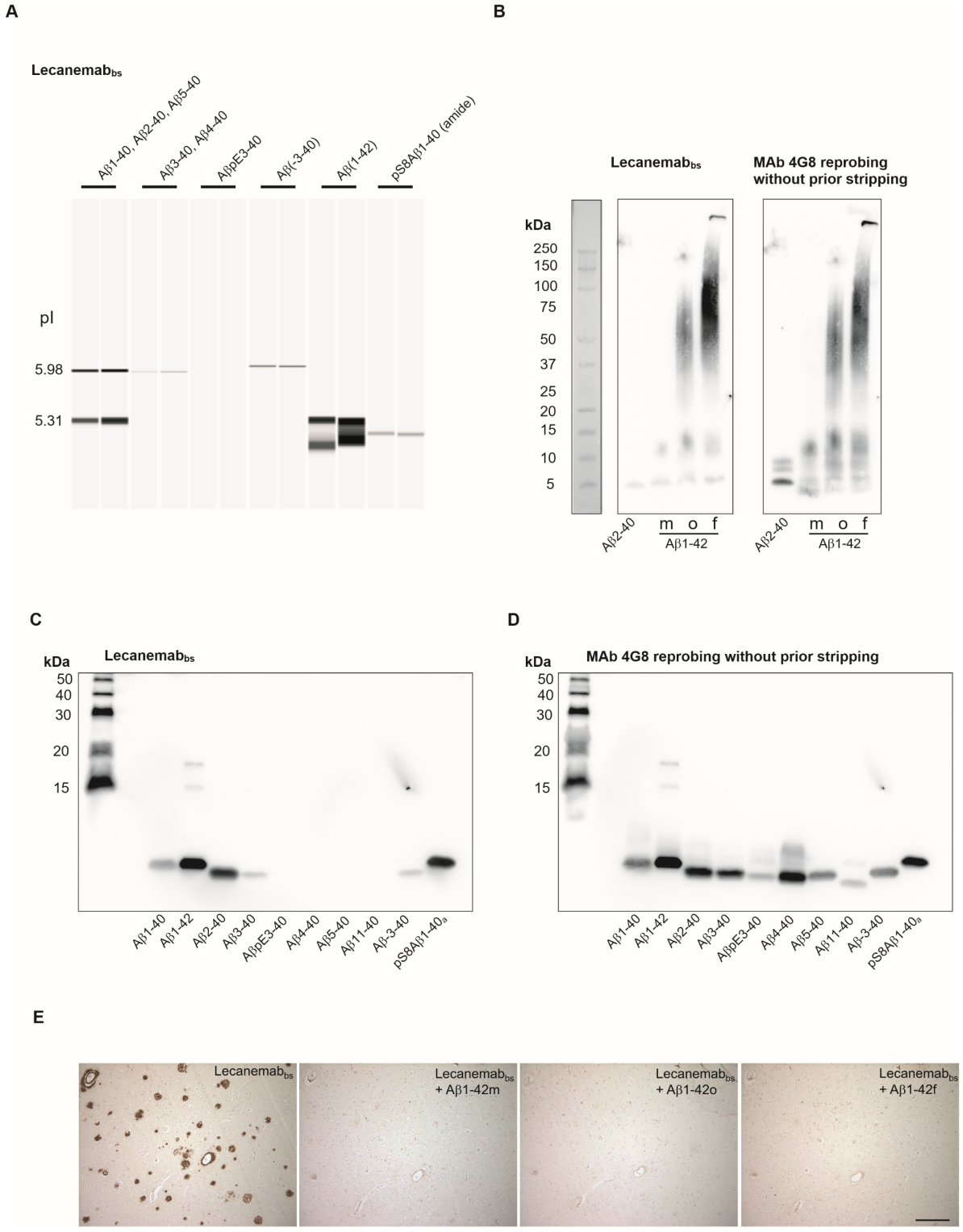

Figure 6: **Lecanemab$_{bs}$ recognizes an epitope located in the N-terminal region.** (A) shows an example of CIEF-immunoassay results for Lecanemab$_{bs}$ displayed as lane view (Western blot simulation). The indicated Aβ peptides were separated by isoelectric focusing in microcapillaries on a Peggy Sue device, immobilized photochemically to the inner capillary wall and subjected to immunological detection. Under the tested conditions, Lecanemab$_{bs}$ detected Aβ1-40 (pI 5.31), Aβ2-40 (pI 5.98), Aβ3-40 (pI 5.97), Aβ-3-40 (pI 6.04), Aβ1-42 (pI approx. 5.3) and pSer8Aβ1-40 (amide) (pI 5.13-5.14). (B) Synthetic Aβ2-40 (361 ng), and monomerized (m), oligomeric (o) and fibrillar (f) preparations of Aβ1-42 (361 ng of each) were

585 separated by 4-12% Bistris SDS-PAGE, blotted onto nitrocellulose and probed with
586 Lecanemab$_{bs}$ (0.5 µg/mL). Exposure: 2 min 7.5 sec; F 0.84; image display: high: 47545; low:
587 0; gamma: 1.0. After blot development, the blot membrane was reprobed with mAb 4G8
588 without prior stripping. That way the 4G8 signals were essentially added on top of the initial
589 Lecanemab$_{bs}$ signals and background artifacts. Exposure: 1 min F 0.84; image display: high:
590 46277; low: 0; gamma: 1.0. (C) The indicated Aβ peptides (50 ng of each) were separated by
591 Bicine Tris (peptide) SDS-PAGE, blotted on PVDF, and probed with Lecanemab$_{bs}$. Exposure:
592 5 min F 0.84, image display: high: 65535; low: 0; gamma: 0.85. (D) To confirm loading and
593 successful blotting of all Aβ peptides, the blot membrane was re-probed with mAb 4G8 without
594 prior stripping (see above). Exposure: 5 min F 0.84; image display: high: 65535; low: 0;
595 gamma: 1.0. (E) Parallel sections from an AD patient were stained with Lecanemab$_{bs}$ and
596 Lecanemab$_{bs}$ that had been pre-adsorbed with either Aβ1-42 monomers (Aβ1-42m), Aβ1-42
597 oligomers (Aβ1-42o) or Aβ1-42 fibrils (Aβ1-42f). Scale bar: 200 µm.

598

599 On CIEF-immunoassay and Bicine-Tris SDS-PAGE/Western blot, Donanemab$_{bs}$ detected
600 AβpE3-40 and Aβ3-40 (both at a pI of approximately 5.95) with a clear preference for the Aβ
601 variant starting with the cyclized N-terminal pE. Other N-terminal Aβ variants that were tested
602 produced no or very small signals (**Figure 7 B, C**). On gradient Bistris SDS-PAGE/Western
603 Blot, Donanemab$_{bs}$ detected multiple AβpE3-40 bands in the low Mr range, presumably
604 representing monomers and low order oligomers which were formed during sample preparation
605 or SDS electrophoresis [82]. The HFIP-treated monomeric, oligomeric and fibrillar Aβ1-42
606 preparations produced very faint signals with Donanemab$_{bs}$ (**Figure 7D**). Re-probing of the
607 blot (without stripping) with mAb4G8 showed multiple Aβ1-42 bands in the low molecular
608 weight range (<15 kDa) in the HFIP treated preparation (presumably monomers and low order
609 oligomers). The Aβ1-42 oligomer preparation showed a similar pattern of bands < 15 kDa and
610 a poorly resolved smear in the range between approximately 25 kDa and 100 kDa. The Aβ1-
611 42 fibril preparation showed low order oligomeric Aβ1-42 bands, a poorly resolved smear in
612 the molecular weight range of 37.5 – 150 kDa and highly aggregated Aβ1-42 which,
613 apparently, did not even enter the stacking gel. On immunohistochemistry, the detection of Aβ
614 vascular and parenchymal deposits by Donanemab$_{bs}$ in AD brain sections was efficiently
615 suppressed by pre-adsorption of the antibody with synthetic AβpE3-40, but not with Aβ1-40
616 or Aβ3-40 peptides (**Figure 7E**).

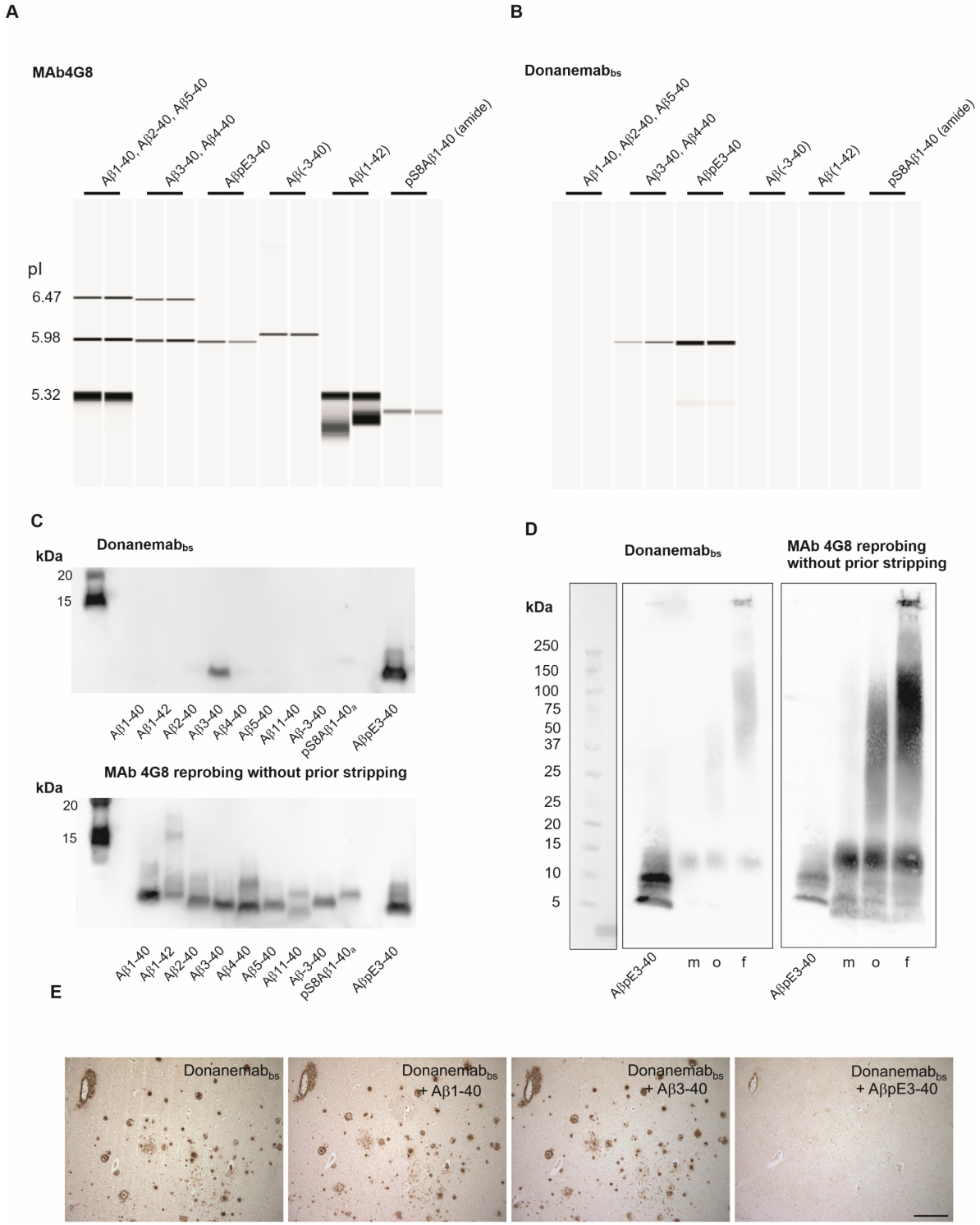

Figure 7: Donanemab$_{bs}$ shows high preference for pyroglutamate bearing pEAβ3-40. The upper panel shows lane views (Western blots simulation) of a CIEF-immunoassay for assessing the detection of different Aβ variants by (A) mAb 4G8 (positive control antibody) and (B) Donanemab$_{bs}$. The indicated Aβ variants were separated by isoelectric focusing in microcapillaries on a Peggy-Sue device, immobilized photochemically to the inner capillary wall and subjected to immunological detection by (A) mAb 4G8 and (B) Donanemab$_{bs}$. (C) Synthetic Aβ peptides (50 ng per lane) were separated by Bicine Tris (peptide) SDS-PAGE, blotted on PVDF and probed with Donanemab$_{bs}$ (0.5 µg/mL) (upper image). Exposure: 5 min F 0.84; image display: high: 59406; low: 0; Gamma: 0.65. To confirm that all Aβ variants were

627 loaded and blotted, the blot membrane was reprobed with mAb 4G8 without prior stripping.
628 That way, the 4G8 signals were essentially added on top of the initial Donanemab$_{bs}$ signals and
629 background artifacts (lower image). Exposure: 5 min F 0.84; image display: high: 65535; low:
630 0; gamma: 0.77. (D) AβpE3-40 and Aβ1-42 monomer (m), oligomer (o) and fibril preparations
631 (f) were separated by 4-12% Bistris SDS-PAGE, blotted onto nitrocellulose and probed with
632 Donanemab$_{bs}$ (image display: High: 64091; Low: 0; Gamma: 0.75), followed by reprobing
633 without prior stripping with mAb4G8 (image display: High: 46984; Low: 0; Gamma: 1.0). The
634 positions of prestained protein marker bands on the blot membrane are shown on the left-hand
635 side. (E) A pre-adsorption experiment employing synthetic Aβ peptides in human AD brain
636 tissue showed that the immunoreactivity of Donanemab$_{bs}$ was not suppressed by pre-adsorption
637 of the antibody with excess amounts of synthetic Aβ1-40 and Aβ3-40 peptides. In contrast, a
638 pre-incubation with AβpE3-40 effectively attenuated the antibody signal in extracellular Aβ
639 deposits as well as in the vasculature.

640 Conclusion

641 Aβ-Abs are pivotal in AD research, in particular those which have the capacity to selectively
642 target specific Aβ variants. Our systematic microarray analysis combined with complementary
643 methodologies provided a comprehensive data set for a panel of research and biosimilar Aβ-
644 Abs. By leveraging the resolution and throughput of microarrays for screening of Aβ fragments
645 in the form of 20.000 peptide-antibody interactions, the individual epitope specificities, and
646 the influence of PTMs or point-mutants at single amino acid resolution were investigated.
647 While Aβ microarrays have proven useful for antibody screening and determining the
648 localization of monomeric binding regions, complementary studies with additional
649 methodologies, including IP-MS, CIEF immunoassay, SDS-PAGE/Western blot, and
650 immunohistochemistry applied here, are necessary since different methods may yield different
651 insights into Aβ-Ab binding requirements and thus into the Abs' mode of action.

652 In view of the biosimilar Abs studied here, our findings recapitulated the strong selectivity of
653 Donanemab$_{bs}$ for Aβ fragments starting with a cyclized AβE3-X and comprising a core epitope
654 at residues 3-10. The core epitope of Lecanemab$_{bs}$ for an N-terminally truncated Aβ2-x
655 fragment was identified at residues 3-7. Also, in the case of Aducanumab$_{bs}$, the microarray
656 experiments provided very detailed insights into the antibody-antigen interactions in this
657 specific setup. However, as these findings were obtained with short monomeric Aβ fragments,
658 they do not seem to fully reflect and explain the preferential binding of Aducanumab to
659 aggregated Aβ [41], which was confirmed here. Nevertheless, our microarray data can still
660 generate hypotheses as to the molecular details underpinning the observed selectivity for short
661 phospho-Aβ fragments, even if this may not be directly relevant for the mode of aggregate
662 binding. Moreover, the reduced binding strength of Aducanumab$_{bs}$ on microarray to N-terminal

Aβ fragments carrying the rare H6R mutation exemplifies that genetic variability might affect therapeutic responses. Finally, the Aducanumab$_{bs}$ specificity profiling provides experimental evidence for different mono- and multivalent [81] Aβ binding modes, offering valuable insights that could guide the design of novel monoclonal antibodies.

In summary, we have systematically compared the binding requirements of 20 Aβ-Abs commonly used for research, diagnostic and therapeutic applications by addressing sequence (including genetic and species variants), PTM, and structural aspects. Our work may not only serve the purpose of a resource facilitating the selection of Aβ-Ab for particular research applications, but also provides systematic insights into the mode of action of biosimilars of the currently available therapeutic Aβ-Abs, which may help to improve the benefit-risk ratio of future generations of this new class of therapeutics for AD.

Methods

Human AD Brains

Paraffin-embedded human brain samples from individuals with sporadic Alzheimer's disease (AD) were obtained from the Netherlands Brain Bank (NBB), Netherlands Institute for Neuroscience, Amsterdam (open access: www.brainbank.nl). All material has been collected from donors for or from whom a written informed consent for a brain autopsy and the use of material and clinical information for research purposes had been obtained by the NBB. For our analysis, we utilized sections from the medial frontal gyrus region of the brain. All procedures involving human tissue were approved by the ethical committee at the University Medical Center Göttingen (Protocol number 12/1/15).

Preparation of Functionalized Cellulose Discs

Paper functionalization was performed by introducing some variations to the previous protocol [83] aimed at increasing the output of discs per session. In brief, Whatman paper grade 50 (45 × 25 cm) was cut into 4mm diameter discs using an OMTech 50-watt CO2 laser at 7.8% power and 150 mm/s speed. To reduce mechanical stress and facilitate transfer into a 384-plate, each disc was cut with a semi-circular pattern. The pre-cut layout (15 x 10 cm) was then treated for 3 hours with a solution of 9-fluorenylmethyloxycarbonyl-β-alanine (Fmoc-β-Ala-OH),

691 diisopropylmethanediimine (DIC) and 1-Methylimidazole (NMI). The Fmoc absorption of
692 each batch of functionalized cellulose membrane was determined at 290nm after 20 minutes of
693 deprotection with 20% (v/v) piperidine (pip) in DMF. The average loading was 130nmol/disc.

694 Microarray Synthesis

695 The µSPOT assay was performed as previously described [84]. First, the APP sequence
696 (UniProtKB: P05067) was displayed in microarray format as 15mer overlapping peptide
697 library. Peptide arrays were synthesized [85-87] using MultiPep RSi robot (CEM GmbH,
698 Kamp-Lintford, Germany) on cellulose discs containing Fmoc-β-Ala linkers. Natural amino
699 acid building blocks were purchased from IRIS (IRIS Biotech GmbH, Marktredwitz,
700 Germany). Special building blocks employed in this study such as isomers, stereoisomers,
701 phosphorylation and pyroglutamination post-transcriptional modifications are listed here:
702 Fmoc-L-Ser(PO(OBzl)OH)-OH (Iris – FAA1423), L-Pyroglutamic acid pentachlorophenyl
703 ester (Novabiochem - 8.54203), Fmoc-L-Asp-OtBu (Iris – FAA1356), Fmoc-D-Asp-OtBu
704 (Carbosolutions – CC05095) and Fmoc-D-Asp(tBu)-OH (Iris – FAA1309). Synthesis was
705 carried out by deprotecting the Fmoc-group using 20% piperidine in dimethylformamide
706 (DMF). Peptide chains were elongated using a coupling solution consisting of amino acids
707 (0.5M) with oxyma (1M) and DIC (1M) in DMF (1:1:1). Coupling steps were carried out 3
708 times (30min), followed by capping (4% acetic anhydride in DMF). Discs were transferred into
709 96 deep-well plates for the work-up. Side chains were deprotected using 90% trifluoracetic
710 acid (TFA), 2% dichloromethane (DCM), 5% H_2O and 3% triisopropylsilane (150µL/well) for
711 1h at room temperature (RT). Afterward, the deprotection solution was removed, and the discs
712 were solubilized ON at RT, while shaking, using a solvation mixture containing 88.5% TFA,
713 4% trifluoromethanesulfonic acid (TFMSA), 5% H2O and 2.5% TIPS (250µL/well). The
714 resulting peptide-cellulose conjugates (PCCs) were precipitated with ice-cold ether
715 (700µL/well) and spun down at 2000×g for 10min at 4°C, followed by two additional washes
716 of the formed pellet with ice-cold ether. The resulting pellets were dissolved in DMSO
717 (250µL/well).

718 Microarray Quality Control

719 LC-MS was carried out using peptide quality controls that were cleaved from the solid support.
720 To ensure cleavage, a Rink amide linker (Iris) suitable for SPPS on cellulose support was
721 introduced during the first coupling cycle. In an acidic environment, the quality controls were

722 cleaved off the solid support. To isolate the quality controls, 150 µL of the supernatant (SN)
723 was transferred to 1.5 mL reaction tubes, followed by the addition of 700 µL of diethyl ether.
724 The samples were then vortexed, and the peptides were allowed to precipitate by incubation at
725 -20°C overnight. After centrifugation at 13,300 × g and 4°C for 10 min, the SN was discarded,
726 and 500 µL of diethyl ether was added. The mixture was vortexed, centrifuged for 10 min, and
727 the supernatant was decanted. This process was repeated twice, and the peptides were left to
728 dry for 60 min. Finally, the Rink amides were dissolved in 50 µL of 50% acetonitrile; 0.1%
729 formic acid (v/v) and vortexed briefly before centrifugation at 13,300 × g and room
730 temperature. For analysis, the quality controls were diluted 1:3 and sent to LC-MS (Agilent
731 technologies).

732 Microarray Printing

733 PCCs solutions were mixed 2:1 with saline–sodium citrate buffer (150mM NaCl, 15mM
734 trisodium citrate, pH7.0) and transferred to a 384-well plate. For transfer of the PCC solutions
735 to white-coated CelluSpot blank slides (76×26mm, Intavis AG Peptide Services GmbH and
736 CO. KG), a SlideSpotter (CEM GmbH) was used. After completion of the printing procedure,
737 slides were left to dry ON.

738 Microarray Binding Assay

739 The microarray slides were blocked for 60min in 5% (w/v) skimmed milk powder (Carl Roth)
740 0.05% Tween20 phosphate-buffered saline (PBS; 137mM NaCl, 2.7mM KCl, 10mM
741 Na_2HPO_4, 1.8mM KH_2PO_4, pH7.4). After blocking, the slides were incubated for 30 min with
742 a solution of blocking buffer and monoclonal and polyclonal Aβ-Ab (**Table 1**). They were then
743 washed 3× with PBS 0.05% Tween20 for 1min. IgG antibodies were detected using goat anti
744 mouse IgG-HRP (Thermo Fisher Cat. No31430), Goat anti-Rabbit IgG, Antibody, HRP (Cell
745 Signaling: 7074), Goat anti-Rat IgG (H+L) Secondary Antibody, HRP (TF: 31470) and Goat
746 anti-Human IgG (H+L) Secondary Antibody, HRP (TF: 31410). The chemiluminescence
747 readout was detected with an Azure imaging system c400 (lowest sensitivity, 1s, 5s, 10s, 30s,
748 1m, 2m) using SuperSignal West Femto maximum sensitive substrate (Thermo Scientific
749 GmbH, Schwerte, Germany). The raw grayscale intensities were measured using open-source
750 MARTin software [88].

751 # Dot Blot

752 The purified peptides were printed onto white-coated CelluSpot blank slides using the Slide
753 Spotter at a starting amount of 0.05 µg. The slides were allowed to dry for 3 hours and rinsed
754 once with 1X PBS to remove the unbound peptides. After blocking in 5% (w/v) skimmed milk
755 powder for 1 hour, the slides were incubated with 1nM $Aducanumab_{bs}$ and IgG signals were
756 detected using goat anti-human IgG DL650 (1:1000 - Invitrogen 84545). The fluorescence
757 signal readouts were acquired using Amersham Image Quant 800 (GE Healthcare) with an
758 exposure time of 30 seconds and 4x4 binning.

759 # Molecular Dynamics Simulations

760 For molecular dynamic (MD) simulations the crystal structure of the aducanumab Aβ complex
761 structure (PDB: 6CO3) was used. The complex structure was prepared using MOE (Molecular
762 Operating Environment, 2022.02, Chemical Computing Group ULC, 1010 Sherbooke St.
763 West, Suite #910, Montreal, QC, Canada, H3A2R7, 2023) structure preparation tools with
764 default values. For producing the MD-starting structure the experimentally resolved residues
765 of the Aβ were prolonged by either a serine or a phosphorylated serine in MOE.

766 The MD simulations were conducted using AMBER22 suite [89]. Topology and parameter
767 files were generated in tleap module using the AMBER ff14sb. The simulations were set up in
768 the following way: The peptide-aducanumab complex was energy minimized for 2000 steps
769 using a generalized Born implicit solvent model, neutralized, and solvated using the TIP3P
770 water model. The system was equilibrated by heating the solvent from 100 K to 300 K within
771 500 ps under constant volume conditions with non-solvent atoms assigned with harmonic
772 constraints of 100 kcal·mol-1·Å-2. Cooling the system back to 100 K within 250 ps and
773 lowering the harmonic constraints on non-solvent atoms to 1 kcal·mol-1·Å-2, followed by
774 heating to 300 K within 500 ps period. Afterwards, the non-solvent atoms constraints were set
775 off and the pressure was adjusted to 1 bar using the Berendsen barostat. Each complex
776 (unmodified and phosphorylated) was simulated in triplicates for 200 ns at constant pressure
777 and temperature. All simulations were carried out using periodic boundary and particle mesh
778 Ewald (PME) methodology to handle long-range electrostatics. 2 fs-time steps were used for
779 integration and coordinates of were saved every 500 steps (1 ps). The trajectories were further
780 analysed with CPPTRAJ (4.14.0).

781 **Aβ-Peptides for Peptide SDS-PAGE, CIEF Immunoassay and IP-**

782 **MS**

783 The synthetic peptides Aβ1–40, Aβ1–42, Aβ2–40, Aβ3–40, AβpE3–40, Aβ4–40, Aβ5–40 and
784 Aβ11–40 were obtained from AnaSpec (Fremont, California, USA 94555). Synthetic Aβ−3–
785 40 [90]was kindly provided by H.-J. Knölker, Technische Universität Dresden. Phosphorylated
786 pSer8-Aβ1-40 was synthesized with an amidated C-terminal carboxyl group to remove one
787 negative charge, ensuring that this Aβ variant still falls into the applied separation range of the
788 CIEF immunoassay.

789

790 **Bistris-SDS Gradient PAGE/Western Blots Analysis of Different**

791 **Aβ Aggregation States.**

792 For the assessment of antibody binding to different Aβ aggregation states, we used Aβ1-42
793 monomers (Cat. No SPR-485B), Aβ1-42 oligomers (Cat. No SPR-488B) and preformed Aβ1-
794 42 fibrils (Cat. No SPR-487B) (StressMarq biosciences, Victoria, BC, Canada). The samples
795 for electrophoresis were prepared (starting from stock solutions) with final concentrations of
796 0.1 µg/µL) in LDS sample buffer (247.5 mM Tris-HCl, pH 8.5, 2% (w/v) lithium dodecyl
797 sulfate (LDS), 10% (v/v) glycerol, 0.5 mM EDTA, 0.22 mM Brilliant Blue G250, 0.175 mM
798 Phenol Red) and denatured by heating at 70°C for 10 min. Per lane, 0.361, 0.722 or 1.44 µg of
799 the different Aβ1-42 forms were loaded on a 4-12% Bistris-gel (1mm, 12 wells, Anamed
800 Electrophorese GmbH, Groß-Bieberau / Rodau, Germany) and separated at 200 V using MES-
801 SDS running buffer. Following recommendations provided by the manufacturer of the different
802 Aβ1-42 aggregation forms, electroblotting onto nitrocellulose was done at 100 V for 1 hour
803 with a Biorad mini tank blot. The prechilled transfer buffer contained 25 mM Tris, 192 mM
804 glycine, 20% (v/v) methanol and 0.0375 % Tween-20. After blotting, the membrane was
805 washed for 10 min at room temperature in Tris-buffered saline (TBS) followed by blocking for
806 30 min with 5% powdered milk in TBS containing 0.1% Tween-20 (TBS-T). The blots were
807 then incubated with primary antibodies in 5% milk in TBS-T over night at 4°C and washed 3
808 x for 10 min with TBS-T at room temperature. The secondary antibodies were (i) Peroxidase-
809 conjugated Affini Pure Donkey Anti-Human IgG (H+L), Jackons ImmunoResearch

810 Laboratories Inc., West Grove, PA, (code number 709-035-149)1:20000 in TBS-T for
811 $Donanemab_{bs}$, $Lecanemab_{bs}$ and $Aducanumab_{bs}$ and (ii) anti-mouse IgG-POD
812 (Calbiochem/EMD Millipore, San Diego, California, USA, catalog number 401253-2ML)
813 1:10000 in TBS-T for mAb 1E4E11 and mAb 6E10. After 1 h incubation with the secondary
814 antibodies, the blots were washed 3 x for 10 min with TBS-T and incubated for 5 min with
815 ECL-Prime Western Blotting Detection Reagent (Cytiva Amersham, Little Chalfont, England).
816 Images were recorded on a Vilber-Loumart Fusion SL blot imager. To confirm successful
817 blotting of all Aβ variants, the blot membranes were reprobed without prior stripping with
818 mAb4G8 (0.5 µg/mL in 5% milk in TBS-T over night at 4°C or 1-2 h at room temperature)
819 followed by anti-mouse IgG-POD (1:10000 in TBS-T) for 1 h at room temperature. That way,
820 the 4G8 reprobing signals were essentially added on top of the initial signals and background
821 artifacts.
822

823 **Peptide Bicine-Tris SDS-PAGE / Western Blot**

824 Synthetic Aβ peptides were separated by 15% T/5% C Bicine-Tris SDS-PAGE, essentially
825 according to[91]. After the electrophoresis, the gel was shortly rinsed with 50 mM Tris –HCl,
826 pH 8.0, followed by blotting the peptides on PVDF using a Gravity Blotter (Serva
827 Electrophoresis GmbH, Heidelberg, Germany). The blotting sandwich was assembled on the
828 Gravity blotter from bottom to top by first placing the gel on the lower plate, followed by a
829 precut PVDF membrane (activated with methanol and equilibrated in 50 mM Tris-HCl, pH
830 8.0), one filter paper Whatmann 3mM equilibrated in 50 mM Tris-HCl, pH 8.0, three dry filter
831 papers (Sartorius BF4 blotting paper) and, finally, three 2.25 kg Gravity Blotter metal plates.
832 The gravity/press blotting was done overnight at room temperature. On the next morning, the
833 blot sandwich was disassembled and the PVDF membrane was boiled in PBS for 3min in a
834 microwave oven with the protein side facing downwards. After blocking for 30 min at room
835 temperature with 2% ECL Prime blocking reagent (Cytiva) in PBS containing 0.075% Tween-
836 20 (PBS-T), the blots were incubated for 1 h at room temperature with the primary antibodies
837 (0.5 µg/mL in 2% ECL-Prime Western Blotting Detection Reagent in PBS-T). After 3 x 10
838 min washing with PBS-T, the secondary peroxidase-conjugated Affini Pure Donkey Anti-
839 Human IgG (see above) (1:20000 in PBS-T) was applied for 1-2 hours at room temperature.
840 Following 3 x 10 min washing with PBS-T, the blots were incubated for 5 min with ECL-Prime

841 Western Blot Detection Reagent, and images were recorded. To confirm successful blotting of
842 all Aβ variants, the blot membranes were reprobed without prior stripping with mAb4G8 (0.5
843 µg/mL in 2% ECL Prime blocking reagent in PBS-T over night at 4° C or 1 h at room
844 temperature followed by anti-mouse IgG-POD (1:10000 in PBS-T) for 1 h at room temperature.
845 That way, the 4G8 reprobing signals were essentially added on top of the initial signals and
846 background artifacts.

847 Capillary Isoelectric Focusing Immunoassay

848 Automated capillary isoelectric focusing immunoassays were performed with a Peggy-Sue
849 system (ProteinSimple,San Jose, California, USA), essentially as previously described [92] and
850 [49].

851 In brief, synthetic Aβ peptide variants were separated by isoelectric focusing in
852 microcapillaries followed by photochemical immobilization to the inner capillary walls and
853 probing with the primary antibodies for 120 min. After 2 washes, the horseradish peroxidase
854 conjugated secondary antibodies were loaded and incubated for 60 min. After two washing
855 steps, a luminol/peroxide mix was loaded, and chemiluminescent signals were recorded. The
856 data was analyzed with the Compass for SW software. The following secondary antibodies
857 were used: Anti-human IgG Secondary HRP antibody (Protein Simple, catalog number 043-
858 491), Goat-Anti-Mouse-HRP Secondary Antibody ProteinSimple, catalog number 040-655)
859 and Peroxidase-conjugated Affini Pure Donkey Anti-Human IgG (H+L) (1:100 dilution)
860 (Jackson ImmunoResearch Laboratories Inc., West Grove, PA, code number 709-035-149).

861 Automated Solid Phase Peptide Synthesis

862 The peptides were synthesized using PurePep Chorus (Gyros Protein Technologies, US) with
863 Fmoc chemistry at 0.05mmol scale. Tentagel S RAM (Resin Substitution 0.22mmol/g - Rapp
864 Polymere, Germany) resin was first swollen in dimethylformamide (DMF) for 30-60 minutes.
865 Next, Fmoc was removed using a 20% piperidine in DMF solution for 1-2 minutes and washed
866 3x with DMF. Deprotection steps were performed at 90°C for unphosphorylated peptides and
867 at room temperature from the first phospho-serine coupling. The peptide chain was elongated
868 by adding the premixed amino acid (AA, 125mM and Oxyma 125mM) along with N,N'-
869 diisopropylcarbodiimide (DIC, 250mM). The mixture was heated at 90°C for 2 minutes and
870 then washed 2x with DMF. Capping was done with acetic anhydride (10% in DMF) for 5

871 minutes and washed 3x with DMF. The peptide chain was elongated until completion and dried
872 for 30 minutes after 7x DCM washes. The Fmoc deprotected peptides were cleaved from the
873 resin using a mixture of 90% TFA, 5% water, 3% TIPS, and 2% DCM for 4 h at RT. The
874 peptides were then precipitated in ice-cold ether ON, subsequently purified using HPLC and
875 analysed by LC-MS, as described below.

876 Purification and Characterization of Peptides

877 The crude peptides were purified by reverse phase (RP) HPLC using a water-acetonitrile
878 gradient with 0.1% formic acid (FA). Preparative HPLC was performed on a UltiMate™ 3000
879 HPLC Systems instrument (ThermoFisher Scientific, Waltham, Massachusetts, USA)
880 equipped with RS variable wavelength detector (set to 215nm) and a Kinetex® 5µm EVO C18
881 100 LC column (00D-4633-P0-AX; Phenomenex, Aschaffenburg, Germany). Chromatograms
882 were recorded using Chromeleon software v7.2. Purity and structural identity of the peptides
883 were verified using a DAD equipped 1260 Infinity II HPLC device with a C18 RP column
884 (Onyx Monolithic C18 50×2 mm), coupled to a mass selective detector with a single
885 quadrupole system (Agilent Technologies, Santa Clara, CA, US) in ESI+ mode.

886 Crude phosphorylated pSer8-Aβ1-40 with an amidated C-terminal carboxyl group was purified
887 on a 10x150mm Waters (Milford, Massachusetts, USA) XBridge Protein BEH C4 OBD
888 preparative column (300Å, 5 µm) using 3% acetonitrile/0.2% Formic acid as solvent A and
889 97% acetonitrile/0.2% FA as solvent B. A Beckman System Gold HPLC system with external
890 column oven was used to form the following gradient with a flow rate of 3.8 ml/min at 50°C
891 column temperature: 5-20% B in 2 min, 20-32% B in 22 min, 32-50% in 5 min. Analytical
892 HPLC was performed on a Waters Alliance e2695 HPLC system coupled to a photodiode array
893 (PDA) optic detector and a single quadrupole QDa mass detector. A 4.6x150mm Waters
894 XBridge Protein BEH C4 analytical column (300 Å, 3.5µm) was used at a flow rate of
895 3.8ml/min at 50°C column temperature; the corresponding gradient was 5-20% B in 2 min, 20-
896 32% B in 11 min, 32-50% in 5 min.

897 Biolayer Interferometry

898 The samples were dispensed into a 96 microplate (Greiner bio-one GmbH, Frickenhausen,
899 Germany) at a final volume of 200 µL. The binding of Aducanumab biosimilar and mAb
900 1E4E11 and their phosphorylated, unphosphorylated and H6R epitopes 6xHis-tagged were

901 measured using Biolayer interferometry on an Octet RED 96system (Sartorius, Göttingen,
902 Germany). The peptides were synthesized (purity above 98% - based on UV at 215nm) with
903 Fmoc-Adoa linker (Iris - FAA1435) and C-terminal 6xHis tag. Sensorgrams were measured in
904 double reference against the buffer and the reference sensor signals.

905 NTA biosensors (Sartorius, Göttingen, Germany) were preincubated into 1XPBS buffer pH
906 7.4, 0.2% BSA, 0.02% (v/v) Tween 20 for 10 min. A first baseline was established in the same
907 buffer. The 6xHis peptides were loaded onto NTA biosensors at 20 µg/ml for 200 s. Following
908 a buffer wash of 120s, the biosensors were incubated with serial-dilutions of the respective
909 antibodies for 1200s s to measure association and then into buffer for additional 1500s to
910 observe the dissociation phase. Experiments were performed at 30℃ and sample plates were
911 shaken at 1000 rpm. Sensorgrams were globally fitted using Data Analysis software version
912 12.0.2.3 (Sartorius, Göttingen, Germany) with a 1:1 binding model.

913 Immunoprecipitation and Mass Spectrometry

914 The monoclonal biosimilar antibodies Aducanumab$_{bs}$, Lecanemab$_{bs}$, and Donanemab$_{bs}$ were
915 covalently coupled to Dynabeads M-270 Epoxy (Invitrogen/ThermoFisher Scientific,
916 Waltham, Massachusetts, USA Cat. No. 14311 D), essentially following the manufacturer's
917 instructions. Tween-20 was omitted from all wash and storage buffers for specific use in IP-
918 MS. In brief, 5 mg of M-270 epoxy beads were weighed into a 1.5-mL reaction vial and washed
919 with 1 mL of buffer C1 (kit component). The bead suspension was divided in aliquots of 200
920 µL (containing 1mg of beads). The vials were placed on a magnetic stand for a few minutes,
921 and the supernatant was carefully removed and discarded. Washed beads were resuspended in
922 40 µL of buffer C1 and 10 µL of antibody stock solution (1 mg/mL). After gentle mixing by
923 pipetting, 50 µL of buffer C2 (kit component) was added and incubated overnight at 37 °C on
924 a mixer. After coupling, the beads were washed 1 time with 400 µL of buffer HB (kit
925 component), 1 time with 400 µL of buffer LB (kit component) and 2 times with 400 µL of PBS.
926 After a final wash with PBS for 15 min with continuous agitation, the beads were resuspended
927 in 100 µL PBS/0.1% BSA/0.02% NaN_3 and stored at 4 °C.

928 The synthetic Aβ peptides Aβ1–40, pSer8-Aβ1–40, Aβ1–42, Aβ2–40, Aβ3–40, AβpyGlu–40,
929 Aβ4–40, Aβ5–40 and Aβ11–40 Aβ−3–40 (see above), were mixed and diluted to final
930 concentrations of 10ng/mL of each in PBS/0.1%BSA containing phosphatase inhibitors
931 (PhosphoStop Mini, Roche, Ref 04906837001) and protease inhibitors (Complete Mini Roche,

932 Ref 04693124001). For immunoprecipitation of Aβ peptides, 250 µL of the Aβ mix was
933 combined with an equal volume of 100 mM Tris-HCl, pH 7.4, containing 0.2% (w/v) nonyl-β-
934 d-thiomaltoside (NTM) and 0.2% (w/v) n-dodecyl-β-d-maltoside (DDM) and 15 µL of
935 functionalized M270 epoxy beads. After overnight incubation at 4 °C with constant mixing,
936 the beads were washed five times with 0.5 mL of 50 mM Tris-HCl, pH 7.4, 150 mM NaCl,
937 0.1% (w/v) DDM, 0.1% (w/v) NTM and resuspended in 0.5 mL of 50 mM ammonium acetate
938 (pH approximately 7.0). The beads were immediately forwarded to sample preparation for
939 mass spectrometry. There, the beads were immobilised on a magnet, the supernatant was
940 removed, and the beads were washed one time with 0.5 mL of 50 mM ammonium acetate, and
941 one time with 0.5 mL H_2O. The bound Aβ peptides were eluted in 2.5 µL of 70% acetonitrile
942 containing 5 mM HCl.

943 Analysis by MALDI-TOF-MS was essentially performed as described [21, 93]. Briefly, the
944 eluates (0.5 µL) were spotted onto a pre-structured MALDI sample support (MTP AnchorChip
945 384 BC; Cat. No. 8280790, Bruker, Bremen, Germany), followed by the addition of 0.5 µl
946 TOPAC matrix solution, a matrix recently developed for the improved detection of intact
947 phosphorylated Aβ peptides [80]. A 1:1 mixture of Peptide Calibration Standard II (Cat. No.
948 8222570, Bruker, Bremen, Germany) and PepMix2 (Cat. No. C102, LaserBio Labs, Valbonne,
949 France) was used as calibrant. The samples were dried in a vacuum desiccator and a total of
950 5000 mass spectra per spot were recorded using an ultrafleXtreme MALDI-TOF/TOF mass
951 spectrometer in reflector mode operated under the software flexControl 3.4 (Bruker, Bremen,
952 Germany).

953 Immunohistochemistry and Antibody Preabsorption

954 Immunohistochemistry was performed on 4-µm paraffin sections. In brief, brain sections were
955 deparaffinized in Roticlear (Carl Roth, Karlsruhe, Germany) and rehydrated in a descending
956 series of ethanol. Activity of endogenous peroxidases was blocked by incubation in 0.3% H_2O_2
957 in PBS for 30 min. Antigen retrieval was achieved by initial boiling of the sections in 0.01 M
958 citrate buffer (pH 6.0) and subsequent incubation in 88% formic acid for 3 min. Unspecific
959 binding sites were blocked by incubation in PBS containing 4% skim milk and 10% fetal calf
960 serum (FCS) for 1 h at room temperature, prior to the overnight incubation with the primary
961 antibodies. The following antibodies were used for the detection of different Aβ variants:
962 $Aducanumab_{bs}$ (0.5 µg/µl), $Donanemab_{bs}$ (1 µg/ml), $Lecanemab_{bs}$ (0.06 µg/ml).

963 Antibody pre-adsorption with synthetic Aβ peptides (Aβ1-40, Aβ3-40 (both from Anaspec),
964 AβpyGlu3-40 (Peptide Speciality Laboratory, Heidelberg, Germany), Aβ1-42 monomers,
965 Aβ1-42 oligomers and Aβ1-42 fibrils (StressMarq, Victoria, Canada) was carried out as
966 described previously [52]. In brief, 1 µg Donanemab$_{bs}$ was blocked with 2.5 µg of Aβ1-40,
967 Aβ3-40 or AβpyGlu3-40 in 0.01 M PBS including 10% FCS. In the case of Aducanumab$_{bs}$, 0.5
968 µg of the antibody were blocked with 10 µg of Aβ1-42 monomers or 5 µg of Aβ1-42 fibrils,
969 while for Lecanemab$_{bs}$, 0.06 µg of antibody was blocked with 0.25 µg of Aβ1-42 monomers,
970 oligomers or fibrils. Antibodies and peptides were incubated on a rotator for 3 h at room
971 temperature and reaction tubes were centrifuged at 13000 rpm for 5 min at the end of the
972 incubation period. Control conditions included antibodies in 0.01 M PBS including 10% FCS
973 without synthetic peptides. Adjacent paraffin-embedded sections from a human AD case were
974 incubated overnight with the supernatants and sections were washed with 0.01 M PBS
975 including 0.1 % Tergitol. For detection, biotinylated anti-human antibodies (6 µg/ml, Jackson
976 ImmunoResearch, West Grove, Pennsylvania, USA #109-065-003) were used and staining was
977 visualized with the ABC method with a Vectastain kit (Vector Laboratories, Newark,
978 California, USA), diaminobenzidine as a chromogen and counterstaining with hematoxylin.

979 Author contributions

980 The following section was based on the CRediT system. Conceptualization: IT, HMM;
981 Methodology: IT, HMM, HWK, OJ, OW; Formal Analysis: IT, HMM, TLe, HWK, OJ, OW,
982 SB, LvW, TLi; Investigation: IT, TLe, HWK, MMH, SA, BM, SB, LvW, TLi; Visualization:
983 IT, TLe; Writing – Original Draft: HMM, IT; Writing – review & editing: all the co-authors;
984 Project administration: IT, HMM; Supervision: HMM, HWK, OJ, OW, JW, HS, JoW, JeW;
985 Funding Acquisition, HMM.

986 Acknowledgements

987 First, we thank Sonja Kachler, Gabriele Paetzold and Sandra Theil for the excellent technical
988 assistance. Also, we would like to thank Prof. S. Weggen (Heinrich Heine University,
989 Germany) to have kindly provided the IC16 Antibody. We thank Prof. H.-J. Knölker
990 (Technische Universität Dresden, Germany) for providing the synthetic Aβ-3-40 peptide.
991 H.M.M. acknowledge funding by the Interdisziplinäres Zentrum für Klinische Forschung
992 (IZKF) of Würzburg, project number A-F-N-419. H.M.M. acknowledges the Junior Group

Leader program of the Rudolf Virchow Center, the excellent ideas programme of the University of Würzburg and support through the Emmy Noether Programme of the Deutsche Forschungsgemeinschaft (DFG) (MA6957/1-1). T.L. acknowledges funding by the Graduate School of Life Sciences of the University of Würzburg. O.W. acknowledges funding by the DFG (WI3472/11-1 and Research Training Group 2824 (GRK2824)). J.W acknowledges funding by the DFG WA1477/6-6

Competing interests

The authors declare that there are no competing interests related to this manuscript.

References

1. Colvin, M.T. et al. (2016) Atomic Resolution Structure of Monomorphic Aβ42 Amyloid Fibrils. Journal of the American Chemical Society 138 (30), 9663-9674.
2. Yang, Y. et al. (2022) Cryo-EM structures of amyloid-β 42 filaments from human brains. Science 375 (6577), 167-172.
3. Tzioras, M. et al. (2023) Synaptic degeneration in Alzheimer disease. Nature Reviews Neurology 19 (1), 19-38.
4. Kent, S.A. et al. (2020) The physiological roles of tau and Aβ: implications for Alzheimer's disease pathology and therapeutics. Acta Neuropathologica 140 (4), 417-447.
5. Vassar, R. et al. (1999) β-Secretase Cleavage of Alzheimer's Amyloid Precursor Protein by the Transmembrane Aspartic Protease BACE. Science 286 (5440), 735-741.
6. Wolfe, M.S. et al. (1999) Two transmembrane aspartates in presenilin-1 required for presenilin endoproteolysis and γ-secretase activity. Nature 398 (6727), 513-517.
7. Wiltfang, J. et al. (2002) Highly conserved and disease-specific patterns of carboxyterminally truncated Aβ peptides 1–37/38/39 in addition to 1–40/42 in Alzheimer's disease and in patients with chronic neuroinflammation. Journal of Neurochemistry 81 (3), 481-496.
8. Mukherjee, S. et al. (2021) Citrullination of Amyloid-β Peptides in Alzheimer's Disease. ACS Chemical Neuroscience 12 (19), 3719-3732.
9. Scheidt, H.A. et al. (2020) Structural characteristics of oligomers formed by pyroglutamate-modified amyloid β peptides studied by solid-state NMR. Physical Chemistry Chemical Physics 22 (29), 16887-16895.
10. Grochowska, K.M. et al. (2017) Posttranslational modification impact on the mechanism by which amyloid-β induces synaptic dysfunction. EMBO reports 18 (6), 962-981.
11. Roher, A.E. et al. (1993) Structural alterations in the peptide backbone of beta-amyloid core protein may account for its deposition and stability in Alzheimer's disease. Journal of Biological Chemistry 268 (5), 3072-3083.
12. Moro, M.L. et al. (2018) Pyroglutamate and Isoaspartate modified Amyloid-Beta in ageing and Alzheimer's disease. Acta Neuropathologica Communications 6 (1), 3.
13. Schrempel, S. et al. (2024) Identification of isoAsp7-Aβ as a major Aβ variant in Alzheimer's disease, dementia with Lewy bodies and vascular dementia. Acta Neuropathologica 148 (1), 78.

14. Kumar, S. et al. (2021) Novel Phosphorylation-State Specific Antibodies Reveal Differential Deposition of Ser26 Phosphorylated Aβ Species in a Mouse Model of Alzheimer's Disease. Frontiers in Molecular Neuroscience 13.
15. Ashby, E.L. et al. (2015) Investigation of Aβ phosphorylated at serine 8 (pAβ) in Alzheimer's disease, dementia with Lewy bodies and vascular dementia. Neuropathology and Applied Neurobiology 41 (4), 428-444.
16. Kumar, S. et al. (2012) Phosphorylation of Amyloid-β Peptide at Serine 8 Attenuates Its Clearance via Insulin-degrading and Angiotensin-converting Enzymes*. Journal of Biological Chemistry 287 (11), 8641-8651.
17. Wirths, O. and Zampar, S. (2019) Emerging roles of N- and C-terminally truncated Aβ species in Alzheimer's disease. Expert Opinion on Therapeutic Targets 23 (12), 991-1004.
18. Shinohara, M. et al. (2017) Distinct spatiotemporal accumulation of N-truncated and full-length amyloid-β42 in Alzheimer's disease. Brain 140 (12), 3301-3316.
19. Reinert, J. et al. (2016) Deposition of C-terminally truncated Aβ species Aβ37 and Aβ39 in Alzheimer's disease and transgenic mouse models. Acta Neuropathologica Communications 4 (1), 24.
20. Moro, M.L. et al. (2012) APP mutations in the Aβ coding region are associated with abundant cerebral deposition of Aβ38. Acta Neuropathologica 124 (6), 809-821.
21. Wirths, O. et al. (2024) Amino-terminally elongated Aβ peptides are generated by the secreted metalloprotease ADAMTS4 and deposit in a subset of Alzheimer's disease brains. Neuropathology and Applied Neurobiology 50 (3), e12991.
22. Sinha, S. et al. (1999) Purification and cloning of amyloid precursor protein β-secretase from human brain. Nature 402 (6761), 537-540.
23. Walter, S. et al. (2019) The metalloprotease ADAMTS4 generates N-truncated Aβ4–x species and marks oligodendrocytes as a source of amyloidogenic peptides in Alzheimer's disease. Acta Neuropathologica 137 (2), 239-257.
24. Wirths, O. et al. (2017) N-truncated Aβ4–x peptides in sporadic Alzheimer's disease cases and transgenic Alzheimer mouse models. Alzheimer's Research & Therapy 9 (1), 80.
25. Seuma, M. et al. (2021) The genetic landscape for amyloid beta fibril nucleation accurately discriminates familial Alzheimer's disease mutations. eLife 10, e63364.
26. Paravastu, A.K. et al. (2008) Molecular structural basis for polymorphism in Alzheimer's β-amyloid fibrils. Proceedings of the National Academy of Sciences 105 (47), 18349-18354.
27. Tycko, R. (2015) Amyloid Polymorphism: Structural Basis and Neurobiological Relevance. Neuron 86 (3), 632-645.
28. Qiang, W. et al. (2017) Structural variation in amyloid-β fibrils from Alzheimer's disease clinical subtypes. Nature 541 (7636), 217-221.
29. Lu, J.-X. et al. (2013) Molecular Structure of β-Amyloid Fibrils in Alzheimer's Disease Brain Tissue. Cell 154 (6), 1257-1268.
30. Rasmussen, J. et al. (2017) Amyloid polymorphisms constitute distinct clouds of conformational variants in different etiological subtypes of Alzheimer's disease. Proceedings of the National Academy of Sciences 114 (49), 13018-13023.
31. Barykin, E.P. et al. (2017) Amyloid β Modification: A Key to the Sporadic Alzheimer's Disease? Frontiers in Genetics 8.
32. Kummer, M.P. and Heneka, M.T. (2014) Truncated and modified amyloid-beta species. Alzheimer's Research & Therapy 6 (3), 28.
33. Roher, A.E. et al. (2017) APP/Aβ structural diversity and Alzheimer's disease pathogenesis. Neurochemistry International 110, 1-13.

34. Gómez-Castro, C.Z. et al. (2024) An N-terminal acidic β-sheet domain is responsible for the metal-accumulation properties of amyloid-β protofibrils: a molecular dynamics study. JBIC Journal of Biological Inorganic Chemistry.
35. Gessel, M.M. et al. (2012) Familial Alzheimer's Disease Mutations Differentially Alter Amyloid β-Protein Oligomerization. ACS Chemical Neuroscience 3 (11), 909-918.
36. Hatami, A. et al. (2017) Familial Alzheimer's Disease Mutations within the Amyloid Precursor Protein Alter the Aggregation and Conformation of the Amyloid-β Peptide* *This work was supported by National Institutes of Health Grants AG033069 and AG00538 and a grant from the Cure Alzheimer's fund. The authors declare that they have no conflicts of interest with the contents of this article. The content is solely the responsibility of the authors and does not necessarily represent the official views of the National Institutes of Health. Journal of Biological Chemistry 292 (8), 3172-3185.
37. Jang, H. et al. (2013) Familial Alzheimer's Disease Osaka Mutant (ΔE22) β-Barrels Suggest an Explanation for the Different Aβ1–40/42 Preferred Conformational States Observed by Experiment. The Journal of Physical Chemistry B 117 (39), 11518-11529.
38. Söderberg, L. et al. (2024) Amyloid-beta antibody binding to cerebral amyloid angiopathy fibrils and risk for amyloid-related imaging abnormalities. Scientific Reports 14 (1), 10868.
39. van Dyck, C.H. (2018) Anti-Amyloid-β Monoclonal Antibodies for Alzheimer's Disease: Pitfalls and Promise. Biological Psychiatry 83 (4), 311-319.
40. Sevigny, J. et al. (2016) The antibody aducanumab reduces Aβ plaques in Alzheimer's disease. Nature 537 (7618), 50-56.
41. Arndt, J.W. et al. (2018) Structural and kinetic basis for the selectivity of aducanumab for aggregated forms of amyloid-β. Scientific Reports 8 (1), 6412.
42. Feinberg, H. et al. (2014) Crystal structure reveals conservation of amyloid-β conformation recognized by 3D6 following humanization to bapineuzumab. Alzheimer's Research & Therapy 6 (3), 31.
43. Dyer, O. (2024) Aduhelm: Biogen abandons Alzheimer's drug after controversial approval left it unfunded by Medicare. BMJ 384, q281.
44. Dyck, C.H.v. et al. (2023) Lecanemab in Early Alzheimer's Disease. New England Journal of Medicine 388 (1), 9-21.
45. Mintun, M.A. et al. (2021) Donanemab in Early Alzheimer's Disease. New England Journal of Medicine 384 (18), 1691-1704.
46. Shcherbinin, S. et al. (2022) Association of Amyloid Reduction After Donanemab Treatment With Tau Pathology and Clinical Outcomes: The TRAILBLAZER-ALZ Randomized Clinical Trial. JAMA Neurology 79 (10), 1015-1024.
47. Britschgi, M. et al. (2009) Neuroprotective natural antibodies to assemblies of amyloidogenic peptides decrease with normal aging and advancing Alzheimer's disease. Proceedings of the National Academy of Sciences 106 (29), 12145-12150.
48. Klafki, H.-W. et al. (2022) Is plasma amyloid-β 1–42/1–40 a better biomarker for Alzheimer's disease than AβX–42/X–40? Fluids and Barriers of the CNS 19 (1), 96.
49. Zampar, S. et al. (2020) N-terminal heterogeneity of parenchymal and vascular amyloid-β deposits in Alzheimer's disease. Neuropathology and Applied Neurobiology 46 (7), 673-685.
50. Savastano, A. et al. (2016) N-Truncated Aβ 2-X Starting with Position Two in Sporadic Alzheimer's Disease Cases and Two Alzheimer Mouse Models. Journal of Alzheimer's Disease 49, 101-110.
51. Baghallab, I. et al. (2018) Epitomic Characterization of the Specificity of the Anti-Amyloid Aβ Monoclonal Antibodies 6E10 and 4G8. Journal of Alzheimer's Disease 66, 1235-1244.
52. Bader, A.S. et al. (2023) Brain Region-Specific Differences in Amyloid-β Plaque Composition in 5XFAD Mice. Life 13 (4), 1053.

53. Kumar, S. et al. (2013) Early intraneuronal accumulation and increased aggregation of phosphorylated Abeta in a mouse model of Alzheimer's disease. Acta Neuropathologica 125 (5), 699-709.
54. Nussbaum, J.M. et al. (2012) Prion-like behaviour and tau-dependent cytotoxicity of pyroglutamylated amyloid-β. Nature 485 (7400), 651-655.
55. Bayer, T.A. and Wirths, O. (2014) Focusing the amyloid cascade hypothesis on N-truncated Abeta peptides as drug targets against Alzheimer's disease. Acta Neuropathologica 127 (6), 787-801.
56. Klafki, H.W. et al. (2020) Development and Technical Validation of an Immunoassay for the Detection of APP669–711 (Aβ–3–40) in Biological Samples. International Journal of Molecular Sciences 21 (18), 6564.
57. Richter, L. et al. (2010) Amyloid beta 42 peptide (Aβ42)-lowering compounds directly bind to Aβ and interfere with amyloid precursor protein (APP) transmembrane dimerization. Proceedings of the National Academy of Sciences 107 (33), 14597-14602.
58. Dornieden, S. et al. (2013) Characterization of a Single-Chain Variable Fragment Recognizing a Linear Epitope of Aβ: A Biotechnical Tool for Studies on Alzheimer's Disease? PLOS ONE 8 (3), e59820.
59. Jäger, S. et al. (2009) α-secretase mediated conversion of the amyloid precursor protein derived membrane stub C99 to C83 limits Aβ generation. Journal of Neurochemistry 111 (6), 1369-1382.
60. Sims, J.R. et al. (2023) Donanemab in Early Symptomatic Alzheimer Disease: The TRAILBLAZER-ALZ 2 Randomized Clinical Trial. JAMA 330 (6), 512-527.
61. DeMattos, Ronald B. et al. (2012) A Plaque-Specific Antibody Clears Existing β-amyloid Plaques in Alzheimer's Disease Mice. Neuron 76 (5), 908-920.
62. Englund, H. et al. (2007) Sensitive ELISA detection of amyloid-β protofibrils in biological samples. Journal of Neurochemistry 103 (1), 334-345.
63. Kaneko, N. et al. (2014) Novel plasma biomarker surrogating cerebral amyloid deposition. Proceedings of the Japan Academy, Series B 90 (9), 353-364.
64. Nakamura, A. et al. (2018) High performance plasma amyloid-β biomarkers for Alzheimer's disease. Nature 554 (7691), 249-254.
65. Van Cauwenberghe, C. et al. (2016) The genetic landscape of Alzheimer disease: clinical implications and perspectives. Genetics in Medicine 18 (5), 421-430.
66. Weggen, S. and Beher, D. (2012) Molecular consequences of amyloid precursor protein and presenilin mutations causing autosomal-dominant Alzheimer's disease. Alzheimer's Research & Therapy 4 (2), 9.
67. Chen, W.T. et al. (2012) Amyloid-beta (Aβ) D7H mutation increases oligomeric Aβ42 and alters properties of Aβ-zinc/copper assemblies. PLoS One 7 (4), e35807.
68. Wakutani, Y. et al. (2004) Novel amyloid precursor protein gene missense mutation (D678N) in probable familial Alzheimer's disease. Journal of Neurology, Neurosurgery & Psychiatry 75 (7), 1039.
69. Janssen, J.C. et al. (2003) Early onset familial Alzheimer's disease. Neurology 60 (2), 235-239.
70. Jones, C.T. et al. (1992) Mutation in codon 713 of the β amyloid precursor protein gene presenting with schizophrenia. Nature Genetics 1 (4), 306-309.
71. Peacock, M.L. et al. (1993) Novel polymorphism in the A4 region of the amyloid precursor protein gene in a patient without Alzheimer's disease. Neurology 43 (6), 1254-1254.
72. Jonsson, T. et al. (2012) A mutation in APP protects against Alzheimer's disease and age-related cognitive decline. Nature 488 (7409), 96-99.
73. Yi, Y. et al. (2020) An APP mutation family exhibiting white matter hyperintensities and cortical calcification in East China. Neurological Sciences 41 (10), 2921-2928.

74. Jiang, B. et al. (2019) Mutation screening in Chinese patients with familial Alzheimer's disease by whole-exome sequencing. Neurobiology of Aging 76, 215.e15-215.e21.
75. Obici, L. et al. (2005) A novel AβPP mutation exclusively associated with cerebral amyloid angiopathy. Annals of Neurology 58 (4), 639-644.
76. Aggarwal, L. and Biswas, P. (2021) Hydration Thermodynamics of the N-Terminal FAD Mutants of Amyloid-β. Journal of Chemical Information and Modeling 61 (1), 298-310.
77. Murakami, K. et al. (2003) Neurotoxicity and Physicochemical Properties of Aβ Mutant Peptides from Cerebral Amyloid Angiopathy: IMPLICATION FOR THE PATHOGENESIS OF CEREBRAL AMYLOID ANGIOPATHY AND ALZHEIMER'S DISEASE*. Journal of Biological Chemistry 278 (46), 46179-46187.
78. Schlenzig, D. et al. (2009) Pyroglutamate Formation Influences Solubility and Amyloidogenicity of Amyloid Peptides. Biochemistry 48 (29), 7072-7078.
79. Kumar, S. et al. (2011) Extracellular phosphorylation of the amyloid β‐peptide promotes formation of toxic aggregates during the pathogenesis of Alzheimer's disease. The EMBO Journal 30 (11), 2255-2265.
80. Liepold, T. et al. (2023) Matrix Development for the Detection of Phosphorylated Amyloid-β Peptides by MALDI-TOF-MS. Journal of the American Society for Mass Spectrometry 34 (3), 505-512.
81. Frost, C.V. and Zacharias, M. (2020) From monomer to fibril: Abeta-amyloid binding to Aducanumab antibody studied by molecular dynamics simulation. Proteins: Structure, Function, and Bioinformatics 88 (12), 1592-1606.
82. Watt, A.D. et al. (2013) Oligomers, fact or artefact? SDS-PAGE induces dimerization of β-amyloid in human brain samples. Acta Neuropathologica 125 (4), 549-564.
83. Schulte, C. et al. (2021) Low-cost synthesis of peptide libraries and their use for binding studies via temperature-related intensity change. STAR Protocols 2 (3), 100605.
84. Talucci, I. et al. (2024) Molecular dissection of an immunodominant epitope in Kv1.2-exclusive autoimmunity. Frontiers in Immunology 15.
85. Dikmans, A. et al. (2006) SC2: A Novel Process for Manufacturing Multipurpose High-Density Chemical Microarrays. QSAR & Combinatorial Science 25 (11), 1069-1080.
86. Frank, R. (1992) Spot-synthesis: an easy technique for the positionally addressable, parallel chemical synthesis on a membrane support. Tetrahedron 48 (42), 9217-9232.
87. Talucci, I. and Maric, H.M. (2023) Peptide Microarrays for Studying Autoantibodies in Neurological Disease. In Peptide Microarrays: Methods and Protocols (Cretich, M. and Gori, A. eds), pp. 17-25, Springer US.
88. Kreissner, K.O. et al. (2024) MARTin—an open-source platform for microarray analysis. Frontiers in Bioinformatics 4.
89. Case, D.A. et al. (2023) AmberTools. Journal of Chemical Information and Modeling 63 (20), 6183-6191.
90. Beyer, I. et al. (2016) Solid-Phase Synthesis and Characterization of N-Terminally Elongated Aβ−3–-Peptides. Chemistry – A European Journal 22 (25), 8685-8693.
91. Wiltfang, J. et al. (1991) A new multiphasic buffer system for sodium dodecyl sulfate-polyacrylamide gel electrophoresis of proteins and peptides with molecular masses 100 000–1000, and their detection with picomolar sensitivity. ELECTROPHORESIS 12 (5), 352-366.
92. Haußmann, U. et al. (2013) Analysis of Amino-Terminal Variants of Amyloid-β Peptides by Capillary Isoelectric Focusing Immunoassay. Analytical Chemistry 85 (17), 8142-8149.
93. Klafki, H.-W. et al. (2022) Detection and quantification of Aβ−3–40 (APP669-711) in cerebrospinal fluid. Journal of Neurochemistry 160 (5), 578-589.

1228 # Appendix. Chromatographic and mass spectrometric

1229 analytical data

1230 ## A1 - µSPOT (l)-Asp 1-15 LC-MS QC

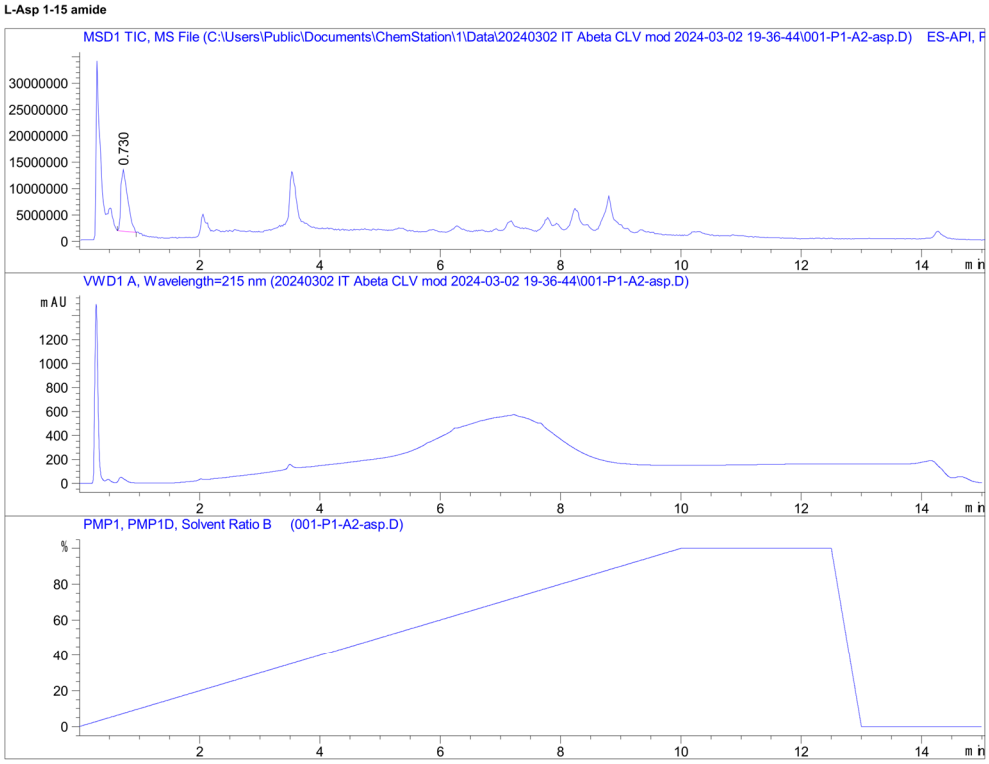

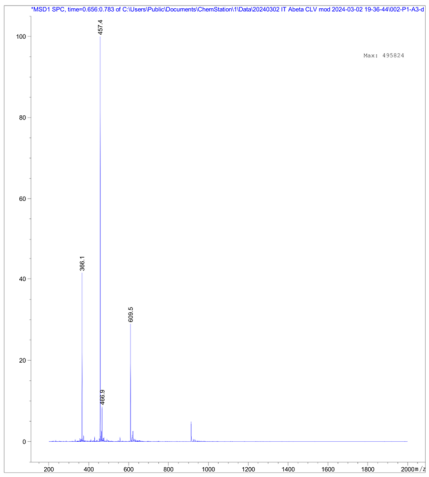

Calculated m/z

365.9 (+4)
457.2 (+3)
609.3 (+2)

1231

1232

A2 - µSPOT (d)-Asp 1-15 LC-MS QC

D-Asp 1-15 amide

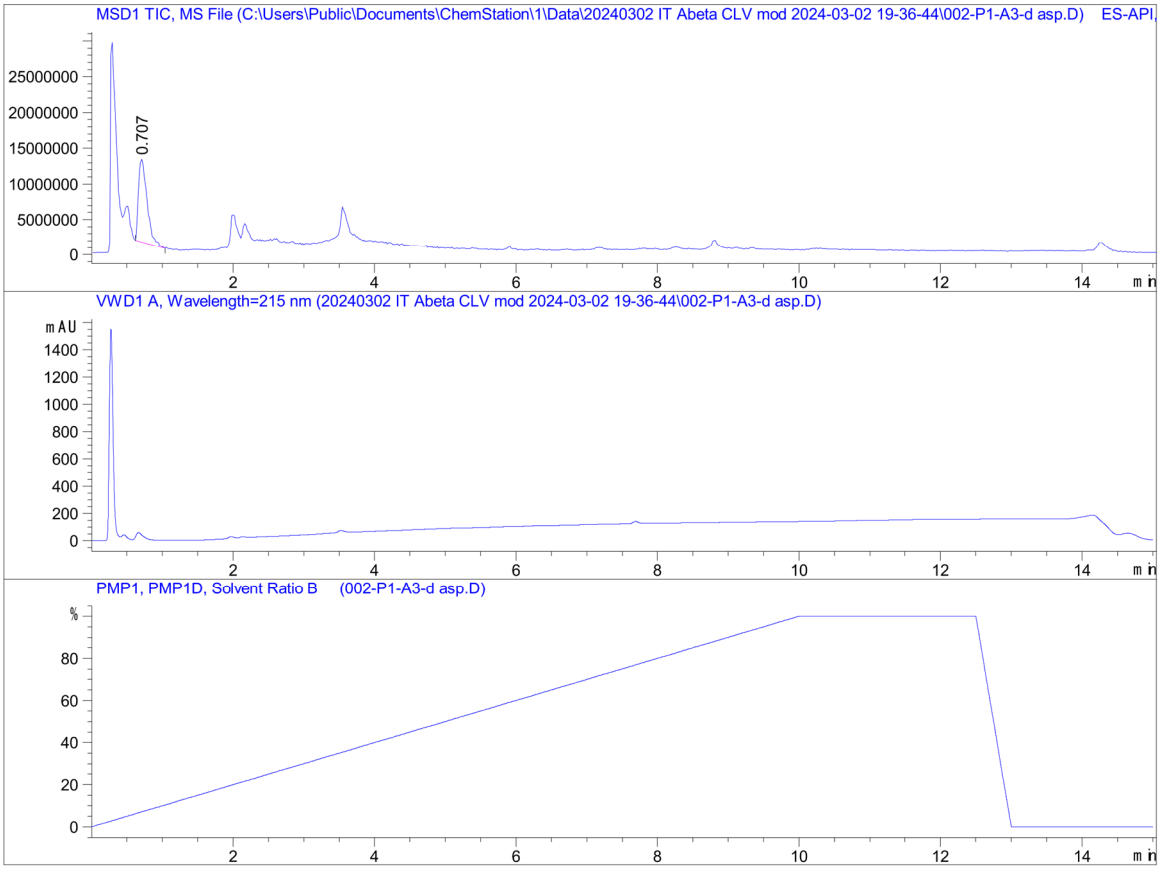

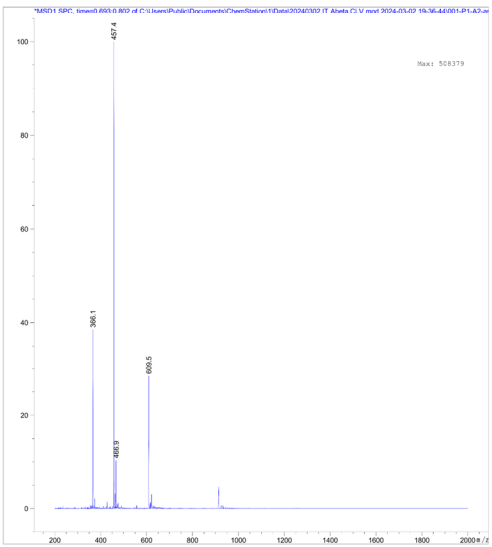

Calculated m/z

365.9 (+4)
457.2 (+3)
609.3 (+2)

1235 **A3 - µSPOT (l)-iso-Asp 1-15 LC-MS QC**

L-iso-Asp 1-15 amide

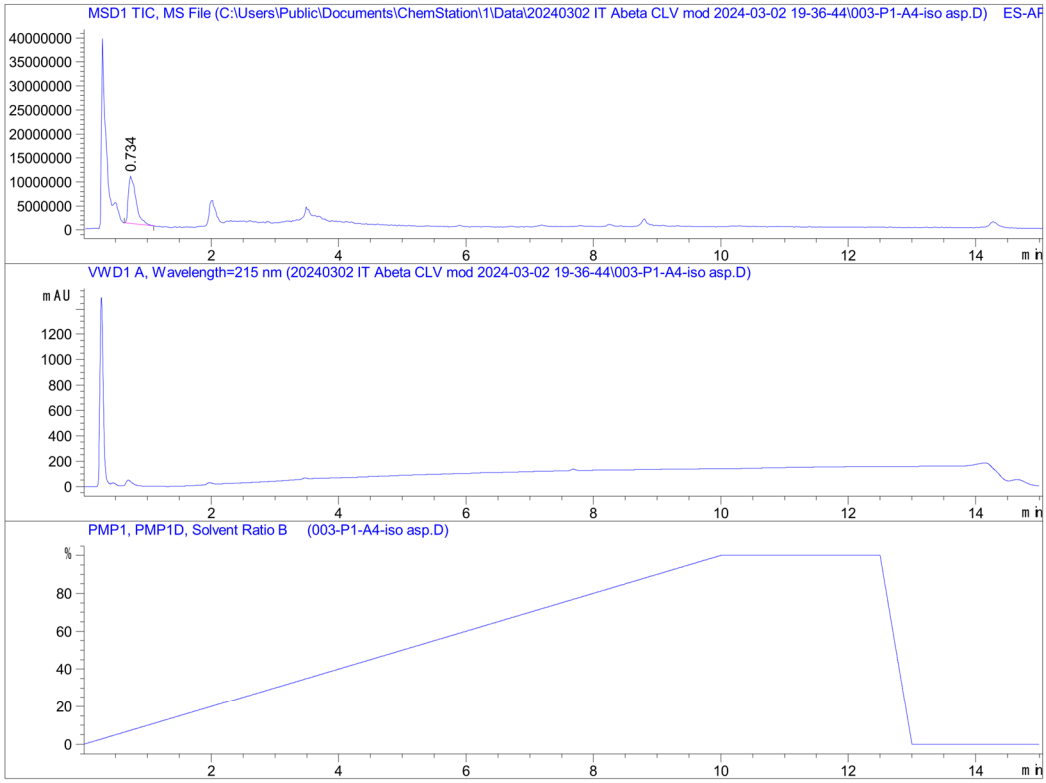

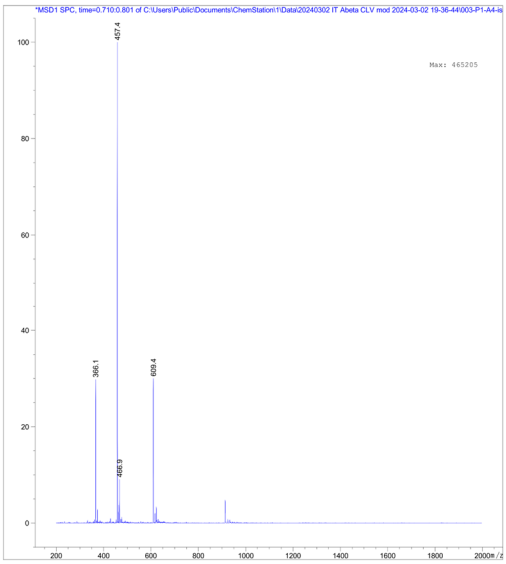

Calculated m/z

365.9 (+4)
457.2 (+3)
609.3 (+2)

1236

1237

A4 - µSPOT (d)-iso-Asp 1-15 LC-MS QC

D-iso-Asp 1-15 amide

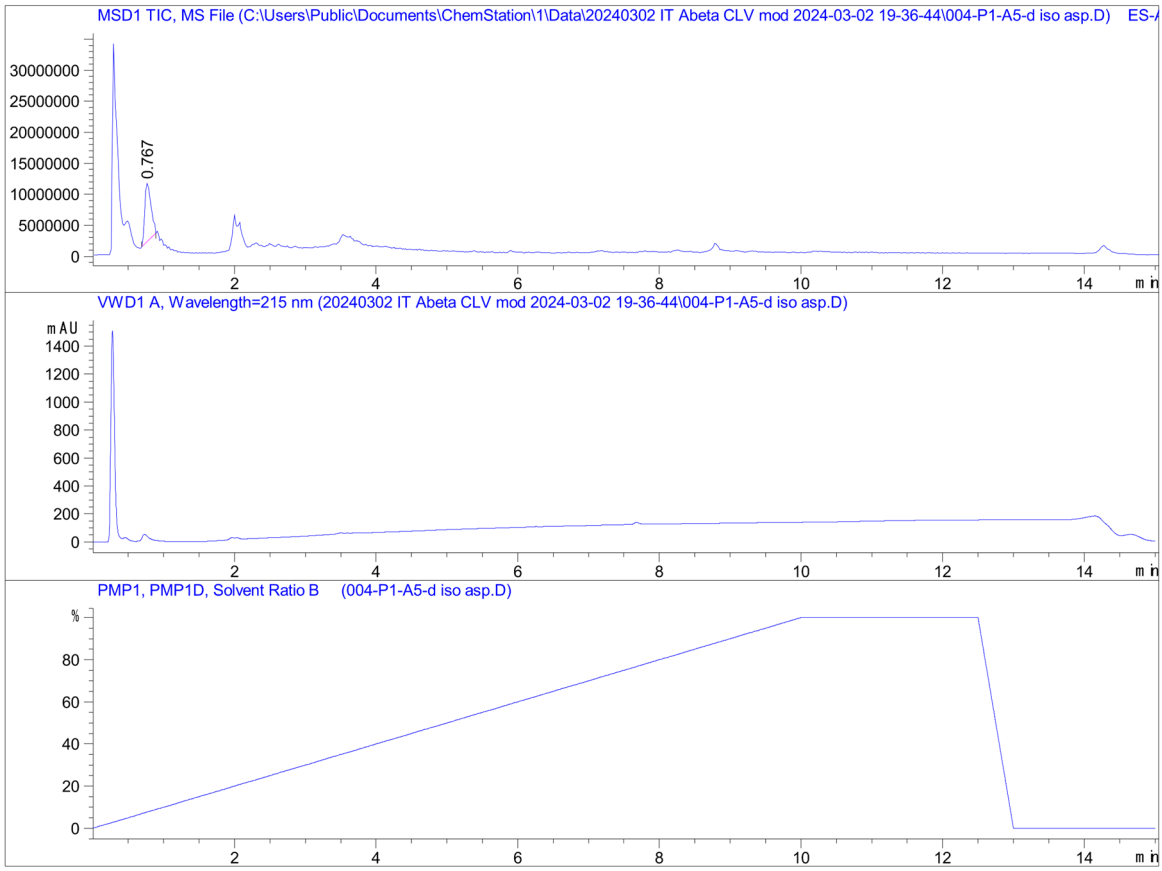

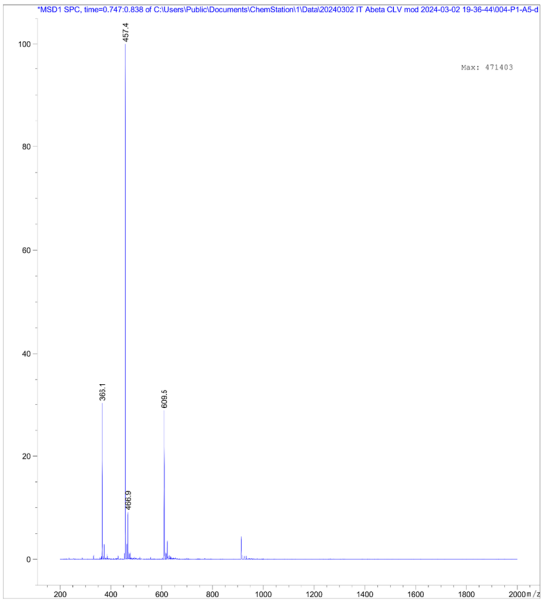

Calculated m/z

365.9 (+4)
457.2 (+3)
609.3 (+2)

A5 - µSPOT pyro-Glu 3-17 LC-MS QC

pyro-Glu 3-17 amide

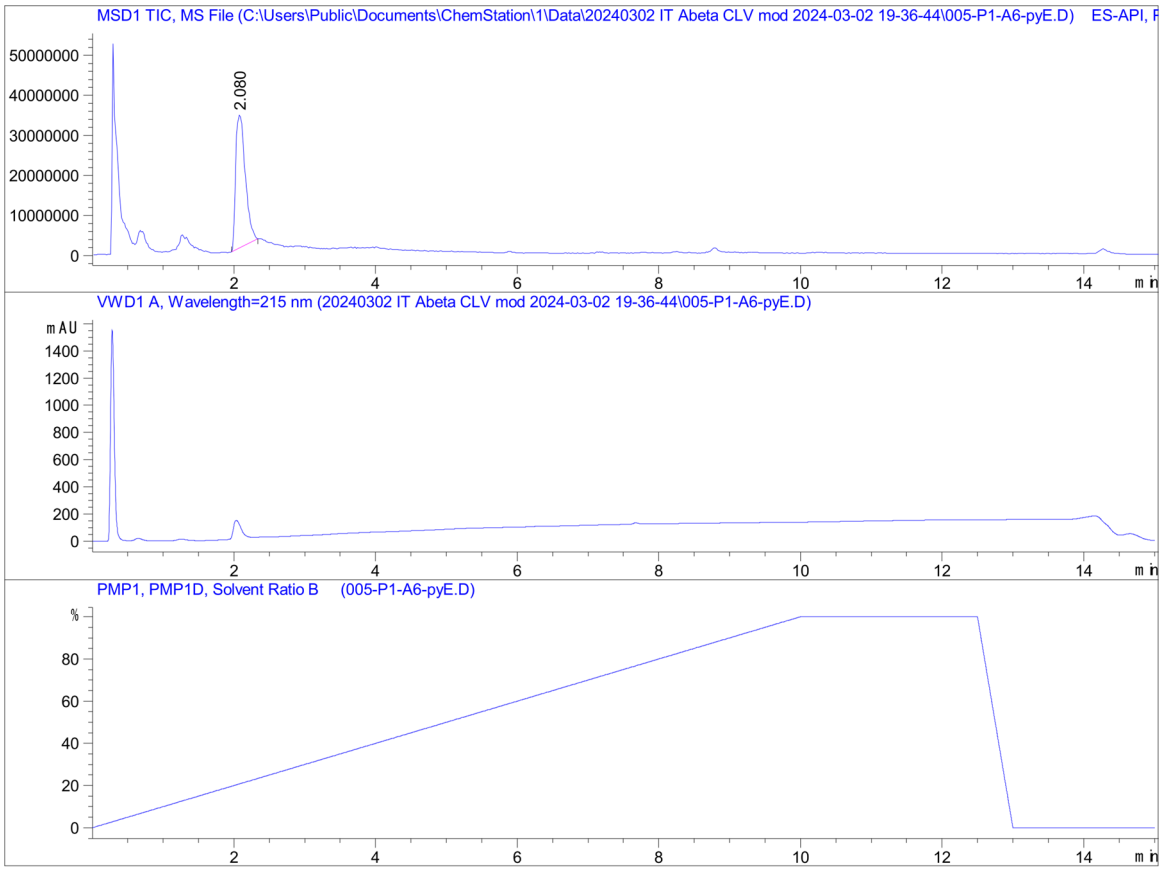

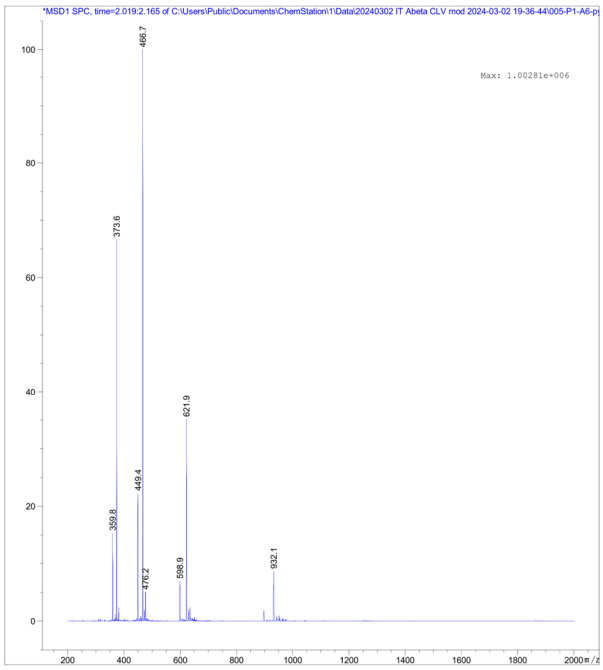

Calculated m/z

931.9 (+2)
466.7 (+4)
621.9 (+3)

A6 - µSPOT pSerine 1-15 LC-MS QC

pSer-1-15 amide

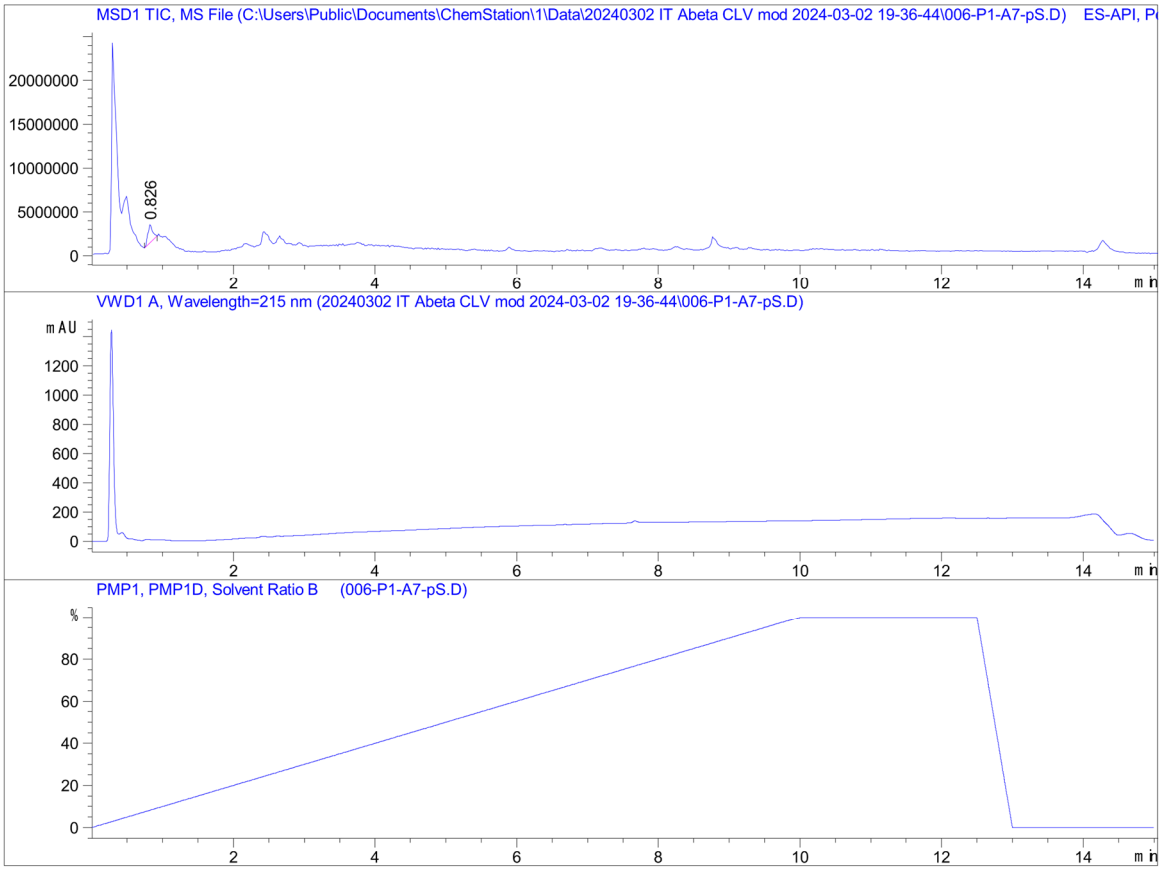

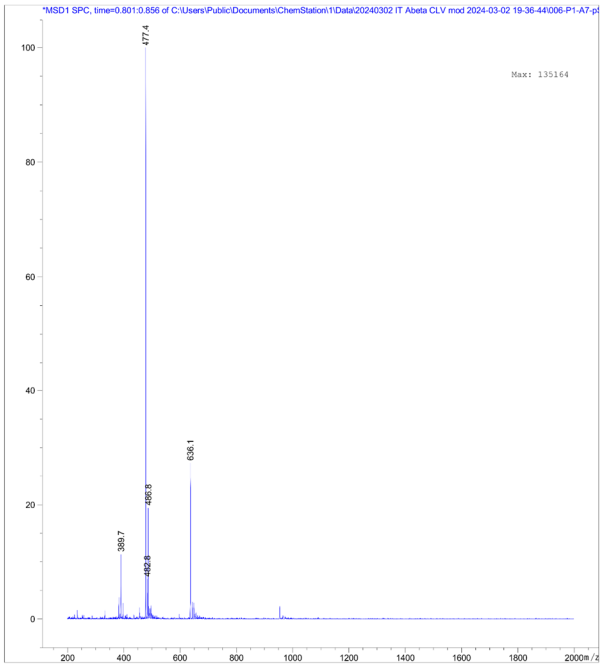

Calculated m/z

953.4 (+2)
477.2 (+4)
635.9 (+3)

1244 **A7 - µSPOT peptide library**

INDEX	NAME	PEPTIDE SEQUENCE
1	FLAG_01	DYKDDDDK
2	FLAG_02	DYKDDDDA
3	FLAG_03	DYKDDDAK
4	Abeta_fineMapping_001	GLTTRPGSGLTNIKT
5	Abeta_fineMapping_002	LTTRPGSGLTNIKTE
6	Abeta_fineMapping_003	TTRPGSGLTNIKTEE
7	Abeta_fineMapping_004	TRPGSGLTNIKTEEI
8	Abeta_fineMapping_005	RPGSGLTNIKTEEIS
9	Abeta_fineMapping_006	PGSGLTNIKTEEISE
10	Abeta_fineMapping_007	GSGLTNIKTEEISEV
11	Abeta_fineMapping_008	SGLTNIKTEEISEVK
12	Abeta_fineMapping_009	GLTNIKTEEISEVKM
13	Abeta_fineMapping_010	LTNIKTEEISEVKMD
14	Abeta_fineMapping_011	TNIKTEEISEVKMDA
15	Abeta_fineMapping_012	NIKTEEISEVKMDAE
16	Abeta_fineMapping_013	IKTEEISEVKMDAEF
17	Abeta_fineMapping_014	KTEEISEVKMDAEFR
18	Abeta_fineMapping_015	TEEISEVKMDAEFRH
19	Abeta_fineMapping_016	EEISEVKMDAEFRHD
20	Abeta_fineMapping_017	EISEVKMDAEFRHDS
21	Abeta_fineMapping_018	ISEVKMDAEFRHDSG
22	Abeta_fineMapping_019	SEVKMDAEFRHDSGY
23	Abeta_fineMapping_020	EVKMDAEFRHDSGYE
24	Abeta_fineMapping_021	VKMDAEFRHDSGYEV
25	Abeta_fineMapping_022	KMDAEFRHDSGYEVH
26	Abeta_fineMapping_023	MDAEFRHDSGYEVHH
27	Abeta_fineMapping_024	DAEFRHDSGYEVHHQ
28	Abeta_fineMapping_025	AEFRHDSGYEVHHQK
29	Abeta_fineMapping_026	EFRHDSGYEVHHQKL
30	Abeta_fineMapping_027	FRHDSGYEVHHQKLV
31	Abeta_fineMapping_028	RHDSGYEVHHQKLVF
32	Abeta_fineMapping_029	HDSGYEVHHQKLVFF
33	Abeta_fineMapping_030	DSGYEVHHQKLVFFA
34	Abeta_fineMapping_031	SGYEVHHQKLVFFAE
35	Abeta_fineMapping_032	GYEVHHQKLVFFAED
36	Abeta_fineMapping_033	YEVHHQKLVFFAEDV
37	Abeta_fineMapping_034	EVHHQKLVFFAEDVG
38	Abeta_fineMapping_035	VHHQKLVFFAEDVGS
39	Abeta_fineMapping_036	HHQKLVFFAEDVGSN
40	Abeta_fineMapping_037	HQKLVFFAEDVGSNK

41	Abeta_fineMapping_038	QKLVFFAEDVGSNKG
42	Abeta_fineMapping_039	KLVFFAEDVGSNKGA
43	Abeta_fineMapping_040	LVFFAEDVGSNKGAI
44	Abeta_fineMapping_041	VFFAEDVGSNKGAII
45	Abeta_fineMapping_042	FFAEDVGSNKGAIIG
46	Abeta_fineMapping_043	FAEDVGSNKGAIIGL
47	Abeta_fineMapping_044	AEDVGSNKGAIIGLM
48	Abeta_fineMapping_045	EDVGSNKGAIIGLMV
49	Abeta_fineMapping_046	DVGSNKGAIIGLMVG
50	Abeta_fineMapping_047	VGSNKGAIIGLMVGG
51	Abeta_fineMapping_048	GSNKGAIIGLMVGGV
52	Abeta_fineMapping_049	SNKGAIIGLMVGGVV
53	Abeta_fineMapping_050	NKGAIIGLMVGGVVI
54	Abeta_fineMapping_051	KGAIIGLMVGGVVIA
55	Abeta_fineMapping_052	GAIIGLMVGGVVIAT
56	Abeta_fineMapping_053	AIIGLMVGGVVIATV
57	Abeta_fineMapping_054	IIGLMVGGVVIATVI
58	Abeta_fineMapping_055	IGLMVGGVVIATVIV
59	Abeta_fineMapping_056	GLMVGGVVIATVIVI
60	Abeta_fineMapping_057	LMVGGVVIATVIVIT
61	Abeta_fineMapping_058	MVGGVVIATVIVITL
62	Abeta_fineMapping_059	VGGVVIATVIVITLV
63	Abeta_fineMapping_060	GGVVIATVIVITLVM
64	FP_-K10-S8_001	ATEEISEVKMDAEFRHDS
65	FP_-K10-S8_002	CTEEISEVKMDAEFRHDS
66	FP_-K10-S8_003	DTEEISEVKMDAEFRHDS
67	FP_-K10-S8_004	ETEEISEVKMDAEFRHDS
68	FP_-K10-S8_005	FTEEISEVKMDAEFRHDS
69	FP_-K10-S8_006	GTEEISEVKMDAEFRHDS
70	FP_-K10-S8_007	HTEEISEVKMDAEFRHDS
71	FP_-K10-S8_008	ITEEISEVKMDAEFRHDS
72	FP_-K10-S8_009	KTEEISEVKMDAEFRHDS
73	FP_-K10-S8_010	LTEEISEVKMDAEFRHDS
74	FP_-K10-S8_011	MTEEISEVKMDAEFRHDS
75	FP_-K10-S8_012	NTEEISEVKMDAEFRHDS
76	FP_-K10-S8_013	PTEEISEVKMDAEFRHDS
77	FP_-K10-S8_014	QTEEISEVKMDAEFRHDS
78	FP_-K10-S8_015	RTEEISEVKMDAEFRHDS
79	FP_-K10-S8_016	STEEISEVKMDAEFRHDS
80	FP_-K10-S8_017	TTEEISEVKMDAEFRHDS
81	FP_-K10-S8_018	VTEEISEVKMDAEFRHDS
82	FP_-K10-S8_019	WTEEISEVKMDAEFRHDS
83	FP_-K10-S8_020	YTEEISEVKMDAEFRHDS

84	FP_-K10-S8_021	KAEEISEVKMDAEFRHDS
85	FP_-K10-S8_022	KCEEISEVKMDAEFRHDS
86	FP_-K10-S8_023	KDEEISEVKMDAEFRHDS
87	FP_-K10-S8_024	KEEEISEVKMDAEFRHDS
88	FP_-K10-S8_025	KFEEISEVKMDAEFRHDS
89	FP_-K10-S8_026	KGEEISEVKMDAEFRHDS
90	FP_-K10-S8_027	KHEEISEVKMDAEFRHDS
91	FP_-K10-S8_028	KIEEISEVKMDAEFRHDS
92	FP_-K10-S8_029	KKEEISEVKMDAEFRHDS
93	FP_-K10-S8_030	KLEEISEVKMDAEFRHDS
94	FP_-K10-S8_031	KMEEISEVKMDAEFRHDS
95	FP_-K10-S8_032	KNEEISEVKMDAEFRHDS
96	FP_-K10-S8_033	KPEEISEVKMDAEFRHDS
97	FP_-K10-S8_034	KQEEISEVKMDAEFRHDS
98	FP_-K10-S8_035	KREEISEVKMDAEFRHDS
99	FP_-K10-S8_036	KSEEISEVKMDAEFRHDS
100	FP_-K10-S8_037	KTEEISEVKMDAEFRHDS
101	FP_-K10-S8_038	KVEEISEVKMDAEFRHDS
102	FP_-K10-S8_039	KWEEISEVKMDAEFRHDS
103	FP_-K10-S8_040	KYEEISEVKMDAEFRHDS
104	FP_-K10-S8_041	KTAEISEVKMDAEFRHDS
105	FP_-K10-S8_042	KTCEISEVKMDAEFRHDS
106	FP_-K10-S8_043	KTDEISEVKMDAEFRHDS
107	FP_-K10-S8_044	KTEEISEVKMDAEFRHDS
108	FP_-K10-S8_045	KTFEISEVKMDAEFRHDS
109	FP_-K10-S8_046	KTGEISEVKMDAEFRHDS
110	FP_-K10-S8_047	KTHEISEVKMDAEFRHDS
111	FP_-K10-S8_048	KTIEISEVKMDAEFRHDS
112	FP_-K10-S8_049	KTKEISEVKMDAEFRHDS
113	FP_-K10-S8_050	KTLEISEVKMDAEFRHDS
114	FP_-K10-S8_051	KTMEISEVKMDAEFRHDS
115	FP_-K10-S8_052	KTNEISEVKMDAEFRHDS
116	FP_-K10-S8_053	KTPEISEVKMDAEFRHDS
117	FP_-K10-S8_054	KTQEISEVKMDAEFRHDS
118	FP_-K10-S8_055	KTREISEVKMDAEFRHDS
119	FP_-K10-S8_056	KTSEISEVKMDAEFRHDS
120	FP_-K10-S8_057	KTTEISEVKMDAEFRHDS
121	FP_-K10-S8_058	KTVEISEVKMDAEFRHDS
122	FP_-K10-S8_059	KTWEISEVKMDAEFRHDS
123	FP_-K10-S8_060	KTYEISEVKMDAEFRHDS
124	FP_-K10-S8_061	KTEAISEVKMDAEFRHDS
125	FP_-K10-S8_062	KTECISEVKMDAEFRHDS
126	FP_-K10-S8_063	KTEDISEVKMDAEFRHDS

127	FP_-K10-S8_064	KTEEISEVKMDAEFRHDS
128	FP_-K10-S8_065	KTEFISEVKMDAEFRHDS
129	FP_-K10-S8_066	KTEGISEVKMDAEFRHDS
130	FP_-K10-S8_067	KTEHISEVKMDAEFRHDS
131	FP_-K10-S8_068	KTEIISEVKMDAEFRHDS
132	FP_-K10-S8_069	KTEKISEVKMDAEFRHDS
133	FP_-K10-S8_070	KTELISEVKMDAEFRHDS
134	FP_-K10-S8_071	KTEMISEVKMDAEFRHDS
135	FP_-K10-S8_072	KTENISEVKMDAEFRHDS
136	FP_-K10-S8_073	KTEPISEVKMDAEFRHDS
137	FP_-K10-S8_074	KTEQISEVKMDAEFRHDS
138	FP_-K10-S8_075	KTERISEVKMDAEFRHDS
139	FP_-K10-S8_076	KTESISEVKMDAEFRHDS
140	FP_-K10-S8_077	KTETISEVKMDAEFRHDS
141	FP_-K10-S8_078	KTEVISEVKMDAEFRHDS
142	FP_-K10-S8_079	KTEWISEVKMDAEFRHDS
143	FP_-K10-S8_080	KTEYISEVKMDAEFRHDS
144	FP_-K10-S8_081	KTEEASEVKMDAEFRHDS
145	FP_-K10-S8_082	KTEECSEVKMDAEFRHDS
146	FP_-K10-S8_083	KTEEDSEVKMDAEFRHDS
147	FP_-K10-S8_084	KTEEESEVKMDAEFRHDS
148	FP_-K10-S8_085	KTEEFSEVKMDAEFRHDS
149	FP_-K10-S8_086	KTEEGSEVKMDAEFRHDS
150	FP_-K10-S8_087	KTEEHSEVKMDAEFRHDS
151	FP_-K10-S8_088	KTEEISEVKMDAEFRHDS
152	FP_-K10-S8_089	KTEEKSEVKMDAEFRHDS
153	FP_-K10-S8_090	KTEELSEVKMDAEFRHDS
154	FP_-K10-S8_091	KTEEMSEVKMDAEFRHDS
155	FP_-K10-S8_092	KTEENSEVKMDAEFRHDS
156	FP_-K10-S8_093	KTEEPSEVKMDAEFRHDS
157	FP_-K10-S8_094	KTEEQSEVKMDAEFRHDS
158	FP_-K10-S8_095	KTEERSEVKMDAEFRHDS
159	FP_-K10-S8_096	KTEESSEVKMDAEFRHDS
160	FP_-K10-S8_097	KTEETSEVKMDAEFRHDS
161	FP_-K10-S8_098	KTEEVSEVKMDAEFRHDS
162	FP_-K10-S8_099	KTEEWSEVKMDAEFRHDS
163	FP_-K10-S8_100	KTEEYSEVKMDAEFRHDS
164	FP_-K10-S8_101	KTEEIAEVKMDAEFRHDS
165	FP_-K10-S8_102	KTEEICEVKMDAEFRHDS
166	FP_-K10-S8_103	KTEEIDEVKMDAEFRHDS
167	FP_-K10-S8_104	KTEEIEEVKMDAEFRHDS
168	FP_-K10-S8_105	KTEEIFEVKMDAEFRHDS
169	FP_-K10-S8_106	KTEEIGEVKMDAEFRHDS

170	FP_-K10-S8_107	KTEEIHEVKMDAEFRHDS
171	FP_-K10-S8_108	KTEEIIEVKMDAEFRHDS
172	FP_-K10-S8_109	KTEEIKEVKMDAEFRHDS
173	FP_-K10-S8_110	KTEEILEVKMDAEFRHDS
174	FP_-K10-S8_111	KTEEIMEVKMDAEFRHDS
175	FP_-K10-S8_112	KTEEINEVKMDAEFRHDS
176	FP_-K10-S8_113	KTEEIPEVKMDAEFRHDS
177	FP_-K10-S8_114	KTEEIQEVKMDAEFRHDS
178	FP_-K10-S8_115	KTEEIREVKMDAEFRHDS
179	FP_-K10-S8_116	KTEEISEVKMDAEFRHDS
180	FP_-K10-S8_117	KTEEITEVKMDAEFRHDS
181	FP_-K10-S8_118	KTEEIVEVKMDAEFRHDS
182	FP_-K10-S8_119	KTEEIWEVKMDAEFRHDS
183	FP_-K10-S8_120	KTEEIYEVKMDAEFRHDS
184	FP_-K10-S8_121	KTEEISAVKMDAEFRHDS
185	FP_-K10-S8_122	KTEEISCVKMDAEFRHDS
186	FP_-K10-S8_123	KTEEISDVKMDAEFRHDS
187	FP_-K10-S8_124	KTEEISEVKMDAEFRHDS
188	FP_-K10-S8_125	KTEEISFVKMDAEFRHDS
189	FP_-K10-S8_126	KTEEISGVKMDAEFRHDS
190	FP_-K10-S8_127	KTEEISHVKMDAEFRHDS
191	FP_-K10-S8_128	KTEEISIVKMDAEFRHDS
192	FP_-K10-S8_129	KTEEISKVKMDAEFRHDS
193	FP_-K10-S8_130	KTEEISLVKMDAEFRHDS
194	FP_-K10-S8_131	KTEEISMVKMDAEFRHDS
195	FP_-K10-S8_132	KTEEISNVKMDAEFRHDS
196	FP_-K10-S8_133	KTEEISPVKMDAEFRHDS
197	FP_-K10-S8_134	KTEEISQVKMDAEFRHDS
198	FP_-K10-S8_135	KTEEISRVKMDAEFRHDS
199	FP_-K10-S8_136	KTEEISSVKMDAEFRHDS
200	FP_-K10-S8_137	KTEEISTVKMDAEFRHDS
201	FP_-K10-S8_138	KTEEISVVKMDAEFRHDS
202	FP_-K10-S8_139	KTEEISWVKMDAEFRHDS
203	FP_-K10-S8_140	KTEEISYVKMDAEFRHDS
204	FP_-K10-S8_141	KTEEISEAKMDAEFRHDS
205	FP_-K10-S8_142	KTEEISECKMDAEFRHDS
206	FP_-K10-S8_143	KTEEISEDKMDAEFRHDS
207	FP_-K10-S8_144	KTEEISEEKMDAEFRHDS
208	FP_-K10-S8_145	KTEEISEFKMDAEFRHDS
209	FP_-K10-S8_146	KTEEISEGKMDAEFRHDS
210	FP_-K10-S8_147	KTEEISEHKMDAEFRHDS
211	FP_-K10-S8_148	KTEEISEIKMDAEFRHDS
212	FP_-K10-S8_149	KTEEISEKKMDAEFRHDS

213	FP_-K10-S8_150	KTEEISELKMDAEFRHDS
214	FP_-K10-S8_151	KTEEISEMKMDAEFRHDS
215	FP_-K10-S8_152	KTEEISENKMDAEFRHDS
216	FP_-K10-S8_153	KTEEISEPKMDAEFRHDS
217	FP_-K10-S8_154	KTEEISEQKMDAEFRHDS
218	FP_-K10-S8_155	KTEEISERKMDAEFRHDS
219	FP_-K10-S8_156	KTEEISESKMDAEFRHDS
220	FP_-K10-S8_157	KTEEISETKMDAEFRHDS
221	FP_-K10-S8_158	KTEEISEVKMDAEFRHDS
222	FP_-K10-S8_159	KTEEISEWKMDAEFRHDS
223	FP_-K10-S8_160	KTEEISEYKMDAEFRHDS
224	FP_-K10-S8_161	KTEEISEVAMDAEFRHDS
225	FP_-K10-S8_162	KTEEISEVCMDAEFRHDS
226	FP_-K10-S8_163	KTEEISEVDMDAEFRHDS
227	FP_-K10-S8_164	KTEEISEVEMDAEFRHDS
228	FP_-K10-S8_165	KTEEISEVFMDAEFRHDS
229	FP_-K10-S8_166	KTEEISEVGMDAEFRHDS
230	FP_-K10-S8_167	KTEEISEVHMDAEFRHDS
231	FP_-K10-S8_168	KTEEISEVIMDAEFRHDS
232	FP_-K10-S8_169	KTEEISEVKMDAEFRHDS
233	FP_-K10-S8_170	KTEEISEVLMDAEFRHDS
234	FP_-K10-S8_171	KTEEISEVMMDAEFRHDS
235	FP_-K10-S8_172	KTEEISEVNMDAEFRHDS
236	FP_-K10-S8_173	KTEEISEVPMDAEFRHDS
237	FP_-K10-S8_174	KTEEISEVQMDAEFRHDS
238	FP_-K10-S8_175	KTEEISEVRMDAEFRHDS
239	FP_-K10-S8_176	KTEEISEVSMDAEFRHDS
240	FP_-K10-S8_177	KTEEISEVTMDAEFRHDS
241	FP_-K10-S8_178	KTEEISEVVMDAEFRHDS
242	FP_-K10-S8_179	KTEEISEVWMDAEFRHDS
243	FP_-K10-S8_180	KTEEISEVYMDAEFRHDS
244	FP_-K10-S8_181	KTEEISEVKADAEFRHDS
245	FP_-K10-S8_182	KTEEISEVKCDAEFRHDS
246	FP_-K10-S8_183	KTEEISEVKDDAEFRHDS
247	FP_-K10-S8_184	KTEEISEVKEDAEFRHDS
248	FP_-K10-S8_185	KTEEISEVKFDAEFRHDS
249	FP_-K10-S8_186	KTEEISEVKGDAEFRHDS
250	FP_-K10-S8_187	KTEEISEVKHDAEFRHDS
251	FP_-K10-S8_188	KTEEISEVKIDAEFRHDS
252	FP_-K10-S8_189	KTEEISEVKKDAEFRHDS
253	FP_-K10-S8_190	KTEEISEVKLDAEFRHDS
254	FP_-K10-S8_191	KTEEISEVKMDAEFRHDS
255	FP_-K10-S8_192	KTEEISEVKNDAEFRHDS

256	FP_-K10-S8_193	KTEEISEVKPDAEFRHDS
257	FP_-K10-S8_194	KTEEISEVKQDAEFRHDS
258	FP_-K10-S8_195	KTEEISEVKRDAEFRHDS
259	FP_-K10-S8_196	KTEEISEVKSDAEFRHDS
260	FP_-K10-S8_197	KTEEISEVKTDAEFRHDS
261	FP_-K10-S8_198	KTEEISEVKVDAEFRHDS
262	FP_-K10-S8_199	KTEEISEVKWDAEFRHDS
263	FP_-K10-S8_200	KTEEISEVKYDAEFRHDS
264	FP_-K10-S8_201	KTEEISEVKMAAEFRHDS
265	FP_-K10-S8_202	KTEEISEVKMCAEFRHDS
266	FP_-K10-S8_203	KTEEISEVKMDAEFRHDS
267	FP_-K10-S8_204	KTEEISEVKMEAEFRHDS
268	FP_-K10-S8_205	KTEEISEVKMFAEFRHDS
269	FP_-K10-S8_206	KTEEISEVKMGAEFRHDS
270	FP_-K10-S8_207	KTEEISEVKMHAEFRHDS
271	FP_-K10-S8_208	KTEEISEVKMIAEFRHDS
272	FP_-K10-S8_209	KTEEISEVKMKAEFRHDS
273	FP_-K10-S8_210	KTEEISEVKMLAEFRHDS
274	FP_-K10-S8_211	KTEEISEVKMMAEFRHDS
275	FP_-K10-S8_212	KTEEISEVKMNAEFRHDS
276	FP_-K10-S8_213	KTEEISEVKMPAEFRHDS
277	FP_-K10-S8_214	KTEEISEVKMQAEFRHDS
278	FP_-K10-S8_215	KTEEISEVKMRAEFRHDS
279	FP_-K10-S8_216	KTEEISEVKMSAEFRHDS
280	FP_-K10-S8_217	KTEEISEVKMTAEFRHDS
281	FP_-K10-S8_218	KTEEISEVKMVAEFRHDS
282	FP_-K10-S8_219	KTEEISEVKMWAEFRHDS
283	FP_-K10-S8_220	KTEEISEVKMYAEFRHDS
284	FP_-K10-S8_221	KTEEISEVKMDAEFRHDS
285	FP_-K10-S8_222	KTEEISEVKMDCEFRHDS
286	FP_-K10-S8_223	KTEEISEVKMDDEFRHDS
287	FP_-K10-S8_224	KTEEISEVKMDEEFRHDS
288	FP_-K10-S8_225	KTEEISEVKMDFEFRHDS
289	FP_-K10-S8_226	KTEEISEVKMDGEFRHDS
290	FP_-K10-S8_227	KTEEISEVKMDHEFRHDS
291	FP_-K10-S8_228	KTEEISEVKMDIEFRHDS
292	FP_-K10-S8_229	KTEEISEVKMDKEFRHDS
293	FP_-K10-S8_230	KTEEISEVKMDLEFRHDS
294	FP_-K10-S8_231	KTEEISEVKMDMEFRHDS
295	FP_-K10-S8_232	KTEEISEVKMDNEFRHDS
296	FP_-K10-S8_233	KTEEISEVKMDPEFRHDS
297	FP_-K10-S8_234	KTEEISEVKMDQEFRHDS
298	FP_-K10-S8_235	KTEEISEVKMDREFRHDS

299	FP_-K10-S8_236	KTEEISEVKMDSEFRHDS
300	FP_-K10-S8_237	KTEEISEVKMDTEFRHDS
301	FP_-K10-S8_238	KTEEISEVKMDVEFRHDS
302	FP_-K10-S8_239	KTEEISEVKMDWEFRHDS
303	FP_-K10-S8_240	KTEEISEVKMDYEFRHDS
304	FP_-K10-S8_241	KTEEISEVKMDAAFRHDS
305	FP_-K10-S8_242	KTEEISEVKMDACFRHDS
306	FP_-K10-S8_243	KTEEISEVKMDADFRHDS
307	FP_-K10-S8_244	KTEEISEVKMDAEFRHDS
308	FP_-K10-S8_245	KTEEISEVKMDAFFRHDS
309	FP_-K10-S8_246	KTEEISEVKMDAGFRHDS
310	FP_-K10-S8_247	KTEEISEVKMDAHFRHDS
311	FP_-K10-S8_248	KTEEISEVKMDAIFRHDS
312	FP_-K10-S8_249	KTEEISEVKMDAKFRHDS
313	FP_-K10-S8_250	KTEEISEVKMDALFRHDS
314	FP_-K10-S8_251	KTEEISEVKMDAMFRHDS
315	FP_-K10-S8_252	KTEEISEVKMDANFRHDS
316	FP_-K10-S8_253	KTEEISEVKMDAPFRHDS
317	FP_-K10-S8_254	KTEEISEVKMDAQFRHDS
318	FP_-K10-S8_255	KTEEISEVKMDARFRHDS
319	FP_-K10-S8_256	KTEEISEVKMDASFRHDS
320	FP_-K10-S8_257	KTEEISEVKMDATFRHDS
321	FP_-K10-S8_258	KTEEISEVKMDAVFRHDS
322	FP_-K10-S8_259	KTEEISEVKMDAWFRHDS
323	FP_-K10-S8_260	KTEEISEVKMDAYFRHDS
324	FP_-K10-S8_261	KTEEISEVKMDAEARHDS
325	FP_-K10-S8_262	KTEEISEVKMDAECRHDS
326	FP_-K10-S8_263	KTEEISEVKMDAEDRHDS
327	FP_-K10-S8_264	KTEEISEVKMDAEERHDS
328	FP_-K10-S8_265	KTEEISEVKMDAEFRHDS
329	FP_-K10-S8_266	KTEEISEVKMDAEGRHDS
330	FP_-K10-S8_267	KTEEISEVKMDAEHRHDS
331	FP_-K10-S8_268	KTEEISEVKMDAEIRHDS
332	FP_-K10-S8_269	KTEEISEVKMDAEKRHDS
333	FP_-K10-S8_270	KTEEISEVKMDAELRHDS
334	FP_-K10-S8_271	KTEEISEVKMDAEMRHDS
335	FP_-K10-S8_272	KTEEISEVKMDAENRHDS
336	FP_-K10-S8_273	KTEEISEVKMDAEPRHDS
337	FP_-K10-S8_274	KTEEISEVKMDAEQRHDS
338	FP_-K10-S8_275	KTEEISEVKMDAERRHDS
339	FP_-K10-S8_276	KTEEISEVKMDAESRHDS
340	FP_-K10-S8_277	KTEEISEVKMDAETRHDS
341	FP_-K10-S8_278	KTEEISEVKMDAEVRHDS

342	FP_-K10-S8_279	KTEEISEVKMDAEWRHDS
343	FP_-K10-S8_280	KTEEISEVKMDAEYRHDS
344	FP_-K10-S8_281	KTEEISEVKMDAEFAHDS
345	FP_-K10-S8_282	KTEEISEVKMDAEFCHDS
346	FP_-K10-S8_283	KTEEISEVKMDAEFDHDS
347	FP_-K10-S8_284	KTEEISEVKMDAEFEHDS
348	FP_-K10-S8_285	KTEEISEVKMDAEFFHDS
349	FP_-K10-S8_286	KTEEISEVKMDAEFGHDS
350	FP_-K10-S8_287	KTEEISEVKMDAEFHHDS
351	FP_-K10-S8_288	KTEEISEVKMDAEFIHDS
352	FP_-K10-S8_289	KTEEISEVKMDAEFKHDS
353	FP_-K10-S8_290	KTEEISEVKMDAEFLHDS
354	FP_-K10-S8_291	KTEEISEVKMDAEFMHDS
355	FP_-K10-S8_292	KTEEISEVKMDAEFNHDS
356	FP_-K10-S8_293	KTEEISEVKMDAEFPHDS
357	FP_-K10-S8_294	KTEEISEVKMDAEFQHDS
358	FP_-K10-S8_295	KTEEISEVKMDAEFRHDS
359	FP_-K10-S8_296	KTEEISEVKMDAEFSHDS
360	FP_-K10-S8_297	KTEEISEVKMDAEFTHDS
361	FP_-K10-S8_298	KTEEISEVKMDAEFVHDS
362	FP_-K10-S8_299	KTEEISEVKMDAEFWHDS
363	FP_-K10-S8_300	KTEEISEVKMDAEFYHDS
364	FP_-K10-S8_301	KTEEISEVKMDAEFRADS
365	FP_-K10-S8_302	KTEEISEVKMDAEFRCDS
366	FP_-K10-S8_303	KTEEISEVKMDAEFRDDS
367	FP_-K10-S8_304	KTEEISEVKMDAEFREDS
368	FP_-K10-S8_305	KTEEISEVKMDAEFRFDS
369	FP_-K10-S8_306	KTEEISEVKMDAEFRGDS
370	FP_-K10-S8_307	KTEEISEVKMDAEFRHDS
371	FP_-K10-S8_308	KTEEISEVKMDAEFRIDS
372	FP_-K10-S8_309	KTEEISEVKMDAEFRKDS
373	FP_-K10-S8_310	KTEEISEVKMDAEFRLDS
374	FP_-K10-S8_311	KTEEISEVKMDAEFRMDS
375	FP_-K10-S8_312	KTEEISEVKMDAEFRNDS
376	FP_-K10-S8_313	KTEEISEVKMDAEFRPDS
377	FP_-K10-S8_314	KTEEISEVKMDAEFRQDS
378	FP_-K10-S8_315	KTEEISEVKMDAEFRRDS
379	FP_-K10-S8_316	KTEEISEVKMDAEFRSDS
380	FP_-K10-S8_317	KTEEISEVKMDAEFRTDS
381	FP_-K10-S8_318	KTEEISEVKMDAEFRVDS
382	FP_-K10-S8_319	KTEEISEVKMDAEFRWDS
383	FP_-K10-S8_320	KTEEISEVKMDAEFRYDS
384	FP_-K10-S8_321	KTEEISEVKMDAEFRHAS

385	FP_-K10-S8_322	KTEEISEVKMDAEFRHCS
386	FP_-K10-S8_323	KTEEISEVKMDAEFRHDS
387	FP_-K10-S8_324	KTEEISEVKMDAEFRHES
388	FP_-K10-S8_325	KTEEISEVKMDAEFRHFS
389	FP_-K10-S8_326	KTEEISEVKMDAEFRHGS
390	FP_-K10-S8_327	KTEEISEVKMDAEFRHHS
391	FP_-K10-S8_328	KTEEISEVKMDAEFRHIS
392	FP_-K10-S8_329	KTEEISEVKMDAEFRHKS
393	FP_-K10-S8_330	KTEEISEVKMDAEFRHLS
394	FP_-K10-S8_331	KTEEISEVKMDAEFRHMS
395	FP_-K10-S8_332	KTEEISEVKMDAEFRHNS
396	FP_-K10-S8_333	KTEEISEVKMDAEFRHPS
397	FP_-K10-S8_334	KTEEISEVKMDAEFRHQS
398	FP_-K10-S8_335	KTEEISEVKMDAEFRHRS
399	FP_-K10-S8_336	KTEEISEVKMDAEFRHSS
400	FP_-K10-S8_337	KTEEISEVKMDAEFRHTS
401	FP_-K10-S8_338	KTEEISEVKMDAEFRHVS
402	FP_-K10-S8_339	KTEEISEVKMDAEFRHWS
403	FP_-K10-S8_340	KTEEISEVKMDAEFRHYS
404	FP_-K10-S8_341	KTEEISEVKMDAEFRHDA
405	FP_-K10-S8_342	KTEEISEVKMDAEFRHDC
406	FP_-K10-S8_343	KTEEISEVKMDAEFRHDD
407	FP_-K10-S8_344	KTEEISEVKMDAEFRHDE
408	FP_-K10-S8_345	KTEEISEVKMDAEFRHDF
409	FP_-K10-S8_346	KTEEISEVKMDAEFRHDG
410	FP_-K10-S8_347	KTEEISEVKMDAEFRHDH
411	FP_-K10-S8_348	KTEEISEVKMDAEFRHDI
412	FP_-K10-S8_349	KTEEISEVKMDAEFRHDK
413	FP_-K10-S8_350	KTEEISEVKMDAEFRHDL
414	FP_-K10-S8_351	KTEEISEVKMDAEFRHDM
415	FP_-K10-S8_352	KTEEISEVKMDAEFRHDN
416	FP_-K10-S8_353	KTEEISEVKMDAEFRHDP
417	FP_-K10-S8_354	KTEEISEVKMDAEFRHDQ
418	FP_-K10-S8_355	KTEEISEVKMDAEFRHDR
419	FP_-K10-S8_356	KTEEISEVKMDAEFRHDS
420	FP_-K10-S8_357	KTEEISEVKMDAEFRHDT
421	FP_-K10-S8_358	KTEEISEVKMDAEFRHDV
422	FP_-K10-S8_359	KTEEISEVKMDAEFRHDW
423	FP_-K10-S8_360	KTEEISEVKMDAEFRHDY
424	FP_-3V-Q15_001	AKMDAEFRHDSGYEVHHQ
425	FP_-3V-Q15_002	CKMDAEFRHDSGYEVHHQ
426	FP_-3V-Q15_003	DKMDAEFRHDSGYEVHHQ
427	FP_-3V-Q15_004	EKMDAEFRHDSGYEVHHQ

428	FP_-3V-Q15_005	FKMDAEFRHDSGYEVHHQ
429	FP_-3V-Q15_006	GKMDAEFRHDSGYEVHHQ
430	FP_-3V-Q15_007	HKMDAEFRHDSGYEVHHQ
431	FP_-3V-Q15_008	IKMDAEFRHDSGYEVHHQ
432	FP_-3V-Q15_009	KKMDAEFRHDSGYEVHHQ
433	FP_-3V-Q15_010	LKMDAEFRHDSGYEVHHQ
434	FP_-3V-Q15_011	MKMDAEFRHDSGYEVHHQ
435	FP_-3V-Q15_012	NKMDAEFRHDSGYEVHHQ
436	FP_-3V-Q15_013	PKMDAEFRHDSGYEVHHQ
437	FP_-3V-Q15_014	QKMDAEFRHDSGYEVHHQ
438	FP_-3V-Q15_015	RKMDAEFRHDSGYEVHHQ
439	FP_-3V-Q15_016	SKMDAEFRHDSGYEVHHQ
440	FP_-3V-Q15_017	TKMDAEFRHDSGYEVHHQ
441	FP_-3V-Q15_018	VKMDAEFRHDSGYEVHHQ
442	FP_-3V-Q15_019	WKMDAEFRHDSGYEVHHQ
443	FP_-3V-Q15_020	YKMDAEFRHDSGYEVHHQ
444	FP_-3V-Q15_021	VAMDAEFRHDSGYEVHHQ
445	FP_-3V-Q15_022	VCMDAEFRHDSGYEVHHQ
446	FP_-3V-Q15_023	VDMDAEFRHDSGYEVHHQ
447	FP_-3V-Q15_024	VEMDAEFRHDSGYEVHHQ
448	FP_-3V-Q15_025	VFMDAEFRHDSGYEVHHQ
449	FP_-3V-Q15_026	VGMDAEFRHDSGYEVHHQ
450	FP_-3V-Q15_027	VHMDAEFRHDSGYEVHHQ
451	FP_-3V-Q15_028	VIMDAEFRHDSGYEVHHQ
452	FP_-3V-Q15_029	VKMDAEFRHDSGYEVHHQ
453	FP_-3V-Q15_030	VLMDAEFRHDSGYEVHHQ
454	FP_-3V-Q15_031	VMMDAEFRHDSGYEVHHQ
455	FP_-3V-Q15_032	VNMDAEFRHDSGYEVHHQ
456	FP_-3V-Q15_033	VPMDAEFRHDSGYEVHHQ
457	FP_-3V-Q15_034	VQMDAEFRHDSGYEVHHQ
458	FP_-3V-Q15_035	VRMDAEFRHDSGYEVHHQ
459	FP_-3V-Q15_036	VSMDAEFRHDSGYEVHHQ
460	FP_-3V-Q15_037	VTMDAEFRHDSGYEVHHQ
461	FP_-3V-Q15_038	VVMDAEFRHDSGYEVHHQ
462	FP_-3V-Q15_039	VWMDAEFRHDSGYEVHHQ
463	FP_-3V-Q15_040	VYMDAEFRHDSGYEVHHQ
464	FP_-3V-Q15_041	VKADAEFRHDSGYEVHHQ
465	FP_-3V-Q15_042	VKCDAEFRHDSGYEVHHQ
466	FP_-3V-Q15_043	VKDDAEFRHDSGYEVHHQ
467	FP_-3V-Q15_044	VKEDAEFRHDSGYEVHHQ
468	FP_-3V-Q15_045	VKFDAEFRHDSGYEVHHQ
469	FP_-3V-Q15_046	VKGDAEFRHDSGYEVHHQ
470	FP_-3V-Q15_047	VKHDAEFRHDSGYEVHHQ

471	FP_-3V-Q15_048	VKIDAEFRHDSGYEVHHQ
472	FP_-3V-Q15_049	VKKDAEFRHDSGYEVHHQ
473	FP_-3V-Q15_050	VKLDAEFRHDSGYEVHHQ
474	FP_-3V-Q15_051	VKMDAEFRHDSGYEVHHQ
475	FP_-3V-Q15_052	VKNDAEFRHDSGYEVHHQ
476	FP_-3V-Q15_053	VKPDAEFRHDSGYEVHHQ
477	FP_-3V-Q15_054	VKQDAEFRHDSGYEVHHQ
478	FP_-3V-Q15_055	VKRDAEFRHDSGYEVHHQ
479	FP_-3V-Q15_056	VKSDAEFRHDSGYEVHHQ
480	FP_-3V-Q15_057	VKTDAEFRHDSGYEVHHQ
481	FP_-3V-Q15_058	VKVDAEFRHDSGYEVHHQ
482	FP_-3V-Q15_059	VKWDAEFRHDSGYEVHHQ
483	FP_-3V-Q15_060	VKYDAEFRHDSGYEVHHQ
484	FP_-3V-Q15_061	VKMAAEFRHDSGYEVHHQ
485	FP_-3V-Q15_062	VKMCAEFRHDSGYEVHHQ
486	FP_-3V-Q15_063	VKMDAEFRHDSGYEVHHQ
487	FP_-3V-Q15_064	VKMEAEFRHDSGYEVHHQ
488	FP_-3V-Q15_065	VKMFAEFRHDSGYEVHHQ
489	FP_-3V-Q15_066	VKMGAEFRHDSGYEVHHQ
490	FP_-3V-Q15_067	VKMHAEFRHDSGYEVHHQ
491	FP_-3V-Q15_068	VKMIAEFRHDSGYEVHHQ
492	FP_-3V-Q15_069	VKMKAEFRHDSGYEVHHQ
493	FP_-3V-Q15_070	VKMLAEFRHDSGYEVHHQ
494	FP_-3V-Q15_071	VKMMAEFRHDSGYEVHHQ
495	FP_-3V-Q15_072	VKMNAEFRHDSGYEVHHQ
496	FP_-3V-Q15_073	VKMPAEFRHDSGYEVHHQ
497	FP_-3V-Q15_074	VKMQAEFRHDSGYEVHHQ
498	FP_-3V-Q15_075	VKMRAEFRHDSGYEVHHQ
499	FP_-3V-Q15_076	VKMSAEFRHDSGYEVHHQ
500	FP_-3V-Q15_077	VKMTAEFRHDSGYEVHHQ
501	FP_-3V-Q15_078	VKMVAEFRHDSGYEVHHQ
502	FP_-3V-Q15_079	VKMWAEFRHDSGYEVHHQ
503	FP_-3V-Q15_080	VKMYAEFRHDSGYEVHHQ
504	FP_-3V-Q15_081	VKMDAEFRHDSGYEVHHQ
505	FP_-3V-Q15_082	VKMDCEFRHDSGYEVHHQ
506	FP_-3V-Q15_083	VKMDDEFRHDSGYEVHHQ
507	FP_-3V-Q15_084	VKMDEEFRHDSGYEVHHQ
508	FP_-3V-Q15_085	VKMDFEFRHDSGYEVHHQ
509	FP_-3V-Q15_086	VKMDGEFRHDSGYEVHHQ
510	FP_-3V-Q15_087	VKMDHEFRHDSGYEVHHQ
511	FP_-3V-Q15_088	VKMDIEFRHDSGYEVHHQ
512	FP_-3V-Q15_089	VKMDKEFRHDSGYEVHHQ
513	FP_-3V-Q15_090	VKMDLEFRHDSGYEVHHQ

514	FP_-3V-Q15_091	VKMDMEFRHDSGYEVHHQ
515	FP_-3V-Q15_092	VKMDNEFRHDSGYEVHHQ
516	FP_-3V-Q15_093	VKMDPEFRHDSGYEVHHQ
517	FP_-3V-Q15_094	VKMDQEFRHDSGYEVHHQ
518	FP_-3V-Q15_095	VKMDREFRHDSGYEVHHQ
519	FP_-3V-Q15_096	VKMDSEFRHDSGYEVHHQ
520	FP_-3V-Q15_097	VKMDTEFRHDSGYEVHHQ
521	FP_-3V-Q15_098	VKMDVEFRHDSGYEVHHQ
522	FP_-3V-Q15_099	VKMDWEFRHDSGYEVHHQ
523	FP_-3V-Q15_100	VKMDYEFRHDSGYEVHHQ
524	FP_-3V-Q15_101	VKMDAAFRHDSGYEVHHQ
525	FP_-3V-Q15_102	VKMDACFRHDSGYEVHHQ
526	FP_-3V-Q15_103	VKMDADFRHDSGYEVHHQ
527	FP_-3V-Q15_104	VKMDAEFRHDSGYEVHHQ
528	FP_-3V-Q15_105	VKMDAFFRHDSGYEVHHQ
529	FP_-3V-Q15_106	VKMDAGFRHDSGYEVHHQ
530	FP_-3V-Q15_107	VKMDAHFRHDSGYEVHHQ
531	FP_-3V-Q15_108	VKMDAIFRHDSGYEVHHQ
532	FP_-3V-Q15_109	VKMDAKFRHDSGYEVHHQ
533	FP_-3V-Q15_110	VKMDALFRHDSGYEVHHQ
534	FP_-3V-Q15_111	VKMDAMFRHDSGYEVHHQ
535	FP_-3V-Q15_112	VKMDANFRHDSGYEVHHQ
536	FP_-3V-Q15_113	VKMDAPFRHDSGYEVHHQ
537	FP_-3V-Q15_114	VKMDAQFRHDSGYEVHHQ
538	FP_-3V-Q15_115	VKMDARFRHDSGYEVHHQ
539	FP_-3V-Q15_116	VKMDASFRHDSGYEVHHQ
540	FP_-3V-Q15_117	VKMDATFRHDSGYEVHHQ
541	FP_-3V-Q15_118	VKMDAVFRHDSGYEVHHQ
542	FP_-3V-Q15_119	VKMDAWFRHDSGYEVHHQ
543	FP_-3V-Q15_120	VKMDAYFRHDSGYEVHHQ
544	FP_-3V-Q15_121	VKMDAEARHDSGYEVHHQ
545	FP_-3V-Q15_122	VKMDAECRHDSGYEVHHQ
546	FP_-3V-Q15_123	VKMDAEDRHDSGYEVHHQ
547	FP_-3V-Q15_124	VKMDAEERHDSGYEVHHQ
548	FP_-3V-Q15_125	VKMDAEFRHDSGYEVHHQ
549	FP_-3V-Q15_126	VKMDAEGRHDSGYEVHHQ
550	FP_-3V-Q15_127	VKMDAEHRHDSGYEVHHQ
551	FP_-3V-Q15_128	VKMDAEIRHDSGYEVHHQ
552	FP_-3V-Q15_129	VKMDAEKRHDSGYEVHHQ
553	FP_-3V-Q15_130	VKMDAELRHDSGYEVHHQ
554	FP_-3V-Q15_131	VKMDAEMRHDSGYEVHHQ
555	FP_-3V-Q15_132	VKMDAENRHDSGYEVHHQ
556	FP_-3V-Q15_133	VKMDAEPRHDSGYEVHHQ

557	FP_-3V-Q15_134	VKMDAEQRHDSGYEVHHQ
558	FP_-3V-Q15_135	VKMDAERRHDSGYEVHHQ
559	FP_-3V-Q15_136	VKMDAESRHDSGYEVHHQ
560	FP_-3V-Q15_137	VKMDAETRHDSGYEVHHQ
561	FP_-3V-Q15_138	VKMDAEVRHDSGYEVHHQ
562	FP_-3V-Q15_139	VKMDAEWRHDSGYEVHHQ
563	FP_-3V-Q15_140	VKMDAEYRHDSGYEVHHQ
564	FP_-3V-Q15_141	VKMDAEFAHDSGYEVHHQ
565	FP_-3V-Q15_142	VKMDAEFCHDSGYEVHHQ
566	FP_-3V-Q15_143	VKMDAEFDHDSGYEVHHQ
567	FP_-3V-Q15_144	VKMDAEFEHDSGYEVHHQ
568	FP_-3V-Q15_145	VKMDAEFFHDSGYEVHHQ
569	FP_-3V-Q15_146	VKMDAEFGHDSGYEVHHQ
570	FP_-3V-Q15_147	VKMDAEFHHDSGYEVHHQ
571	FP_-3V-Q15_148	VKMDAEFIHDSGYEVHHQ
572	FP_-3V-Q15_149	VKMDAEFKHDSGYEVHHQ
573	FP_-3V-Q15_150	VKMDAEFLHDSGYEVHHQ
574	FP_-3V-Q15_151	VKMDAEFMHDSGYEVHHQ
575	FP_-3V-Q15_152	VKMDAEFNHDSGYEVHHQ
576	FP_-3V-Q15_153	VKMDAEFPHDSGYEVHHQ
577	FP_-3V-Q15_154	VKMDAEFQHDSGYEVHHQ
578	FP_-3V-Q15_155	VKMDAEFRHDSGYEVHHQ
579	FP_-3V-Q15_156	VKMDAEFSHDSGYEVHHQ
580	FP_-3V-Q15_157	VKMDAEFTHDSGYEVHHQ
581	FP_-3V-Q15_158	VKMDAEFVHDSGYEVHHQ
582	FP_-3V-Q15_159	VKMDAEFWHDSGYEVHHQ
583	FP_-3V-Q15_160	VKMDAEFYHDSGYEVHHQ
584	FP_-3V-Q15_161	VKMDAEFRADSGYEVHHQ
585	FP_-3V-Q15_162	VKMDAEFRCDSGYEVHHQ
586	FP_-3V-Q15_163	VKMDAEFRDDSGYEVHHQ
587	FP_-3V-Q15_164	VKMDAEFREDSGYEVHHQ
588	FP_-3V-Q15_165	VKMDAEFRFDSGYEVHHQ
589	FP_-3V-Q15_166	VKMDAEFRGDSGYEVHHQ
590	FP_-3V-Q15_167	VKMDAEFRHDSGYEVHHQ
591	FP_-3V-Q15_168	VKMDAEFRIDSGYEVHHQ
592	FP_-3V-Q15_169	VKMDAEFRKDSGYEVHHQ
593	FP_-3V-Q15_170	VKMDAEFRLDSGYEVHHQ
594	FP_-3V-Q15_171	VKMDAEFRMDSGYEVHHQ
595	FP_-3V-Q15_172	VKMDAEFRNDSGYEVHHQ
596	FP_-3V-Q15_173	VKMDAEFRPDSGYEVHHQ
597	FP_-3V-Q15_174	VKMDAEFRQDSGYEVHHQ
598	FP_-3V-Q15_175	VKMDAEFRRDSGYEVHHQ
599	FP_-3V-Q15_176	VKMDAEFRSDSGYEVHHQ

600	FP_-3V-Q15_177	VKMDAEFRTDSGYEVHHQ
601	FP_-3V-Q15_178	VKMDAEFRVDSGYEVHHQ
602	FP_-3V-Q15_179	VKMDAEFRWDSGYEVHHQ
603	FP_-3V-Q15_180	VKMDAEFRYDSGYEVHHQ
604	FP_-3V-Q15_181	VKMDAEFRHASGYEVHHQ
605	FP_-3V-Q15_182	VKMDAEFRHCSGYEVHHQ
606	FP_-3V-Q15_183	VKMDAEFRHDSGYEVHHQ
607	FP_-3V-Q15_184	VKMDAEFRHESGYEVHHQ
608	FP_-3V-Q15_185	VKMDAEFRHFSGYEVHHQ
609	FP_-3V-Q15_186	VKMDAEFRHGSGYEVHHQ
610	FP_-3V-Q15_187	VKMDAEFRHHSGYEVHHQ
611	FP_-3V-Q15_188	VKMDAEFRHISGYEVHHQ
612	FP_-3V-Q15_189	VKMDAEFRHKSGYEVHHQ
613	FP_-3V-Q15_190	VKMDAEFRHLSGYEVHHQ
614	FP_-3V-Q15_191	VKMDAEFRHMSGYEVHHQ
615	FP_-3V-Q15_192	VKMDAEFRHNSGYEVHHQ
616	FP_-3V-Q15_193	VKMDAEFRHPSGYEVHHQ
617	FP_-3V-Q15_194	VKMDAEFRHQSGYEVHHQ
618	FP_-3V-Q15_195	VKMDAEFRHRSGYEVHHQ
619	FP_-3V-Q15_196	VKMDAEFRHSSGYEVHHQ
620	FP_-3V-Q15_197	VKMDAEFRHTSGYEVHHQ
621	FP_-3V-Q15_198	VKMDAEFRHVSGYEVHHQ
622	FP_-3V-Q15_199	VKMDAEFRHWSGYEVHHQ
623	FP_-3V-Q15_200	VKMDAEFRHYSGYEVHHQ
624	FP_-3V-Q15_201	VKMDAEFRHDAGYEVHHQ
625	FP_-3V-Q15_202	VKMDAEFRHDCGYEVHHQ
626	FP_-3V-Q15_203	VKMDAEFRHDDGYEVHHQ
627	FP_-3V-Q15_204	VKMDAEFRHDEGYEVHHQ
628	FP_-3V-Q15_205	VKMDAEFRHDFGYEVHHQ
629	FP_-3V-Q15_206	VKMDAEFRHDGGYEVHHQ
630	FP_-3V-Q15_207	VKMDAEFRHDHGYEVHHQ
631	FP_-3V-Q15_208	VKMDAEFRHDIGYEVHHQ
632	FP_-3V-Q15_209	VKMDAEFRHDKGYEVHHQ
633	FP_-3V-Q15_210	VKMDAEFRHDLGYEVHHQ
634	FP_-3V-Q15_211	VKMDAEFRHDMGYEVHHQ
635	FP_-3V-Q15_212	VKMDAEFRHDNGYEVHHQ
636	FP_-3V-Q15_213	VKMDAEFRHDPGYEVHHQ
637	FP_-3V-Q15_214	VKMDAEFRHDQGYEVHHQ
638	FP_-3V-Q15_215	VKMDAEFRHDRGYEVHHQ
639	FP_-3V-Q15_216	VKMDAEFRHDSGYEVHHQ
640	FP_-3V-Q15_217	VKMDAEFRHDTGYEVHHQ
641	FP_-3V-Q15_218	VKMDAEFRHDVGYEVHHQ
642	FP_-3V-Q15_219	VKMDAEFRHDWGYEVHHQ

643	FP_-3V-Q15_220	VKMDAEFRHDYGYEVHHQ
644	FP_-3V-Q15_221	VKMDAEFRHDSAYEVHHQ
645	FP_-3V-Q15_222	VKMDAEFRHDSCYEVHHQ
646	FP_-3V-Q15_223	VKMDAEFRHDSDYEVHHQ
647	FP_-3V-Q15_224	VKMDAEFRHDSEYEVHHQ
648	FP_-3V-Q15_225	VKMDAEFRHDSFYEVHHQ
649	FP_-3V-Q15_226	VKMDAEFRHDSGYEVHHQ
650	FP_-3V-Q15_227	VKMDAEFRHDSHYEVHHQ
651	FP_-3V-Q15_228	VKMDAEFRHDSIYEVHHQ
652	FP_-3V-Q15_229	VKMDAEFRHDSKYEVHHQ
653	FP_-3V-Q15_230	VKMDAEFRHDSLYEVHHQ
654	FP_-3V-Q15_231	VKMDAEFRHDSMYEVHHQ
655	FP_-3V-Q15_232	VKMDAEFRHDSNYEVHHQ
656	FP_-3V-Q15_233	VKMDAEFRHDSPYEVHHQ
657	FP_-3V-Q15_234	VKMDAEFRHDSQYEVHHQ
658	FP_-3V-Q15_235	VKMDAEFRHDSRYEVHHQ
659	FP_-3V-Q15_236	VKMDAEFRHDSSYEVHHQ
660	FP_-3V-Q15_237	VKMDAEFRHDSTYEVHHQ
661	FP_-3V-Q15_238	VKMDAEFRHDSVYEVHHQ
662	FP_-3V-Q15_239	VKMDAEFRHDSWYEVHHQ
663	FP_-3V-Q15_240	VKMDAEFRHDSYYEVHHQ
664	FP_-3V-Q15_241	VKMDAEFRHDSGAEVHHQ
665	FP_-3V-Q15_242	VKMDAEFRHDSGCEVHHQ
666	FP_-3V-Q15_243	VKMDAEFRHDSGDEVHHQ
667	FP_-3V-Q15_244	VKMDAEFRHDSGEEVHHQ
668	FP_-3V-Q15_245	VKMDAEFRHDSGFEVHHQ
669	FP_-3V-Q15_246	VKMDAEFRHDSGGEVHHQ
670	FP_-3V-Q15_247	VKMDAEFRHDSGHEVHHQ
671	FP_-3V-Q15_248	VKMDAEFRHDSGIEVHHQ
672	FP_-3V-Q15_249	VKMDAEFRHDSGKEVHHQ
673	FP_-3V-Q15_250	VKMDAEFRHDSGLEVHHQ
674	FP_-3V-Q15_251	VKMDAEFRHDSGMEVHHQ
675	FP_-3V-Q15_252	VKMDAEFRHDSGNEVHHQ
676	FP_-3V-Q15_253	VKMDAEFRHDSGPEVHHQ
677	FP_-3V-Q15_254	VKMDAEFRHDSGQEVHHQ
678	FP_-3V-Q15_255	VKMDAEFRHDSGREVHHQ
679	FP_-3V-Q15_256	VKMDAEFRHDSGSEVHHQ
680	FP_-3V-Q15_257	VKMDAEFRHDSGTEVHHQ
681	FP_-3V-Q15_258	VKMDAEFRHDSGVEVHHQ
682	FP_-3V-Q15_259	VKMDAEFRHDSGWEVHHQ
683	FP_-3V-Q15_260	VKMDAEFRHDSGYEVHHQ
684	FP_-3V-Q15_261	VKMDAEFRHDSGYAVHHQ
685	FP_-3V-Q15_262	VKMDAEFRHDSGYCVHHQ

686	FP_-3V-Q15_263	VKMDAEFRHDSGYDVHHQ
687	FP_-3V-Q15_264	VKMDAEFRHDSGYEVHHQ
688	FP_-3V-Q15_265	VKMDAEFRHDSGYFVHHQ
689	FP_-3V-Q15_266	VKMDAEFRHDSGYGVHHQ
690	FP_-3V-Q15_267	VKMDAEFRHDSGYHVHHQ
691	FP_-3V-Q15_268	VKMDAEFRHDSGYIVHHQ
692	FP_-3V-Q15_269	VKMDAEFRHDSGYKVHHQ
693	FP_-3V-Q15_270	VKMDAEFRHDSGYLVHHQ
694	FP_-3V-Q15_271	VKMDAEFRHDSGYMVHHQ
695	FP_-3V-Q15_272	VKMDAEFRHDSGYNVHHQ
696	FP_-3V-Q15_273	VKMDAEFRHDSGYPVHHQ
697	FP_-3V-Q15_274	VKMDAEFRHDSGYQVHHQ
698	FP_-3V-Q15_275	VKMDAEFRHDSGYRVHHQ
699	FP_-3V-Q15_276	VKMDAEFRHDSGYSVHHQ
700	FP_-3V-Q15_277	VKMDAEFRHDSGYTVHHQ
701	FP_-3V-Q15_278	VKMDAEFRHDSGYVVHHQ
702	FP_-3V-Q15_279	VKMDAEFRHDSGYWVHHQ
703	FP_-3V-Q15_280	VKMDAEFRHDSGYYVHHQ
704	FP_-3V-Q15_281	VKMDAEFRHDSGYEAHHQ
705	FP_-3V-Q15_282	VKMDAEFRHDSGYECHHQ
706	FP_-3V-Q15_283	VKMDAEFRHDSGYEDHHQ
707	FP_-3V-Q15_284	VKMDAEFRHDSGYEEHHQ
708	FP_-3V-Q15_285	VKMDAEFRHDSGYEFHHQ
709	FP_-3V-Q15_286	VKMDAEFRHDSGYEGHHQ
710	FP_-3V-Q15_287	VKMDAEFRHDSGYEHHHQ
711	FP_-3V-Q15_288	VKMDAEFRHDSGYEIHHQ
712	FP_-3V-Q15_289	VKMDAEFRHDSGYEKHHQ
713	FP_-3V-Q15_290	VKMDAEFRHDSGYELHHQ
714	FP_-3V-Q15_291	VKMDAEFRHDSGYEMHHQ
715	FP_-3V-Q15_292	VKMDAEFRHDSGYENHHQ
716	FP_-3V-Q15_293	VKMDAEFRHDSGYEPHHQ
717	FP_-3V-Q15_294	VKMDAEFRHDSGYEQHHQ
718	FP_-3V-Q15_295	VKMDAEFRHDSGYERHHQ
719	FP_-3V-Q15_296	VKMDAEFRHDSGYESHHQ
720	FP_-3V-Q15_297	VKMDAEFRHDSGYETHHQ
721	FP_-3V-Q15_298	VKMDAEFRHDSGYEVHHQ
722	FP_-3V-Q15_299	VKMDAEFRHDSGYEWHHQ
723	FP_-3V-Q15_300	VKMDAEFRHDSGYEYHHQ
724	FP_-3V-Q15_301	VKMDAEFRHDSGYEVAHQ
725	FP_-3V-Q15_302	VKMDAEFRHDSGYEVCHQ
726	FP_-3V-Q15_303	VKMDAEFRHDSGYEVDHQ
727	FP_-3V-Q15_304	VKMDAEFRHDSGYEVEHQ
728	FP_-3V-Q15_305	VKMDAEFRHDSGYEVFHQ

729	FP_-3V-Q15_306	VKMDAEFRHDSGYEVGHQ
730	FP_-3V-Q15_307	VKMDAEFRHDSGYEVHHQ
731	FP_-3V-Q15_308	VKMDAEFRHDSGYEVIHQ
732	FP_-3V-Q15_309	VKMDAEFRHDSGYEVKHQ
733	FP_-3V-Q15_310	VKMDAEFRHDSGYEVLHQ
734	FP_-3V-Q15_311	VKMDAEFRHDSGYEVMHQ
735	FP_-3V-Q15_312	VKMDAEFRHDSGYEVNHQ
736	FP_-3V-Q15_313	VKMDAEFRHDSGYEVPHQ
737	FP_-3V-Q15_314	VKMDAEFRHDSGYEVQHQ
738	FP_-3V-Q15_315	VKMDAEFRHDSGYEVRHQ
739	FP_-3V-Q15_316	VKMDAEFRHDSGYEVSHQ
740	FP_-3V-Q15_317	VKMDAEFRHDSGYEVTHQ
741	FP_-3V-Q15_318	VKMDAEFRHDSGYEVVHQ
742	FP_-3V-Q15_319	VKMDAEFRHDSGYEVWHQ
743	FP_-3V-Q15_320	VKMDAEFRHDSGYEVYHQ
744	FP_-3V-Q15_321	VKMDAEFRHDSGYEVHAQ
745	FP_-3V-Q15_322	VKMDAEFRHDSGYEVHCQ
746	FP_-3V-Q15_323	VKMDAEFRHDSGYEVHDQ
747	FP_-3V-Q15_324	VKMDAEFRHDSGYEVHEQ
748	FP_-3V-Q15_325	VKMDAEFRHDSGYEVHFQ
749	FP_-3V-Q15_326	VKMDAEFRHDSGYEVHGQ
750	FP_-3V-Q15_327	VKMDAEFRHDSGYEVHHQ
751	FP_-3V-Q15_328	VKMDAEFRHDSGYEVHIQ
752	FP_-3V-Q15_329	VKMDAEFRHDSGYEVHKQ
753	FP_-3V-Q15_330	VKMDAEFRHDSGYEVHLQ
754	FP_-3V-Q15_331	VKMDAEFRHDSGYEVHMQ
755	FP_-3V-Q15_332	VKMDAEFRHDSGYEVHNQ
756	FP_-3V-Q15_333	VKMDAEFRHDSGYEVHPQ
757	FP_-3V-Q15_334	VKMDAEFRHDSGYEVHQQ
758	FP_-3V-Q15_335	VKMDAEFRHDSGYEVHRQ
759	FP_-3V-Q15_336	VKMDAEFRHDSGYEVHSQ
760	FP_-3V-Q15_337	VKMDAEFRHDSGYEVHTQ
761	FP_-3V-Q15_338	VKMDAEFRHDSGYEVHVQ
762	FP_-3V-Q15_339	VKMDAEFRHDSGYEVHWQ
763	FP_-3V-Q15_340	VKMDAEFRHDSGYEVHYQ
764	FP_-3V-Q15_341	VKMDAEFRHDSGYEVHHA
765	FP_-3V-Q15_342	VKMDAEFRHDSGYEVHHC
766	FP_-3V-Q15_343	VKMDAEFRHDSGYEVHHD
767	FP_-3V-Q15_344	VKMDAEFRHDSGYEVHHE
768	FP_-3V-Q15_345	VKMDAEFRHDSGYEVHHF
769	FP_-3V-Q15_346	VKMDAEFRHDSGYEVHHG
770	FP_-3V-Q15_347	VKMDAEFRHDSGYEVHHH
771	FP_-3V-Q15_348	VKMDAEFRHDSGYEVHHI

772	FP_-3V-Q15_349	VKMDAEFRHDSGYEVHHK
773	FP_-3V-Q15_350	VKMDAEFRHDSGYEVHHL
774	FP_-3V-Q15_351	VKMDAEFRHDSGYEVHHM
775	FP_-3V-Q15_352	VKMDAEFRHDSGYEVHHN
776	FP_-3V-Q15_353	VKMDAEFRHDSGYEVHHP
777	FP_-3V-Q15_354	VKMDAEFRHDSGYEVHHQ
778	FP_-3V-Q15_355	VKMDAEFRHDSGYEVHHR
779	FP_-3V-Q15_356	VKMDAEFRHDSGYEVHHS
780	FP_-3V-Q15_357	VKMDAEFRHDSGYEVHHT
781	FP_-3V-Q15_358	VKMDAEFRHDSGYEVHHV
782	FP_-3V-Q15_359	VKMDAEFRHDSGYEVHHW
783	FP_-3V-Q15_360	VKMDAEFRHDSGYEVHHY
784	FP_D1-V18_001	AAEFRHDSGYEVHHQKLV
785	FP_D1-V18_002	CAEFRHDSGYEVHHQKLV
786	FP_D1-V18_003	DAEFRHDSGYEVHHQKLV
787	FP_D1-V18_004	EAEFRHDSGYEVHHQKLV
788	FP_D1-V18_005	FAEFRHDSGYEVHHQKLV
789	FP_D1-V18_006	GAEFRHDSGYEVHHQKLV
790	FP_D1-V18_007	HAEFRHDSGYEVHHQKLV
791	FP_D1-V18_008	IAEFRHDSGYEVHHQKLV
792	FP_D1-V18_009	KAEFRHDSGYEVHHQKLV
793	FP_D1-V18_010	LAEFRHDSGYEVHHQKLV
794	FP_D1-V18_011	MAEFRHDSGYEVHHQKLV
795	FP_D1-V18_012	NAEFRHDSGYEVHHQKLV
796	FP_D1-V18_013	PAEFRHDSGYEVHHQKLV
797	FP_D1-V18_014	QAEFRHDSGYEVHHQKLV
798	FP_D1-V18_015	RAEFRHDSGYEVHHQKLV
799	FP_D1-V18_016	SAEFRHDSGYEVHHQKLV
800	FP_D1-V18_017	TAEFRHDSGYEVHHQKLV
801	FP_D1-V18_018	VAEFRHDSGYEVHHQKLV
802	FP_D1-V18_019	WAEFRHDSGYEVHHQKLV
803	FP_D1-V18_020	YAEFRHDSGYEVHHQKLV
804	FP_D1-V18_021	DAEFRHDSGYEVHHQKLV
805	FP_D1-V18_022	DCEFRHDSGYEVHHQKLV
806	FP_D1-V18_023	DDEFRHDSGYEVHHQKLV
807	FP_D1-V18_024	DEEFRHDSGYEVHHQKLV
808	FP_D1-V18_025	DFEFRHDSGYEVHHQKLV
809	FP_D1-V18_026	DGEFRHDSGYEVHHQKLV
810	FP_D1-V18_027	DHEFRHDSGYEVHHQKLV
811	FP_D1-V18_028	DIEFRHDSGYEVHHQKLV
812	FP_D1-V18_029	DKEFRHDSGYEVHHQKLV
813	FP_D1-V18_030	DLEFRHDSGYEVHHQKLV
814	FP_D1-V18_031	DMEFRHDSGYEVHHQKLV

815	FP_D1-V18_032	DNEFRHDSGYEVHHQKLV
816	FP_D1-V18_033	DPEFRHDSGYEVHHQKLV
817	FP_D1-V18_034	DQEFRHDSGYEVHHQKLV
818	FP_D1-V18_035	DREFRHDSGYEVHHQKLV
819	FP_D1-V18_036	DSEFRHDSGYEVHHQKLV
820	FP_D1-V18_037	DTEFRHDSGYEVHHQKLV
821	FP_D1-V18_038	DVEFRHDSGYEVHHQKLV
822	FP_D1-V18_039	DWEFRHDSGYEVHHQKLV
823	FP_D1-V18_040	DYEFRHDSGYEVHHQKLV
824	FP_D1-V18_041	DAAFRHDSGYEVHHQKLV
825	FP_D1-V18_042	DACFRHDSGYEVHHQKLV
826	FP_D1-V18_043	DADFRHDSGYEVHHQKLV
827	FP_D1-V18_044	DAEFRHDSGYEVHHQKLV
828	FP_D1-V18_045	DAFFRHDSGYEVHHQKLV
829	FP_D1-V18_046	DAGFRHDSGYEVHHQKLV
830	FP_D1-V18_047	DAHFRHDSGYEVHHQKLV
831	FP_D1-V18_048	DAIFRHDSGYEVHHQKLV
832	FP_D1-V18_049	DAKFRHDSGYEVHHQKLV
833	FP_D1-V18_050	DALFRHDSGYEVHHQKLV
834	FP_D1-V18_051	DAMFRHDSGYEVHHQKLV
835	FP_D1-V18_052	DANFRHDSGYEVHHQKLV
836	FP_D1-V18_053	DAPFRHDSGYEVHHQKLV
837	FP_D1-V18_054	DAQFRHDSGYEVHHQKLV
838	FP_D1-V18_055	DARFRHDSGYEVHHQKLV
839	FP_D1-V18_056	DASFRHDSGYEVHHQKLV
840	FP_D1-V18_057	DATFRHDSGYEVHHQKLV
841	FP_D1-V18_058	DAVFRHDSGYEVHHQKLV
842	FP_D1-V18_059	DAWFRHDSGYEVHHQKLV
843	FP_D1-V18_060	DAYFRHDSGYEVHHQKLV
844	FP_D1-V18_061	DAEARHDSGYEVHHQKLV
845	FP_D1-V18_062	DAECRHDSGYEVHHQKLV
846	FP_D1-V18_063	DAEDRHDSGYEVHHQKLV
847	FP_D1-V18_064	DAEERHDSGYEVHHQKLV
848	FP_D1-V18_065	DAEFRHDSGYEVHHQKLV
849	FP_D1-V18_066	DAEGRHDSGYEVHHQKLV
850	FP_D1-V18_067	DAEHRHDSGYEVHHQKLV
851	FP_D1-V18_068	DAEIRHDSGYEVHHQKLV
852	FP_D1-V18_069	DAEKRHDSGYEVHHQKLV
853	FP_D1-V18_070	DAELRHDSGYEVHHQKLV
854	FP_D1-V18_071	DAEMRHDSGYEVHHQKLV
855	FP_D1-V18_072	DAENRHDSGYEVHHQKLV
856	FP_D1-V18_073	DAEPRHDSGYEVHHQKLV
857	FP_D1-V18_074	DAEQRHDSGYEVHHQKLV

858	FP_D1-V18_075	DAERRHDSGYEVHHQKLV
859	FP_D1-V18_076	DAESRHDSGYEVHHQKLV
860	FP_D1-V18_077	DAETRHDSGYEVHHQKLV
861	FP_D1-V18_078	DAEVRHDSGYEVHHQKLV
862	FP_D1-V18_079	DAEWRHDSGYEVHHQKLV
863	FP_D1-V18_080	DAEYRHDSGYEVHHQKLV
864	FP_D1-V18_081	DAEFAHDSGYEVHHQKLV
865	FP_D1-V18_082	DAEFCHDSGYEVHHQKLV
866	FP_D1-V18_083	DAEFDHDSGYEVHHQKLV
867	FP_D1-V18_084	DAEFEHDSGYEVHHQKLV
868	FP_D1-V18_085	DAEFFHDSGYEVHHQKLV
869	FP_D1-V18_086	DAEFGHDSGYEVHHQKLV
870	FP_D1-V18_087	DAEFHHDSGYEVHHQKLV
871	FP_D1-V18_088	DAEFIHDSGYEVHHQKLV
872	FP_D1-V18_089	DAEFKHDSGYEVHHQKLV
873	FP_D1-V18_090	DAEFLHDSGYEVHHQKLV
874	FP_D1-V18_091	DAEFMHDSGYEVHHQKLV
875	FP_D1-V18_092	DAEFNHDSGYEVHHQKLV
876	FP_D1-V18_093	DAEFPHDSGYEVHHQKLV
877	FP_D1-V18_094	DAEFQHDSGYEVHHQKLV
878	FP_D1-V18_095	DAEFRHDSGYEVHHQKLV
879	FP_D1-V18_096	DAEFSHDSGYEVHHQKLV
880	FP_D1-V18_097	DAEFTHDSGYEVHHQKLV
881	FP_D1-V18_098	DAEFVHDSGYEVHHQKLV
882	FP_D1-V18_099	DAEFWHDSGYEVHHQKLV
883	FP_D1-V18_100	DAEFYHDSGYEVHHQKLV
884	FP_D1-V18_101	DAEFRADSGYEVHHQKLV
885	FP_D1-V18_102	DAEFRCDSGYEVHHQKLV
886	FP_D1-V18_103	DAEFRDDSGYEVHHQKLV
887	FP_D1-V18_104	DAEFREDSGYEVHHQKLV
888	FP_D1-V18_105	DAEFRFDSGYEVHHQKLV
889	FP_D1-V18_106	DAEFRGDSGYEVHHQKLV
890	FP_D1-V18_107	DAEFRHDSGYEVHHQKLV
891	FP_D1-V18_108	DAEFRIDSGYEVHHQKLV
892	FP_D1-V18_109	DAEFRKDSGYEVHHQKLV
893	FP_D1-V18_110	DAEFRLDSGYEVHHQKLV
894	FP_D1-V18_111	DAEFRMDSGYEVHHQKLV
895	FP_D1-V18_112	DAEFRNDSGYEVHHQKLV
896	FP_D1-V18_113	DAEFRPDSGYEVHHQKLV
897	FP_D1-V18_114	DAEFRQDSGYEVHHQKLV
898	FP_D1-V18_115	DAEFRRDSGYEVHHQKLV
899	FP_D1-V18_116	DAEFRSDSGYEVHHQKLV
900	FP_D1-V18_117	DAEFRTDSGYEVHHQKLV

901	FP_D1-V18_118	DAEFRVDSGYEVHHQKLV
902	FP_D1-V18_119	DAEFRWDSGYEVHHQKLV
903	FP_D1-V18_120	DAEFRYDSGYEVHHQKLV
904	FP_D1-V18_121	DAEFRHASGYEVHHQKLV
905	FP_D1-V18_122	DAEFRHCSGYEVHHQKLV
906	FP_D1-V18_123	DAEFRHDSGYEVHHQKLV
907	FP_D1-V18_124	DAEFRHESGYEVHHQKLV
908	FP_D1-V18_125	DAEFRHFSGYEVHHQKLV
909	FP_D1-V18_126	DAEFRHGSGYEVHHQKLV
910	FP_D1-V18_127	DAEFRHHSGYEVHHQKLV
911	FP_D1-V18_128	DAEFRHISGYEVHHQKLV
912	FP_D1-V18_129	DAEFRHKSGYEVHHQKLV
913	FP_D1-V18_130	DAEFRHLSGYEVHHQKLV
914	FP_D1-V18_131	DAEFRHMSGYEVHHQKLV
915	FP_D1-V18_132	DAEFRHNSGYEVHHQKLV
916	FP_D1-V18_133	DAEFRHPSGYEVHHQKLV
917	FP_D1-V18_134	DAEFRHQSGYEVHHQKLV
918	FP_D1-V18_135	DAEFRHRSGYEVHHQKLV
919	FP_D1-V18_136	DAEFRHSSGYEVHHQKLV
920	FP_D1-V18_137	DAEFRHTSGYEVHHQKLV
921	FP_D1-V18_138	DAEFRHVSGYEVHHQKLV
922	FP_D1-V18_139	DAEFRHWSGYEVHHQKLV
923	FP_D1-V18_140	DAEFRHYSGYEVHHQKLV
924	FP_D1-V18_141	DAEFRHDAGYEVHHQKLV
925	FP_D1-V18_142	DAEFRHDCGYEVHHQKLV
926	FP_D1-V18_143	DAEFRHDDGYEVHHQKLV
927	FP_D1-V18_144	DAEFRHDEGYEVHHQKLV
928	FP_D1-V18_145	DAEFRHDFGYEVHHQKLV
929	FP_D1-V18_146	DAEFRHDGGYEVHHQKLV
930	FP_D1-V18_147	DAEFRHDHGYEVHHQKLV
931	FP_D1-V18_148	DAEFRHDIGYEVHHQKLV
932	FP_D1-V18_149	DAEFRHDKGYEVHHQKLV
933	FP_D1-V18_150	DAEFRHDLGYEVHHQKLV
934	FP_D1-V18_151	DAEFRHDMGYEVHHQKLV
935	FP_D1-V18_152	DAEFRHDNGYEVHHQKLV
936	FP_D1-V18_153	DAEFRHDPGYEVHHQKLV
937	FP_D1-V18_154	DAEFRHDQGYEVHHQKLV
938	FP_D1-V18_155	DAEFRHDRGYEVHHQKLV
939	FP_D1-V18_156	DAEFRHDSGYEVHHQKLV
940	FP_D1-V18_157	DAEFRHDTGYEVHHQKLV
941	FP_D1-V18_158	DAEFRHDVGYEVHHQKLV
942	FP_D1-V18_159	DAEFRHDWGYEVHHQKLV
943	FP_D1-V18_160	DAEFRHDYGYEVHHQKLV

944	FP_D1-V18_161	DAEFRHDSAYEVHHQKLV
945	FP_D1-V18_162	DAEFRHDSCYEVHHQKLV
946	FP_D1-V18_163	DAEFRHDSDYEVHHQKLV
947	FP_D1-V18_164	DAEFRHDSEYEVHHQKLV
948	FP_D1-V18_165	DAEFRHDSFYEVHHQKLV
949	FP_D1-V18_166	DAEFRHDSGYEVHHQKLV
950	FP_D1-V18_167	DAEFRHDSHYEVHHQKLV
951	FP_D1-V18_168	DAEFRHDSIYEVHHQKLV
952	FP_D1-V18_169	DAEFRHDSKYEVHHQKLV
953	FP_D1-V18_170	DAEFRHDSLYEVHHQKLV
954	FP_D1-V18_171	DAEFRHDSMYEVHHQKLV
955	FP_D1-V18_172	DAEFRHDSNYEVHHQKLV
956	FP_D1-V18_173	DAEFRHDSPYEVHHQKLV
957	FP_D1-V18_174	DAEFRHDSQYEVHHQKLV
958	FP_D1-V18_175	DAEFRHDSRYEVHHQKLV
959	FP_D1-V18_176	DAEFRHDSSYEVHHQKLV
960	FP_D1-V18_177	DAEFRHDSTYEVHHQKLV
961	FP_D1-V18_178	DAEFRHDSVYEVHHQKLV
962	FP_D1-V18_179	DAEFRHDSWYEVHHQKLV
963	FP_D1-V18_180	DAEFRHDSYYEVHHQKLV
964	FP_D1-V18_181	DAEFRHDSGAEVHHQKLV
965	FP_D1-V18_182	DAEFRHDSGCEVHHQKLV
966	FP_D1-V18_183	DAEFRHDSGDEVHHQKLV
967	FP_D1-V18_184	DAEFRHDSGEEVHHQKLV
968	FP_D1-V18_185	DAEFRHDSGFEVHHQKLV
969	FP_D1-V18_186	DAEFRHDSGGEVHHQKLV
970	FP_D1-V18_187	DAEFRHDSGHEVHHQKLV
971	FP_D1-V18_188	DAEFRHDSGIEVHHQKLV
972	FP_D1-V18_189	DAEFRHDSGKEVHHQKLV
973	FP_D1-V18_190	DAEFRHDSGLEVHHQKLV
974	FP_D1-V18_191	DAEFRHDSGMEVHHQKLV
975	FP_D1-V18_192	DAEFRHDSGNEVHHQKLV
976	FP_D1-V18_193	DAEFRHDSGPEVHHQKLV
977	FP_D1-V18_194	DAEFRHDSGQEVHHQKLV
978	FP_D1-V18_195	DAEFRHDSGREVHHQKLV
979	FP_D1-V18_196	DAEFRHDSGSEVHHQKLV
980	FP_D1-V18_197	DAEFRHDSGTEVHHQKLV
981	FP_D1-V18_198	DAEFRHDSGVEVHHQKLV
982	FP_D1-V18_199	DAEFRHDSGWEVHHQKLV
983	FP_D1-V18_200	DAEFRHDSGYEVHHQKLV
984	FP_D1-V18_201	DAEFRHDSGYAVHHQKLV
985	FP_D1-V18_202	DAEFRHDSGYCVHHQKLV
986	FP_D1-V18_203	DAEFRHDSGYDVHHQKLV

987	FP_D1-V18_204	DAEFRHDSGYEVHHQKLV
988	FP_D1-V18_205	DAEFRHDSGYFVHHQKLV
989	FP_D1-V18_206	DAEFRHDSGYGVHHQKLV
990	FP_D1-V18_207	DAEFRHDSGYHVHHQKLV
991	FP_D1-V18_208	DAEFRHDSGYIVHHQKLV
992	FP_D1-V18_209	DAEFRHDSGYKVHHQKLV
993	FP_D1-V18_210	DAEFRHDSGYLVHHQKLV
994	FP_D1-V18_211	DAEFRHDSGYMVHHQKLV
995	FP_D1-V18_212	DAEFRHDSGYNVHHQKLV
996	FP_D1-V18_213	DAEFRHDSGYPVHHQKLV
997	FP_D1-V18_214	DAEFRHDSGYQVHHQKLV
998	FP_D1-V18_215	DAEFRHDSGYRVHHQKLV
999	FP_D1-V18_216	DAEFRHDSGYSVHHQKLV
1000	FP_D1-V18_217	DAEFRHDSGYTVHHQKLV
1001	FP_D1-V18_218	DAEFRHDSGYVVHHQKLV
1002	FP_D1-V18_219	DAEFRHDSGYWVHHQKLV
1003	FP_D1-V18_220	DAEFRHDSGYYVHHQKLV
1004	FP_D1-V18_221	DAEFRHDSGYEAHHQKLV
1005	FP_D1-V18_222	DAEFRHDSGYECHHQKLV
1006	FP_D1-V18_223	DAEFRHDSGYEDHHQKLV
1007	FP_D1-V18_224	DAEFRHDSGYEEHHQKLV
1008	FP_D1-V18_225	DAEFRHDSGYEFHHQKLV
1009	FP_D1-V18_226	DAEFRHDSGYEGHHQKLV
1010	FP_D1-V18_227	DAEFRHDSGYEHHHQKLV
1011	FP_D1-V18_228	DAEFRHDSGYEIHHQKLV
1012	FP_D1-V18_229	DAEFRHDSGYEKHHQKLV
1013	FP_D1-V18_230	DAEFRHDSGYELHHQKLV
1014	FP_D1-V18_231	DAEFRHDSGYEMHHQKLV
1015	FP_D1-V18_232	DAEFRHDSGYENHHQKLV
1016	FP_D1-V18_233	DAEFRHDSGYEPHHQKLV
1017	FP_D1-V18_234	DAEFRHDSGYEQHHQKLV
1018	FP_D1-V18_235	DAEFRHDSGYERHHQKLV
1019	FP_D1-V18_236	DAEFRHDSGYESHHQKLV
1020	FP_D1-V18_237	DAEFRHDSGYETHHQKLV
1021	FP_D1-V18_238	DAEFRHDSGYEVHHQKLV
1022	FP_D1-V18_239	DAEFRHDSGYEWHHQKLV
1023	FP_D1-V18_240	DAEFRHDSGYEYHHQKLV
1024	FP_D1-V18_241	DAEFRHDSGYEVAHQKLV
1025	FP_D1-V18_242	DAEFRHDSGYEVCHQKLV
1026	FP_D1-V18_243	DAEFRHDSGYEVDHQKLV
1027	FP_D1-V18_244	DAEFRHDSGYEVEHQKLV
1028	FP_D1-V18_245	DAEFRHDSGYEVFHQKLV
1029	FP_D1-V18_246	DAEFRHDSGYEVGHQKLV

1030	FP_D1-V18_247	DAEFRHDSGYEVHHQKLV
1031	FP_D1-V18_248	DAEFRHDSGYEVIHQKLV
1032	FP_D1-V18_249	DAEFRHDSGYEVKHQKLV
1033	FP_D1-V18_250	DAEFRHDSGYEVLHQKLV
1034	FP_D1-V18_251	DAEFRHDSGYEVMHQKLV
1035	FP_D1-V18_252	DAEFRHDSGYEVNHQKLV
1036	FP_D1-V18_253	DAEFRHDSGYEVPHQKLV
1037	FP_D1-V18_254	DAEFRHDSGYEVQHQKLV
1038	FP_D1-V18_255	DAEFRHDSGYEVRHQKLV
1039	FP_D1-V18_256	DAEFRHDSGYEVSHQKLV
1040	FP_D1-V18_257	DAEFRHDSGYEVTHQKLV
1041	FP_D1-V18_258	DAEFRHDSGYEVVHQKLV
1042	FP_D1-V18_259	DAEFRHDSGYEVWHQKLV
1043	FP_D1-V18_260	DAEFRHDSGYEVYHQKLV
1044	FP_D1-V18_261	DAEFRHDSGYEVHAQKLV
1045	FP_D1-V18_262	DAEFRHDSGYEVHCQKLV
1046	FP_D1-V18_263	DAEFRHDSGYEVHDQKLV
1047	FP_D1-V18_264	DAEFRHDSGYEVHEQKLV
1048	FP_D1-V18_265	DAEFRHDSGYEVHFQKLV
1049	FP_D1-V18_266	DAEFRHDSGYEVHGQKLV
1050	FP_D1-V18_267	DAEFRHDSGYEVHHQKLV
1051	FP_D1-V18_268	DAEFRHDSGYEVHIQKLV
1052	FP_D1-V18_269	DAEFRHDSGYEVHKQKLV
1053	FP_D1-V18_270	DAEFRHDSGYEVHLQKLV
1054	FP_D1-V18_271	DAEFRHDSGYEVHMQKLV
1055	FP_D1-V18_272	DAEFRHDSGYEVHNQKLV
1056	FP_D1-V18_273	DAEFRHDSGYEVHPQKLV
1057	FP_D1-V18_274	DAEFRHDSGYEVHQQKLV
1058	FP_D1-V18_275	DAEFRHDSGYEVHRQKLV
1059	FP_D1-V18_276	DAEFRHDSGYEVHSQKLV
1060	FP_D1-V18_277	DAEFRHDSGYEVHTQKLV
1061	FP_D1-V18_278	DAEFRHDSGYEVHVQKLV
1062	FP_D1-V18_279	DAEFRHDSGYEVHWQKLV
1063	FP_D1-V18_280	DAEFRHDSGYEVHYQKLV
1064	FP_D1-V18_281	DAEFRHDSGYEVHHAKLV
1065	FP_D1-V18_282	DAEFRHDSGYEVHHCKLV
1066	FP_D1-V18_283	DAEFRHDSGYEVHHDKLV
1067	FP_D1-V18_284	DAEFRHDSGYEVHHEKLV
1068	FP_D1-V18_285	DAEFRHDSGYEVHHFKLV
1069	FP_D1-V18_286	DAEFRHDSGYEVHHGKLV
1070	FP_D1-V18_287	DAEFRHDSGYEVHHHKLV
1071	FP_D1-V18_288	DAEFRHDSGYEVHHIKLV
1072	FP_D1-V18_289	DAEFRHDSGYEVHHKKLV

1073	FP_D1-V18_290	DAEFRHDSGYEVHHLKLV
1074	FP_D1-V18_291	DAEFRHDSGYEVHHMKLV
1075	FP_D1-V18_292	DAEFRHDSGYEVHHNKLV
1076	FP_D1-V18_293	DAEFRHDSGYEVHHPKLV
1077	FP_D1-V18_294	DAEFRHDSGYEVHHQKLV
1078	FP_D1-V18_295	DAEFRHDSGYEVHHRKLV
1079	FP_D1-V18_296	DAEFRHDSGYEVHHSKLV
1080	FP_D1-V18_297	DAEFRHDSGYEVHHTKLV
1081	FP_D1-V18_298	DAEFRHDSGYEVHHVKLV
1082	FP_D1-V18_299	DAEFRHDSGYEVHHWKLV
1083	FP_D1-V18_300	DAEFRHDSGYEVHHYKLV
1084	FP_D1-V18_301	DAEFRHDSGYEVHHQALV
1085	FP_D1-V18_302	DAEFRHDSGYEVHHQCLV
1086	FP_D1-V18_303	DAEFRHDSGYEVHHQDLV
1087	FP_D1-V18_304	DAEFRHDSGYEVHHQELV
1088	FP_D1-V18_305	DAEFRHDSGYEVHHQFLV
1089	FP_D1-V18_306	DAEFRHDSGYEVHHQGLV
1090	FP_D1-V18_307	DAEFRHDSGYEVHHQHLV
1091	FP_D1-V18_308	DAEFRHDSGYEVHHQILV
1092	FP_D1-V18_309	DAEFRHDSGYEVHHQKLV
1093	FP_D1-V18_310	DAEFRHDSGYEVHHQLLV
1094	FP_D1-V18_311	DAEFRHDSGYEVHHQMLV
1095	FP_D1-V18_312	DAEFRHDSGYEVHHQNLV
1096	FP_D1-V18_313	DAEFRHDSGYEVHHQPLV
1097	FP_D1-V18_314	DAEFRHDSGYEVHHQQLV
1098	FP_D1-V18_315	DAEFRHDSGYEVHHQRLV
1099	FP_D1-V18_316	DAEFRHDSGYEVHHQSLV
1100	FP_D1-V18_317	DAEFRHDSGYEVHHQTLV
1101	FP_D1-V18_318	DAEFRHDSGYEVHHQVLV
1102	FP_D1-V18_319	DAEFRHDSGYEVHHQWLV
1103	FP_D1-V18_320	DAEFRHDSGYEVHHQYLV
1104	FP_D1-V18_321	DAEFRHDSGYEVHHQKAV
1105	FP_D1-V18_322	DAEFRHDSGYEVHHQKCV
1106	FP_D1-V18_323	DAEFRHDSGYEVHHQKDV
1107	FP_D1-V18_324	DAEFRHDSGYEVHHQKEV
1108	FP_D1-V18_325	DAEFRHDSGYEVHHQKFV
1109	FP_D1-V18_326	DAEFRHDSGYEVHHQKGV
1110	FP_D1-V18_327	DAEFRHDSGYEVHHQKHV
1111	FP_D1-V18_328	DAEFRHDSGYEVHHQKIV
1112	FP_D1-V18_329	DAEFRHDSGYEVHHQKKV
1113	FP_D1-V18_330	DAEFRHDSGYEVHHQKLV
1114	FP_D1-V18_331	DAEFRHDSGYEVHHQKMV
1115	FP_D1-V18_332	DAEFRHDSGYEVHHQKNV

1116	FP_D1-V18_333	DAEFRHDSGYEVHHQKPV
1117	FP_D1-V18_334	DAEFRHDSGYEVHHQKQV
1118	FP_D1-V18_335	DAEFRHDSGYEVHHQKRV
1119	FP_D1-V18_336	DAEFRHDSGYEVHHQKSV
1120	FP_D1-V18_337	DAEFRHDSGYEVHHQKTV
1121	FP_D1-V18_338	DAEFRHDSGYEVHHQKVV
1122	FP_D1-V18_339	DAEFRHDSGYEVHHQKWV
1123	FP_D1-V18_340	DAEFRHDSGYEVHHQKYV
1124	FP_D1-V18_341	DAEFRHDSGYEVHHQKLA
1125	FP_D1-V18_342	DAEFRHDSGYEVHHQKLC
1126	FP_D1-V18_343	DAEFRHDSGYEVHHQKLD
1127	FP_D1-V18_344	DAEFRHDSGYEVHHQKLE
1128	FP_D1-V18_345	DAEFRHDSGYEVHHQKLF
1129	FP_D1-V18_346	DAEFRHDSGYEVHHQKLG
1130	FP_D1-V18_347	DAEFRHDSGYEVHHQKLH
1131	FP_D1-V18_348	DAEFRHDSGYEVHHQKLI
1132	FP_D1-V18_349	DAEFRHDSGYEVHHQKLK
1133	FP_D1-V18_350	DAEFRHDSGYEVHHQKLL
1134	FP_D1-V18_351	DAEFRHDSGYEVHHQKLM
1135	FP_D1-V18_352	DAEFRHDSGYEVHHQKLN
1136	FP_D1-V18_353	DAEFRHDSGYEVHHQKLP
1137	FP_D1-V18_354	DAEFRHDSGYEVHHQKLQ
1138	FP_D1-V18_355	DAEFRHDSGYEVHHQKLR
1139	FP_D1-V18_356	DAEFRHDSGYEVHHQKLS
1140	FP_D1-V18_357	DAEFRHDSGYEVHHQKLT
1141	FP_D1-V18_358	DAEFRHDSGYEVHHQKLV
1142	FP_D1-V18_359	DAEFRHDSGYEVHHQKLW
1143	FP_D1-V18_360	DAEFRHDSGYEVHHQKLY
1144	Abeta_S8_scan_WT_01	EEISEVKMDAEFRHD
1145	Abeta_S8_scan_WT_02	EISEVKMDAEFRHDS
1146	Abeta_S8_scan_WT_03	ISEVKMDAEFRHDSG
1147	Abeta_S8_scan_WT_04	SEVKMDAEFRHDSGY
1148	Abeta_S8_scan_WT_05	EVKMDAEFRHDSGYE
1149	Abeta_S8_scan_WT_06	VKMDAEFRHDSGYEV
1150	Abeta_S8_scan_WT_07	KMDAEFRHDSGYEVH
1151	Abeta_S8_scan_WT_08	MDAEFRHDSGYEVHH
1152	Abeta_S8_scan_WT_09	DAEFRHDSGYEVHHQ
1153	Abeta_S8_scan_WT_10	AEFRHDSGYEVHHQK
1154	Abeta_S8_scan_WT_11	EFRHDSGYEVHHQKL
1155	Abeta_S8_scan_WT_12	FRHDSGYEVHHQKLV
1156	Abeta_S8_scan_WT_13	RHDSGYEVHHQKLVF
1157	Abeta_S8_scan_WT_14	HDSGYEVHHQKLVFF
1158	Abeta_S8_scan_WT_15	DSGYEVHHQKLVFFA

1159	Abeta_S8_scan_WT_16	SGYEVHHQKLVFFAE
1160	Abeta_S8_scan_WT_17	GYEVHHQKLVFFAED
1161	Abeta_S8_scan_phospo_01	EEISEVKMDAEFRHD
1162	Abeta_S8_scan_phospo_02	EISEVKMDAEFRHD2
1163	Abeta_S8_scan_phospo_03	ISEVKMDAEFRHD2G
1164	Abeta_S8_scan_phospo_04	SEVKMDAEFRHD2GY
1165	Abeta_S8_scan_phospo_05	EVKMDAEFRHD2GYE
1166	Abeta_S8_scan_phospo_06	VKMDAEFRHD2GYEV
1167	Abeta_S8_scan_phospo_07	KMDAEFRHD2GYEVH
1168	Abeta_S8_scan_phospo_08	MDAEFRHD2GYEVHH
1169	Abeta_S8_scan_phospo_09	DAEFRHD2GYEVHHQ
1170	Abeta_S8_scan_phospo_10	AEFRHD2GYEVHHQK
1171	Abeta_S8_scan_phospo_11	EFRHD2GYEVHHQKL
1172	Abeta_S8_scan_phospo_12	FRHD2GYEVHHQKLV
1173	Abeta_S8_scan_phospo_13	RHD2GYEVHHQKLVF
1174	Abeta_S8_scan_phospo_14	HD2GYEVHHQKLVFF
1175	Abeta_S8_scan_phospo_15	D2GYEVHHQKLVFFA
1176	Abeta_S8_scan_phospo_16	2GYEVHHQKLVFFAE
1177	Abeta_S8_scan_phospo_17	GYEVHHQKLVFFAED
1178	Abeta_S26_scan_WT_01	EVHHQKLVFFAEDVG
1179	Abeta_S26_scan_WT_02	VHHQKLVFFAEDVGS
1180	Abeta_S26_scan_WT_03	HHQKLVFFAEDVGSN
1181	Abeta_S26_scan_WT_04	HQKLVFFAEDVGSNK
1182	Abeta_S26_scan_WT_05	QKLVFFAEDVGSNKG
1183	Abeta_S26_scan_WT_06	KLVFFAEDVGSNKGA
1184	Abeta_S26_scan_WT_07	LVFFAEDVGSNKGAI
1185	Abeta_S26_scan_WT_08	VFFAEDVGSNKGAII
1186	Abeta_S26_scan_WT_09	FFAEDVGSNKGAIIG
1187	Abeta_S26_scan_WT_10	FAEDVGSNKGAIIGL
1188	Abeta_S26_scan_WT_11	AEDVGSNKGAIIGLM
1189	Abeta_S26_scan_WT_12	EDVGSNKGAIIGLMV
1190	Abeta_S26_scan_WT_13	DVGSNKGAIIGLMVG
1191	Abeta_S26_scan_WT_14	VGSNKGAIIGLMVGG
1192	Abeta_S26_scan_WT_15	GSNKGAIIGLMVGGV
1193	Abeta_S26_scan_WT_16	SNKGAIIGLMVGGVV
1194	Abeta_S26_scan_WT_17	NKGAIIGLMVGGVVI
1195	Abeta_S26_scan_phospo_01	EVHHQKLVFFAEDVG
1196	Abeta_S26_scan_phospo_02	VHHQKLVFFAEDVG2
1197	Abeta_S26_scan_phospo_03	HHQKLVFFAEDVG2N
1198	Abeta_S26_scan_phospo_04	HQKLVFFAEDVG2NK
1199	Abeta_S26_scan_phospo_05	QKLVFFAEDVG2NKG
1200	Abeta_S26_scan_phospo_06	KLVFFAEDVG2NKGA
1201	Abeta_S26_scan_phospo_07	LVFFAEDVG2NKGAI

1202	Abeta_S26_scan_phospo_08	VFFAEDVG2NKGAII
1203	Abeta_S26_scan_phospo_09	FFAEDVG2NKGAIIG
1204	Abeta_S26_scan_phospo_10	FAEDVG2NKGAIIGL
1205	Abeta_S26_scan_phospo_11	AEDVG2NKGAIIGLM
1206	Abeta_S26_scan_phospo_12	EDVG2NKGAIIGLMV
1207	Abeta_S26_scan_phospo_13	DVG2NKGAIIGLMVG
1208	Abeta_S26_scan_phospo_14	VG2NKGAIIGLMVGG
1209	Abeta_S26_scan_phospo_15	G2NKGAIIGLMVGGV
1210	Abeta_S26_scan_phospo_16	2NKGAIIGLMVGGVV
1211	Abeta_S26_scan_phospo_17	NKGAIIGLMVGGVVI
1212	Abeta_D1-WT_01	DAEFRHDSGYEVHHQ
1213	Abeta_D1-WT_02	DAEFRHDSGYEVHHQ
1214	Abeta_D1-WT_03	DAEFRHDSGYEVHHQ
1215	Abeta_D1_d_01	5AEFRHDSGYEVHHQ
1216	Abeta_D1_d_02	5AEFRHDSGYEVHHQ
1217	Abeta_D1_d_03	5AEFRHDSGYEVHHQ
1218	Abeta _D1-d,iso_01	7AEFRHDSGYEVHHQ
1219	Abeta _D1-d,iso_02	7AEFRHDSGYEVHHQ
1220	Abeta _D1-d,iso_03	7AEFRHDSGYEVHHQ
1221	Abeta_D1-l,iso_01	6AEFRHDSGYEVHHQ
1222	Abeta_D1-l,iso_02	6AEFRHDSGYEVHHQ
1223	Abeta_D1-l,iso_03	6AEFRHDSGYEVHHQ
1224	Abeta_D1-1_01	MDAEFRHDSGYEVHH
1225	Abeta_D1-1_02	MDAEFRHDSGYEVHH
1226	Abeta_D1-1_03	MDAEFRHDSGYEVHH
1227	Abeta_E3_WT	EFRHDSGYEVHHQKL
1228	Abeta_E3_WT	EFRHDSGYEVHHQKL
1229	Abeta_E3_WT	EFRHDSGYEVHHQKL
1230	Abeta_E3_pyro	8FRHDSGYEVHHQKL
1231	Abeta_E3_pyro	8FRHDSGYEVHHQKL
1232	Abeta_E3_pyro	8FRHDSGYEVHHQKL
1233	Abeta_E11_WT	EVHHQKLVFFAEDVG
1234	Abeta_E11_WT	EVHHQKLVFFAEDVG
1235	Abeta_E11_WT	EVHHQKLVFFAEDVG
1236	Abeta_E11_pyro	8VHHQKLVFFAEDVG
1237	Abeta_E11_pyro	8VHHQKLVFFAEDVG
1238	Abeta_E11_pyro	8VHHQKLVFFAEDVG
		p Ser=2
		d,isoD=6
		l,isoD=7
		d,D=5
		pyE=5

1245 **A8 - Purified 1-15 H6R**

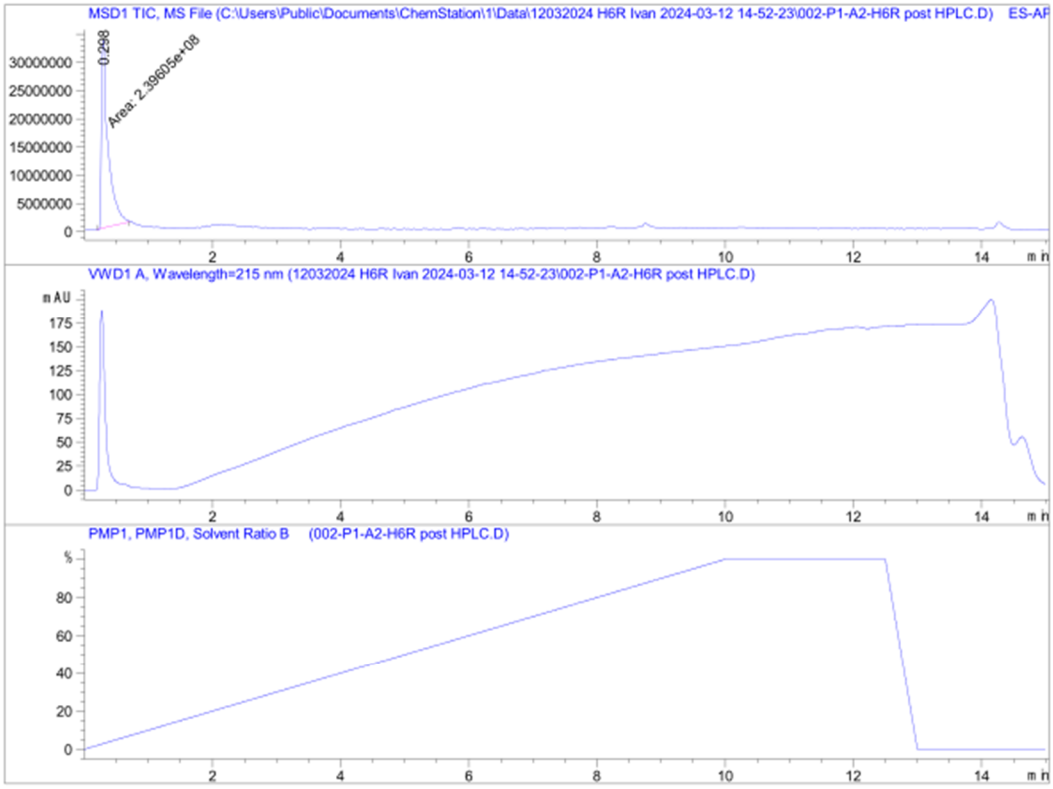

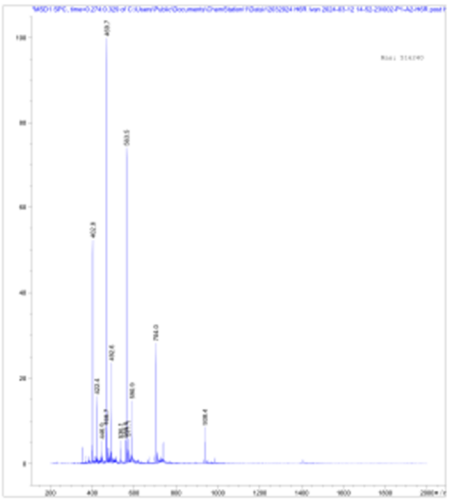

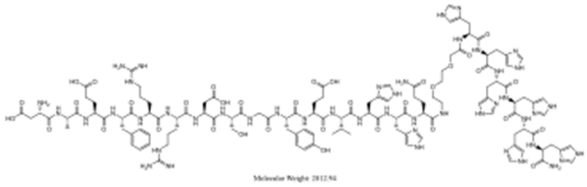

1246

1247 **A9 – Purified 1-15 and p1-15 peptides LC-MS QC**

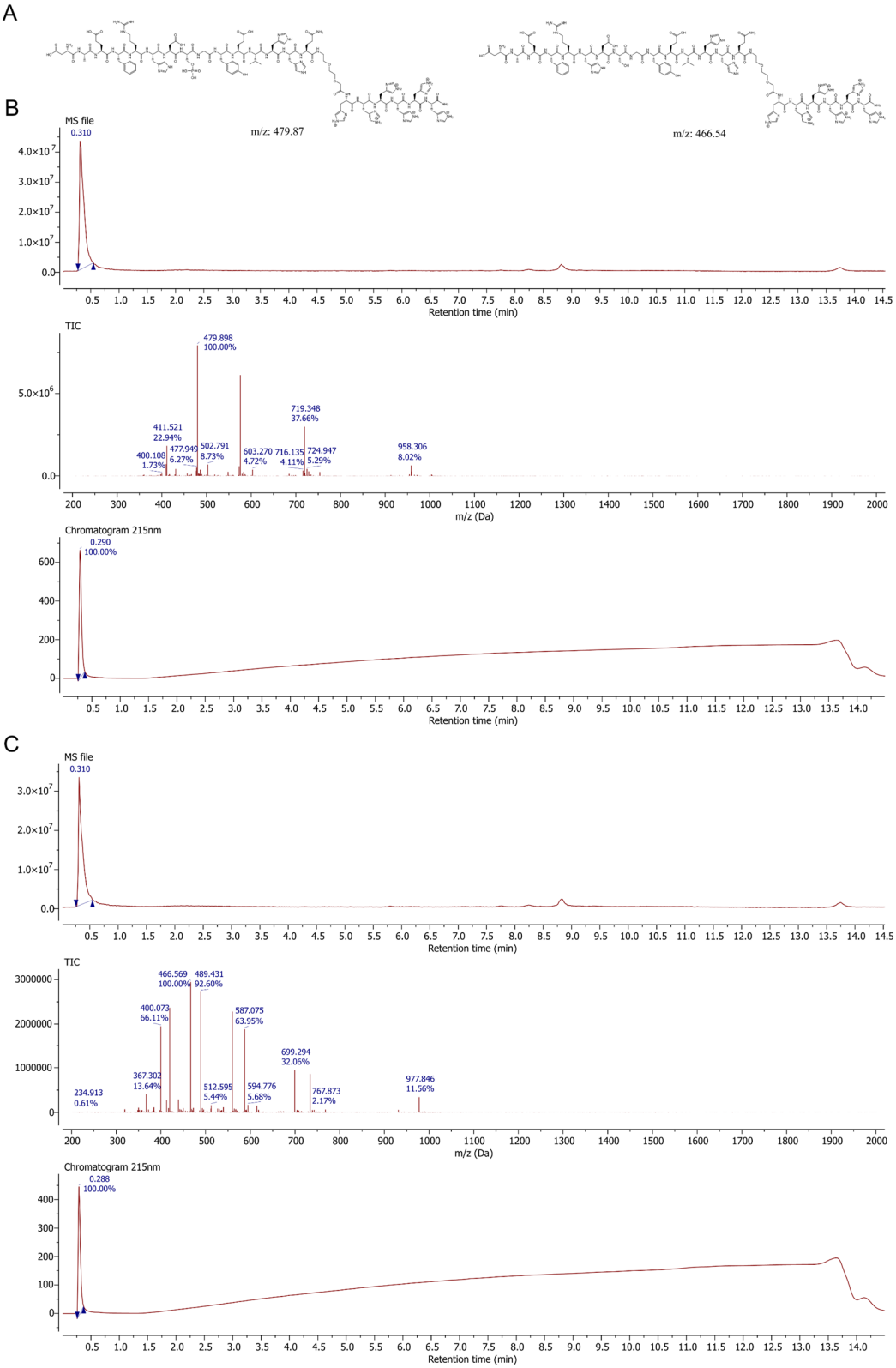

1248

1249 **A10–EC50 values of 1E4E11 and Aducanumab$_{bs}$ on Microarray**

Antibody	Peptide	EC*50* [nmol/L]
Aducanumab$_{bs}$	DAEFRHDSGYEVHHQ	1.17
Aducanumab$_{bs}$	DAEFRHD(p)SGYEVHHQ	0.00361
1E4E11	DAEFRHDSGYEVHHQ	1.69
1E4E11	DAEFRHD(p)SGYEVHHQ	0.099

1250

1251 **A11 - In-house synthetized pSerine 8 Aβ1-40 LC-MS QC**

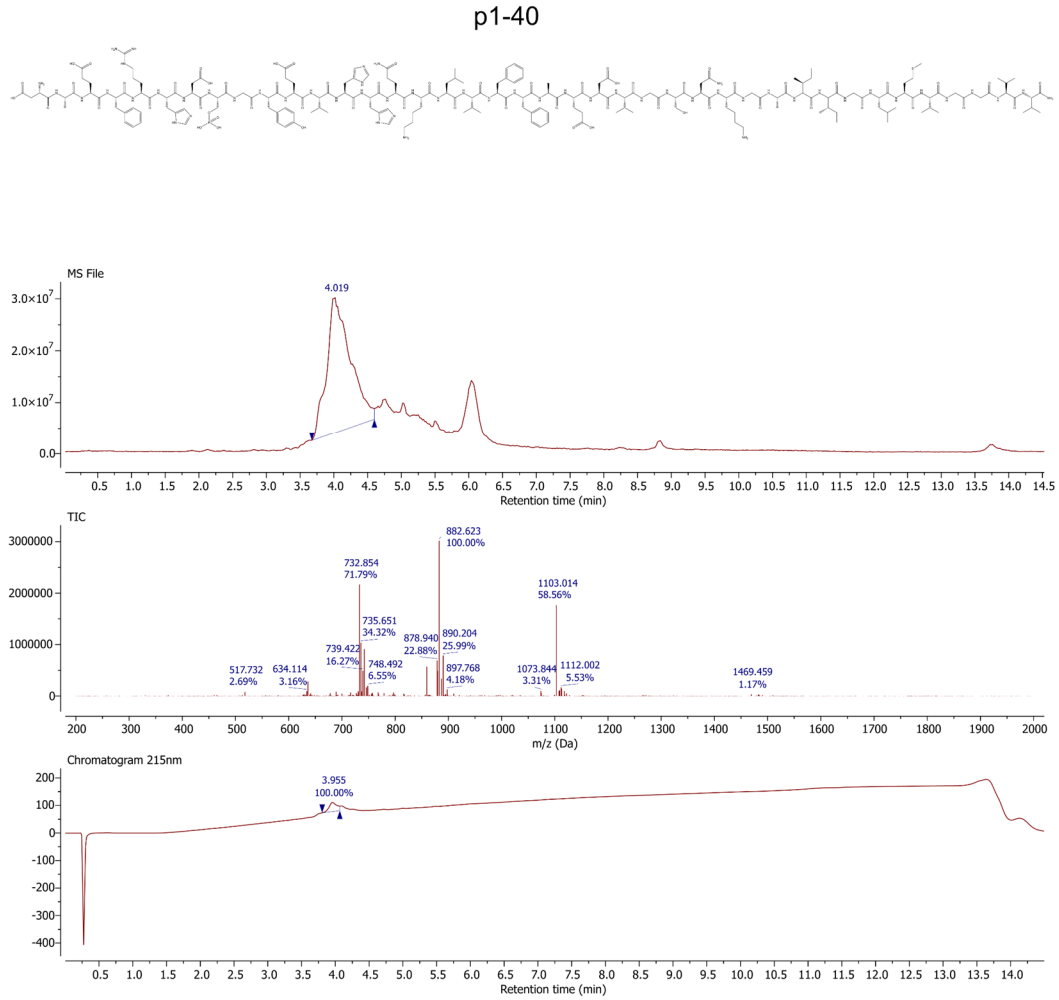

1252

1253 **A12- pSerine 8 Aβ1-40 MALDI-TOF**

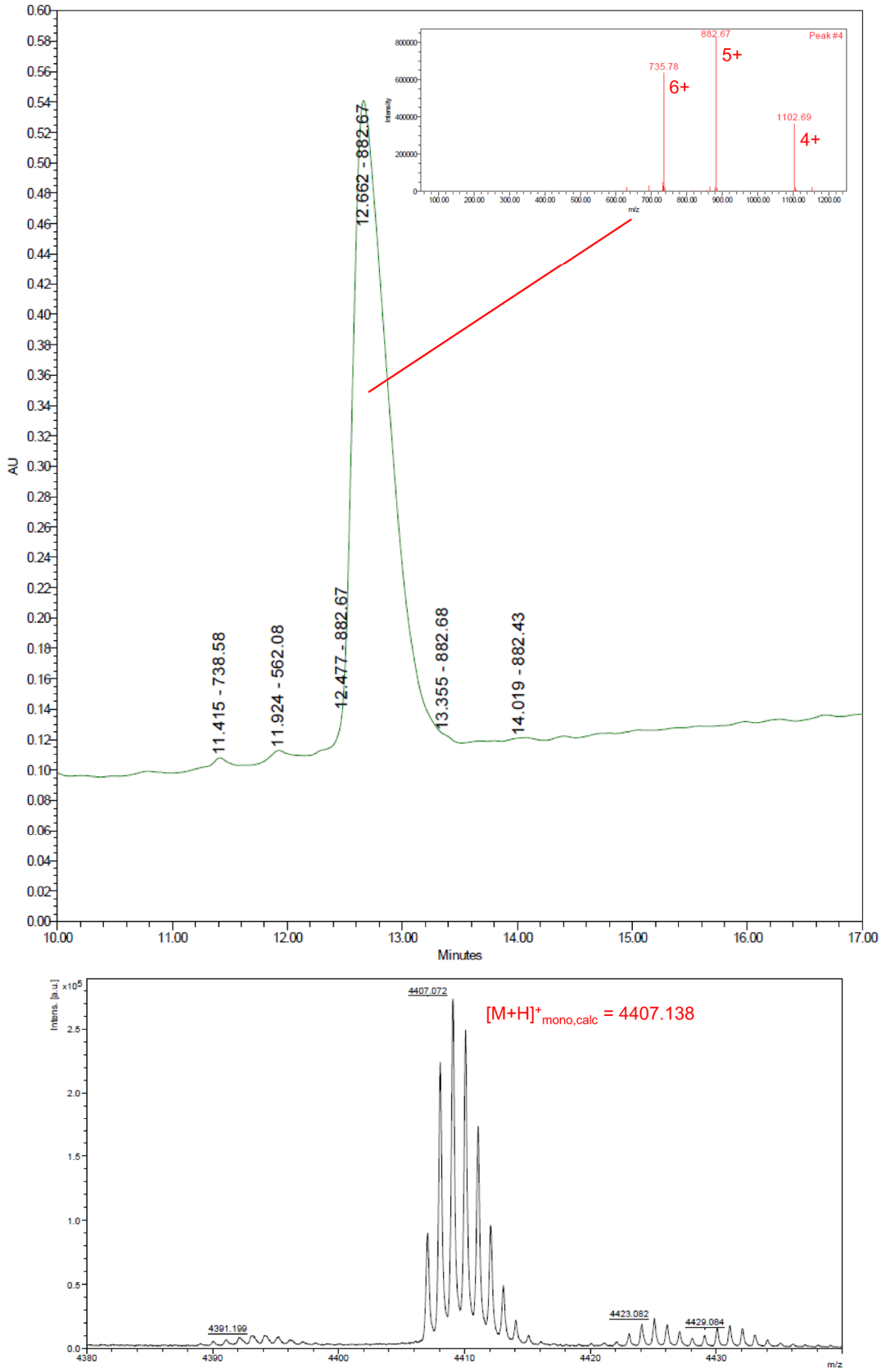

1254